LATVIJAS UNIVERSITĀTES
ZINĀTNISKIE RAKSTI

ACTA UNIVERSITATIS LATVIENSIS

559

ACTUAL PHYSICAL AND CHEMICAL PROBLEMS OF FERROELECTRICS

UNIVERSITY OF LATVIA

Institute of Solid State Physics

ACTUAL PHYSICAL AND CHEMICAL PROBLEMS OF FERROELECTRICS

Scientific Reports

Volume 559

University of Latvia
1991

ACTUAL PHYSICAL AND CHEMICAL PROBLEMS OF FERROELECTRICS / Ed.by A.Sternberg and V.Polmane. - R.: Univ.of Latvia, 1991. - 112 p.

Papers published in this book concern with original experimental and theoretical studies of physical properties of oxygen octahedra ferroelectrics performed from 1988 to 1990 and mainly by the division of ferroelectric physics of the Institute of Solid State Physics of the University of Latvia.

The phase transition dynamics and its crossover features in $BaTiO_3$ single crystals are analyzed in the quasiharmonic rigid ion approximation, the calculated Ti and O ion displacements being related to the experimental data of X-ray diffraction. By measurements of microstructure, dielectric, optical, electrooptical, thermal, elastic, and mechanical parameters and studies of transfer processes phase transitions have been examined in a number of more complex systems like $Pb_xSr_{1-x}TiO_3$ and $NaNbO_3$ solid solutions, SBN single crystals and transparent PLZT ceramics. The most recent results on electric field induced phase transition micromechanism studies in transparent ferroelectric ceramics are also reported as well as on domain structure and polarization switching in pure and metal-doped PLZT ceramics, and on effects of irradiation on PLZT optical and dielectric properties. Some of the papers refer to technology of PLZT ceramics, and problems of the control of stoichiometric changes and admixture concentration.

The present book is assumed to be of professional help to people dealing with physical and chemical properties of ferroelectric materials and the studies of phase transitions, as well as to graduate and senior students in solid state physics. It may be also helpful to scientists of the University of Latvia participating in meetings and business trips in other countries, as well as the guest scientists to get acquainted with the problems being studied and results obtained in the Institute of Solid State Physics.

UDC 537.224.33

LATTICE DYNAMICS IN CUBIC $BaTiO_3$

J.Zvirgzds, J.Cabrusenoks
Institute of Solid State Physics, University of Latvia
8, Kengaraga St., 226063 Riga, Latvia

The rigid ion model in quasiharmonic aproximation was used to investigate the alterations of central force parameters between ions and lattice normal vibration coordinates in the ferroelectric phase transition region in $BaTiO_3$. Phonon dispersion curves, one-phonon diffuse X-ray scattering intensity and the ellipsoids of ion thermal vibration were calculated. The mean-square displacements of the Ti and O ions, being phase transition sensitive, show a crossover feature and are determined by these ions vibration amplitudes along the axes Ti-O in the soft mode.

Specific features of the rigid ion model

The rigid ion model studies of lattice dynamics in barium titanate have been reported in a number of papers [1,2]. However the most interesting phenomenon - the change of dynamics of the cubic lattice near the ferroelectric phase transition (PT) - has not been paid its due attention. We have used the rigid ion model to calculate the parameters of lattice dynamics in cubic barium titanate, mean - square displacements of ions, thermal capacity and X-ray diffuse scattering intensity. The latter provide suggestions concerning the mechanism of the PT.

Interaction potential of the rigid ion model is supposed to include the Coulomb contribution and the short-range Born-Mayer potential [3]. The short-range force calculations as in [3] were limited to the nearest neighbours only: Ba-O(1), Ti-O(2), O-O(3). The short-range interaction potential in the model of central interaction is determined by two parameters A_λ and B_λ. The long-range Coulomb terms $C(kk')$ of the dynamic matrix D have been calculated by the method reported by Cowley

[4]. Since the matrix elements C(kk') and matrix elements of short range terms F(kk') contain unknown parameters and effective charges of ions, the matrix is first written for the wave vector $\vec{q} = 0$. To simplify following calculations the block diagonalization of the matrix D has been performed. The 48 elements of symmetry group O_h being taken into account to obtain unitary matrix U(Γ) at the Γ-point of reciprocal space ($\vec{q} = 0$). The diagonalized matrix D' is obtained by transformation $D' = U^{T}(\Gamma)DU(\Gamma)$. The method of calculation has been reported earlier [5,6,7,8].

Force constants and effective charges of ions

Elastic parameters and effective charges of ions have been found from experimental values of elastic moduli c_{ij} [9] and calculated w(T) [10] from IR reflection by the method of least squares. The charges being assumed as a result of mixed ion-covalent interaction. Ionic contribution in the value of the ion charge is expressed by the coefficient e. Minimization is made seperately for transverse and longitudinal modes, the accuracy of A_i and B_i values being within ±0.1 N/m for a series of e values. Parameters of the model are given in Table 1. Compared to experimental data the best results are obtained with e close to one. For further calculations the value $e = 0.95$ has been chosen. The error of mode frequencies has a small effect on the A_i and B_i values. At the same time the values of elastic moduli are important: the values of c_{ij} are determined within the accuracy of 10-15% and different single crystal specimens provide strongly different sets of elastic moduli. Nevertheless, the calculated values of force parameters and effective charges are in good agreement with the data obtained for similar perovskites by other authors (Table 1). To estimate validity of the model the frequencies of ion vibrations propagating along the main directions of the crystal lattice for different values of wave vector q in the first Brillouin zone were calculated and compared to the data of neutron scattering [11]. A satisfactory agreement is obtained for all vibration modes (Fig.1).

Table 1

Force parameters* A_i for rigid ion model in perovskites

Parameter	$BaTiO_3$	$BaTiO_3$/1/		$PbTiO_3$/1/		$SrTiO_3$/13/	
	Temperature in $T-T_c$, K						
	950 K	3	-103	-470	-10	190	-15
A_1	69	60	47	34	30	24.7	25.8
			51	68	67		
			41	12	13		
A_2	194	194	267	347	353	360	364
			133	88	90		
			197	221	194		
A_3	-19	-23	9.8	8.7	7.0	-2.27	-2.77
			8.2	11.3	7.5		
			9.4				
Z_T	2.46	2.46	2.68	2.47	3.68	3.68	3.68
Z_B	1.47	1.47	1.58	1.69	1.82	1.09	1.09

*) Force parameters A_i values are given in N/m, ionic charges - in electron charge units.

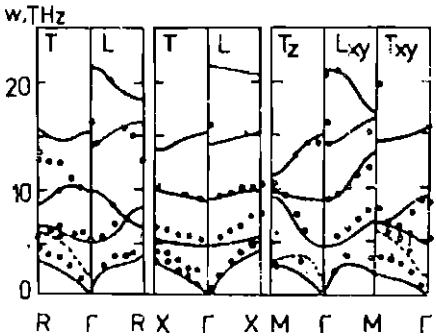

Fig.1. Calculated dispersion curves of $BaTiO_3$ for rigid ion model at $T=T_c+3$ K. Filled circles neutron data [2].

The value of force parameter A_1 (parameter of the A-O bound in perovskite ABO_3) is higher in the case of displacements of the oxygen octahedra (e.g., in $BaTiO_3$) as

compared to rotations (e.g., in $SrTiO_3$). Parameter A_1 is the one describing the force preventing rotation of the octahedron. The value of A_2 suggests that ion B is the most strongly bonded to the oxygen in all perovskites. In $SrTiO_3$ and $PbTiO_3$ where these bonds are the strongest among perovskites displacement and rotation of the octahedra do not distort them. Parameter A_3 characterizing interaction between the oxygen ions is small. Its value being close to zero suggests that the effect of interaction between the oxygen ions on the octahedron stability is weak, the Coulomb forces being repulsive. Parameters B_i describe the force applied to the ion at its displacements normal to the bond direction and mainly are negative. The ion is instable with respect to its displacements normal to the bond. Effective charge values are close in all the three perovskites given in Table 1. They are 0.6-0.7 of the free ion charge.

We have obtained the following symmetry of vibration modes. The high-frequency mode determined by the small values of parameter A_3 and mass of the oxygen ions refers to counterphase vibrations of the oxygen sublattices. The middle-frequency mode corresponds to vibrations of the octahedra including oxygen and titanum with respect to the Ba sublattice, the force parameter A_2 describing the oxygen-barium interaction being the most important. The soft mode relates to the vibration of the titanium ion with respect to the oxygen octahedra. The low value of the vibration frequency of the titanium is possibly due to equilibrium between all the forces at small displacements through the titanum-oxygen bond (characterized by parameter A_2) is the most rigid. The symmetry of the modes is the same as in the tetragonal phase [1].

According to the rigid ion approximation there are considered two basic reasons which may cause the change of force parameters and eigenvectors upon approaching the T_c. Usually only one of them is regarded - the decrease of soft mode frequency, the elastic moduli c_{ij} being assumed not to dependent on temperature. However, the decrease of the elastic moduli values at $T \to T_c^+$ provide at least a comparable contribution.

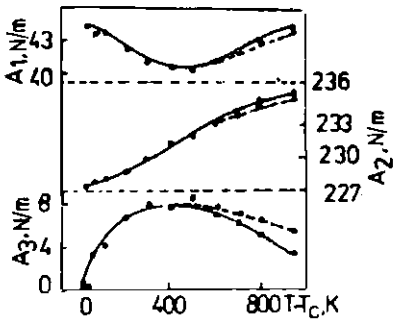

Fig.2. Force parameters A_i for rigid ion model versus temperature in cubic $BaTiO_3$.

Table 2

Force parameters* B_i for rigid ion model versus temperature in cubic $BaTiO_3$

$T-T_c$,K	B_1	B_2	B_3
1	-6.11	-52.3	5.13
3	-4.45	-59.8	5.43
10	-3.69	-59.6	4.71
20	-2.70	-63.3	4.70
50	-2.05	-64.1	4.31
100	-1.63	-65.1	4.18
200	-1.33	-65.1	3.91
400	-1.21	-64.6	3.92
600	-1.59	-62.3	3.49
800	-1.77	-60.9	3.31

* Force parameters B_i values are given in N/m.

Force parameter values at different temperature have been determined from thermal behaviour of frequency $w(T)$ and ε_{11} by minimization according to the procedure used by Powel. Thermal behaviour of force parameters A_i is shown in

Fig.2. In Table 2 are given the values of force constants B_i used in the model for different temperature. Approaching T_c the oxygen-oxygen interaction (A_3) decreases. This is consistent with the assumption that the oxygen is the least strongly bounded ion in the lattice. The low value of B_2 (about -60 N/m) suggesting a comparatively free displacement of the oxygen normal to the Ti-O bond is another argument to regard the symmetric position of the oxygen as a relatively unstable one.

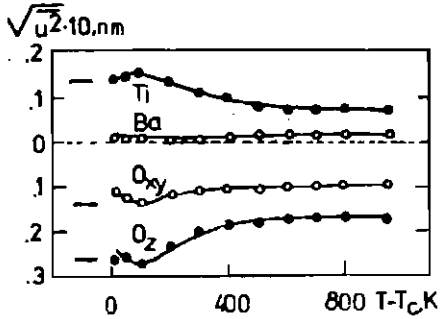

Fig.3. Vibration amplitude of ions in the soft mode versus temperature in $BaTiO_3$ in Brillouin zone center.

Fig. 3 and 4 show the ion amplitudes in different vibration modes as function of temperature. Dependence of ion amplitudes on temperature is due to: the change of eigenvector moduli $e(k,j,\vec{q})$ (mode frequency w, elastic moduli c_{ij}), the change of mode j frequency $w(j,\vec{q})$ and the change of mode energy E.

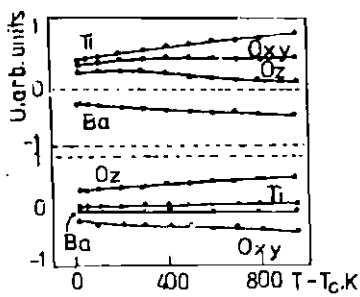

Fig.4. Vibration amplitude of ions in two highfrequency modes versus temperature in $BaTiO_3$ in Brillouin zone center.

As the mode frequency decreases the amplitude of the relevant ion vibration grows which is true for the soft mode as well. However, as the soft mode becomes saturated at $T=T_c+100$ K, the change of the amplitude $U(j\vec{q})$ is determined by the decrease of elastic moduli and mode energy $E(j\vec{q})$ alone. It is important that thermal behaviour of the soft mode frequency and the elastic moduli do not change the sign of eigenvectors and, consequently, the form of normal vibration coordinates at $\vec{q} = 0$ when $T->T_c^+$. Neither the decrease of soft mode frequency nor the decrease of elastic moduli have an effect on the amplitudes of high-frequency vibration modes.

Thermal vibration ellipsoid and the soft mode in $BaTiO_3$

Half-axes of thermal vibration ellipsoids (TVE) for the three basic directions of the crystal lattice, calculated from eigenvectors and eigenfrequencies of the rigid ion model, are shown in Fig.5. Far from the PT vibrations of the Ba and Ti

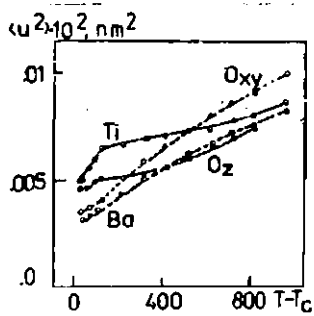

Fig.5. Ellipsoid of thermal vibration versus temperature in $BaTiO_3$. The thermal vibrations of Ba and Ti are isotropic.

are isotropic while vibrations of the O ion form rotational ellipsoid flattened along the axis (the 4-th order axis O-Ti of the lattice). Approaching the PT no change is observed in the thermal behaviour of $\langle u_{11}^2 \rangle$ of the Ba ions while the slope of $\langle u_{11}^2 \rangle$ of the Ti and O ions becomes less pronounced the thermal vibration of the O being extended along the O-Ti axis. Diagonal terms of the thermal vibration tensor $\langle u_{11}^2 \rangle$ of the Ti and O pass through a step of maximum at the temperature of 100 K above T_c corresponding to the soft mode saturation temperature

(the crossover temperature [10]). The amplitudes of ions of the soft mode vibrations are by an order larger than their mean square displacements near the PT.

The PT has collective behaviour not only with respect to seperate ions but as well to some region of wave vector values in the Brillouin zone center. Let us evaluate the size of the region around Γ-point providing essential contribution to thermal vibrations of ions and, consequently, to the PT. Calculated values of amplitude squares of ions of the transverse soft mode vibrations propagating alonge the three basic directions [001], [110], [111] of the crystal lattice at temperature $T=T_c+20$ K are shown in Fig.6. The soft mode has three branches - two transversal and one longitudinal. Only the

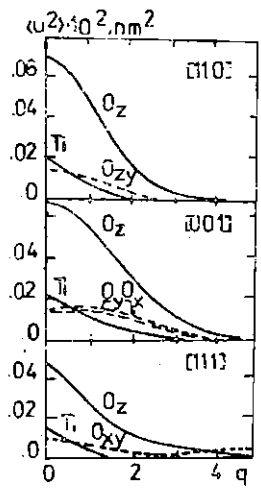

Fig.6. Calculated values of amplitude squares of ions in the transverse soft mode vibrations propagating along the three basic directions [001], [110], [111] at $T=T_c+20$ K in $BaTiO_3$.

transversal modes contribute to the PT. Along [001] and [111] directions transversal vibrations are degenerate, in the [110] direction the branches have different frequency for the same value of the wave vector - they are split. It means that they are split in any other direction except [001] and [111]. In the latter case important is contribution from the branch polarized along [001] (direction of spontaneous deformation of the crystal). From Fig.6 it follows that the most significant

contribution in the TVE of oxygen is due to the soft mode vibration at the zone center - its amplitude square exceed by 10 times the mean-square displacements in the TVE. Regardless to the direction at $T=T_c+20$ K prevailing is the $\langle u^2_{oz}\rangle$ component - vibration of the O along its bond to the Ti. At high temperature dominate $\langle u^2_{oxy}\rangle$ - vibration of the O in the plane perpendicular to the Ti-O axis.

The data show that apart from soft mode vibrations of ions in Brillouin zone center, i.e., vibrations of infinite wavelength, a rather considerable neighbourhood of the zone center contributes to the phase transition. So, up to 80% of the TVE is due to the oxygen soft mode vibrations of q values up to 0.2 while only 50% - to those of q=0.1. Amplitude square of oxygen ion vibration drops most rapidly as q grows in the direction of point R of Brillouin zone. Amplitude square of the soft mode vibration of the Ti ion at the zone center is about five times its mean-square displacements in the TVE.

These data show considerable contribution of the soft mode ion vibrations to the TVE the soft mode being the only one strongly dependent on temperature. Though there is only one soft mode it is the one responsible for mean-square displacements of ions dependent on temperature.

First order X-ray diffuse scattering

Diffuse scattering bands were observed in cubic $KNbO_3$ and $BaTiO_3$ by several authors [12]. The bands were ascribed to static corelated displacements of ions along certain axes. Later on it was supposed that the bands are due to anisotropy of the mode dispersion surfaces [13]. We have checked this assumption by calculations for $BaTiO_3$ the total dynamic matrix of the rigid ion model being used. Diffuse scattering intensities were calculated in planes (001), (-110) and (100) of the reciprocal lattice in the first Brillouin zone around three types of points of the lattice: (001), (110) and (111). The calculations were made with the step 0.005 of the reduced wave vector $\vec{q} = 2\pi/a(q_1;q_2;q_3)$ up to 0.05. The following

points of the reciprocal lattice have been used to find anisotropy of diffuse scattering from the scattering indicatrix and its change: (004), (011), (330), (880), (222), (666). Three basic directions of the lattice were selected and such values of (hkl) for which the effects of Debye-Waller factor on the scattering intensity would be about the same.

The shape of scattered intensity maxima depends only on the reciprocal lattice point, i.e., - (001), (110) or (111). The most anisotropic calculated scattering was found to lay in the plane (110)(or (010), Fig.7). The scattered intensity maximum

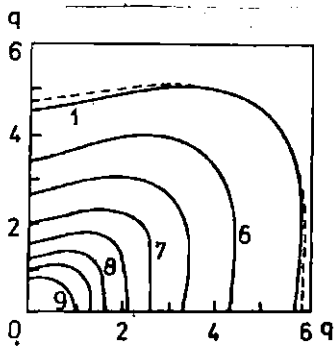

Fig.7. The contours of one-phonon X-ray scattering intensity in the plane (110). The shape of contours changes very little with temperature.

is oriented in [011] direction - intensity maximum is extended in this direction. This extension resembles the bands observed experimentally [12], their shapes being little dependent on temperature. Approaching the PT temperature anisotropy of diffuse scattering somewhat increases - intensity maxima become more extended in the [110] direction (Fig.7, curve 1). It seems to be due to the small change of mode dispersion anisotropy.

Contrary to the angular distribution of scattered intensity, its absolute value strongly depends on temperature. As the sum of index squared amounts to above 120 the thermal behaviour of the intensities become similar to that of ions displacements in the soft mode. This is most pronounced in the [001] direction (the (0011) point of the reciprocal lattice).

Conclusions

1. Lattice dynamics at the Brillouin zone center of barium titanate in the region of phase transition are well described by the rigid ion model in quasi-harmonic approximation. Parameter A_3 of interaction between the oxygen ions is the only rigid ion model parameter having a relatively critical thermal behaviour. It may be assumed that this interaction is the most important in the phase transition mechanism.

2. The soft mode vibration amplitudes of the ions are the largest and increase strongly approaching T_c at cooling, passing a maximum at the mode saturation.

3. Thermal vibration ellipsoid of the oxygen ion in cubic barium titanate at the distance of 200 K from the phase transition point changes its shape from flattened to extended along the Ti-O axes (the direction of spontaneous displacements at the phase transition).

4. A contribution to the phase transition is provided by vibrations at wave vectors in a considerable neighbourhood of the Γ-point of the first Brillouin zone. However, the features of thermal behaviour of mean square displacements of ions of $BaTiO_3$ are due to the soft mode vibration amplitudes near the Γ-point.

5) Anisotropy of the diffuse scattering is little pronounced and little changed at $T \to T_c^+$. Dispersion anisotropy of the modes is not sufficient to form pronounced bands of diffuse scattering.

REFERENCES

1. Freire J.D., Katiyar R.S. // Phys.Rev. - 1988. - Vol.37, N 4. - P.2074-2085.

2. Khatib D., Migoni R., Kugel G.E., Godefroy L. // J.Phys.: Condens. Matter. - 1989. - Vol.1. - P.9811-9822.

3. Cowley R.A. // Phys.Rev. - 1964. - Vol.134, N 4A. - P.A981-A997.

4. Cowley R.A. // Acta Cryst. - 1962. - Vol.15. - P.687-690.

5. Zvirgzds J.A., Gabrusenoks J.V. // Izv.Akad.Nauk Latv.SSR. Ser.Fiz.Tekh.- 1989.- N 4.- P.77-82 (in Russian).

6. Zvirgzds J.A., Gabrusenoks J.V., Zitars I.R. // Izv.Akad.Nauk Latv.SSR. Ser.Fiz.Tekh.- 1989.- N 3.- P.46-54 (in Russian).

7. Ozolinsh V.E., Zvirgzds J.A. // Izv.Akad.Nauk Latv.SSR. Ser.Fiz.Tekh.- 1990.- N 1.- p.35-39 (in Russian).

8. Zvirgzde J.V., Zvirgzds J.A. // Izv.Akad.Nauk Latv.SSR. Ser.Fiz.Tekh.- 1990.- N 1.- P.40-43 (in Russian).

9. Huibregtse E.J., Bessey W.H., Drougard M.E. // J.Appl. Phys. - 1959. - Vol.30, N 6. - P. 899-905.

10. Luspin Y., Servoin J.L., Gervais F. // J.Phys.C.: Solid State Phys. - 1980. - Vol.13. - P.3761-3773.

11. Jannot B., Escribe-Fillipini C., Bouillot J. // J.Phys.C.: Solid State Phys. - 1984. - Vol.17. - P.1327- 1329.

12. Comes M.R., Lambert M., Guinier M.A. // C.R.Acad. Sci. Paris. - 1968. - Vol.266, Ser.B. - P.959-962.

13. Gesi K., Axe J.D., Shirane G. // Phys.Rev.B. - 1972. - Vol.5, N 5. - P.1933-1941.

14. Stirling W.G. // J.Phys. C.: Solid State Phys. - 1972. - Vol.5. - P.2711 - 2730.

Received February 6, 1991.

UDC 537.224.33

THE ONE-PARTICLE POTENTIAL IN $BaTiO_3$ CRYSTAL

J.Zvirgzde, P.Kapostins, J.Zvirgzds
Institute of Solid State Physics, University of Latvia
8, Kengaraga St., 226063 Riga, Latvia

The one-particle potentials of seperate ions in $BaTiO_3$ single crystals has been investigated by X-ray diffraction in the region of ferroelectric phase transition. The probability for the O ion to acquire energy higher than the potential barrier is increasing noticeably near the melting point and the ferroelectric phase transition temperature. The reason of this is the thermal energy growth at high temperatures and the lowering of potential barrier of the O ion due to pretransitional anharmonic interactions.

Introduction

The interpretation of Debye-Waller factors (DWF's) from weakly anharmonic systems in terms of the parameters of an effective one-particle potential (OPP) has become an established technique [1,2]. The effective OPP may be viewed as representing the mean field seen by the atom in question, resulting from the influence of all other atoms. The temperature dependence of OPP's may be related to cooperative effects in the crystal and microscopic mechanisms of phase transition (PT).

OPP for seperate ions in $BaTiO_3$ has been investigated theoretically [3,4] and experimentally [5]. The relief of ion potentials is supposed to be constant with temperature [3-5]. Therefore these investigations do not reveal possible alterations of the OPP with temperature.

In the present study we have investigated the changes of OPP near the PT in $BaTiO_3$ by X-ray diffraction. In the previous paper [5] the scattering from the oxygen was not taken into account. That has resulted in elevated sensitivity of the titanium OPP near T_c. Presently the oxygen has been included in calculations. Some data has been published previously [7].

Theoretical

In the isotropic approximation OPP has the same form for lattice points with symmetry m3m and 4/mmm [2].

$$V_i(u)=V_o+\alpha u^2/2+\gamma u^4. \quad (1)$$

Then for Bragg reflections (00l) the Debye-Waller factor for each ion

$$T(Q)=\exp(8\pi^2\langle u^2\rangle l^2/4a), \quad (2)$$

where general (anharmonic) mean-square displacements for each ion

$$\langle u^2\rangle=\langle u_h^2\rangle(1-20k_bT\gamma/\alpha^2) \quad (3)$$

α and γ are harmonic and anharmonic potential (1) parameters. Harmonic mean-square displacements $\langle u_h^2\rangle$ can be expressed as k_bT/α. Near PT the anharmonicity grows and general (anharmonic) mean-square displacements (MSD) get additional singular component $\langle u_s^2\rangle(T)$ and deviate upward from the $\langle u_r^2\rangle(T)$ slope. The latter is extrapolated from temperatures higher than $T=T_c+100$ K into the PT region

$$\langle u_s^2\rangle(T)=\langle u^2\rangle(T)-\langle u_r^2\rangle(T). \quad (4)$$

In [6] we suggested to describe the growing anharmonicity and related changes in OPP near PT by additional growth $\Delta\gamma$ of the anharmonic parameter γ:

$$\Delta\gamma = -\alpha^3[20(k_bT)^2(\langle u^2\rangle-\langle u_r^2\rangle)]. \quad (5)$$

Then general mean-square displacements near PT

$$\langle u^2\rangle=\langle u_h^2\rangle[1-20k_bT(\Delta\gamma+\gamma)/\alpha^2]. \quad (6)$$

Expressing general MSD by OPP parameters we get

$$\langle u^2\rangle(T)=k_bT(1-T[2\gamma_g\alpha-20k_bT(\gamma+\Delta\gamma)/\alpha^2]) \quad . \quad (7)$$

Experimental

The sample 4x4x1 mm^3 was prepared from a single crystal grown by the topseeded method from TiO_2 rich TiO-BaO melt. The normal of the sample plane was parallel to the cubic a-axis. The integrated intensities of Bragg reflections (0,0,l; l varies from 1 to 11) were measured by"DRON-2" (λ = 0,071 nm) in the temperature range from T_c up to T_c+300 K. Before making analysis, I(0,0,l,T) were corrected for Lorentz, polarization

and therm. diffuse scattering (one phonon procedure of Merisalo and Kurittu, Fig.1). The extinction correction by Becker and

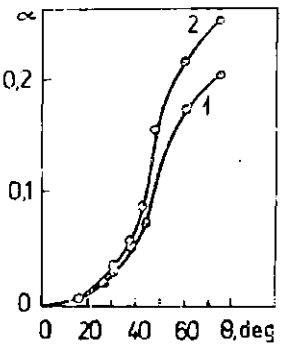

Fig.1. TDS correction $\alpha_T = (I_e/I_t - 1)$ versus scattering angle at two emperatures in cubic $BaTiO_3$: 1 - $T = T_c+90$ K; 2 - $T=T_c+3$ K.

Coppens was included in minimization. Least-square refinements by Powel method were employed to minimize the difference between the observed and calculated intensity. After refinements we get general (anharmonic) MSD $\langle u^2\rangle(T)$ for seperate ions (Fig.2. $\langle u^2\rangle(T)$ of the O_I and O_{II} ions are supposed to be equal). The accuracy of $\langle u^2\rangle(T)$ was determined

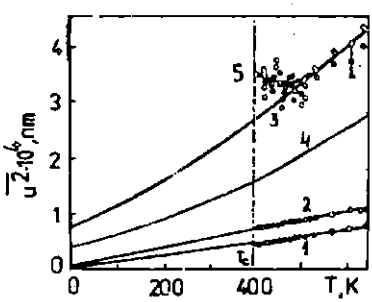

Fig.2. Mean-square displacements versus temperature in $BaTiO_3$. 1 - Ba, 2 - Ti, 3 - O, 4 - approximation $\langle u^2\rangle(T)$ for the O ion [8] by polinom (9), 5 - the deviations of the experimental curve $\langle u^2\rangle(T)$ from polinom (9) near T_c.

by means of statistic modelling. We get the following measurement accuracy values of $\langle u^2\rangle$ for the Ba, Ti, O ions 1; 1,5 and 5% at 1% accuracy for intensity.

For further use of experimental data $\langle u^2\rangle(T)$ (Fig.2) we have to fit [2] them by the polinom in terms of T and

simultaneously determine the absolute term - static component of MSD $\langle u^2_{st}\rangle$.

The experimental data of $\langle u^2\rangle(T)$ for the Ba and Ti ions in $BaTiO_3$ as in the case of the Cs and Pb ions in $PbCsCl_3$ [1], are well fitted by the curve, passing through the origin: T=0, $\langle u^2\rangle=0$ (Fig.2). Consequently, $\langle u^2_{st}\rangle$ is very small for the Ba and Ti ions. MSD could be well fitted by second order polinom with no absolute term

$$\langle u^2\rangle(T)=bT+cT^2. \tag{8}$$

Experimental data of $\langle u^2\rangle(T)$ for the oxygen ion (Fig.2) have an pronounced non-linear character and a considerable singular component $\langle u^2_s\rangle$. To get the growth $\Delta\gamma$ for anharmonic parameter we had to determine statistic component $\langle u^2_{st}\rangle$ for $\langle u^2\rangle$ and parameters α and γ. We used for that purpose experimental data of $\langle u^2\rangle(T)$ from [8] in temperature range from 400 up to 1100 K. These data are of a strongly nonlinear temperature dependence, however, by use of a third order polinom

$$\langle u^2\rangle(T) = a+bT+cT^2+dT^3 \tag{9}$$

the experimental data [8] have been fitted very well. We obtained the following values for polinom coefficients: $a = (0,425\pm0,005)\cdot10^{-4}$ nm^2, $b = (0,274\pm0,002)\cdot10^{-7}$ nm$^2\cdot$T^{-1}, $c = (0,300\pm0,005)\cdot10^{-9}$ nm$^2\cdot$T^{-2}, $d = (0,20\pm0,02)\cdot10^{-13}$ nm$^2\cdot$T^{-3}. By using these values we fit our experimental data $\langle u^2\rangle(T)$ for the oxygen by polinom (9) in the temperature range from T_C up to T_C+300 K. The following values were obtained $a = (0,8\pm0,1)\cdot10^{-4}$ nm^2 and $b = (0,35\pm0,03)\cdot10^{-6}$ nm$^2\cdot$T^{-1}.

The potential parameters were determined by means of comparison the polinom coefficients at corresponding terms of T in (7), (6) and (9)

$$a=k_bT/\alpha, \tag{10}$$

$$\gamma = \alpha^2(2\gamma_s x - \alpha c/k_b)/20k_b. \tag{11}$$

The obtained parameters are given in Table 1. According to Table 1, the tighest coupling in lattice has the Ba ion - the parameter of elastic coupling α is around 6-$7\cdot10^{-2}$ eV$\cdot$nm^2. Different authors had observed similar values for α, anharmonic parameter γ in all papers are positiv - the velocity of $\langle u^2\rangle(T)$ growth decreases with rising temperature.

Table 1

The OPP parameters for ions in $BaTiO_3$

	Ba		Ti			O		
Paper	α	γ	α	γ	$\Delta\gamma$	α	γ	$\Delta\gamma$
/8/	5.82	8.11	3.0	0.76	...	2,46	-2,7	
Present	7.14	...	4.7	...	0,32	...	...	-2,17
/4/	4.85	4.08	14.3	88.7	...	4.2	11.7	
/3/	6.68	6.63	2.17	3.9	...	1.23	0.95	
/5/	6.35	0.34	4.55	4.24	...	1.65^1	-2.49^1	
						6.24^2	18.65^2	

Values of α in 10^{-2} eV·nm^{-2}, γ and $\Delta\gamma$ in 10^{-4} eV·nm^{-4}, 1 and 2 parameters for the oxygen ion in directions x,y, and z correspondingly.

In the same time the parameter values α and γ for the Ti ion differs noticeably from different sources

Experimental data [8] for the oxygen ion testifies, that with rising temperature $\langle u^2\rangle(T)$ are growing faster. However, in [1,2] authors get values $\gamma > 0$, what contradicts to that. The same contradiction is true also for the titanium ion.

Near the phase transition the character of the Ti and O ions MSD temperature dependence changes. The MSD $\langle u^2\rangle(T)$ obtains an additional component in the temperature region from T_c+100 K down to T_c: $\langle u^2\rangle$ deviates up from the slopes (8) and (9). That deviation for the Ti and O ions reaches values $(0,3\pm0,1)\cdot10^{-5}$ nm^2 and $(0,8\pm0,2)\cdot10^{-3}$ nm^2 at T = 400 K, corresponding to values of anharmonicity parameter $\Delta\gamma$ = $(0,3\pm0,1)\cdot10^{-4}$ and $(-2,2\pm0,6)\cdot10^{-4}$ eV·nm^{-4}.

By use of parameters α, γ, $\Delta\gamma$ the OPP for the Ba, Ti and O ions were calculated (Fig.3). The OPP curves testifies, that the Ba and Ti ions are rigider bounded in the lattice. The O ion is less harder bounded in the lattice. The considerable value of anharmonicity parameter (α = $2,7\cdot10^4$ eV·nm^{-4}) results

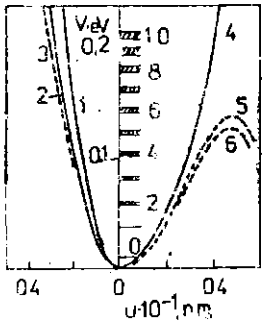

Fig.3. The changes of harmonic oxygen ion OPP and lowering (dashed area) energy levels by rising temperature from 400 K up to 1500 K in cubic $BaTiO_3$. 1 - Ba, 2 - Ti, 4 - O; 3 and 5 - changes in 2 and 4 when near PT increasing anharmonicity is taken into account, 6 - changes in 5 when temperature is rised to 1500 K

in formation a relative low potential barrier around the oxygen ion - only 0,14 eV high. When temperature increases from 400 up to 1500 K , the barrier high lowered by 0,01 eV (Fig.4). To estimate the importance of barrier lowering, we calculate the the O ion's distribution on energy levels in OPP. We used Bose-Einstein distribution. The energy levels are at following values [9]:

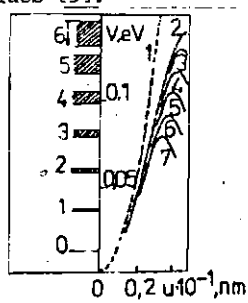

Fig.4. The influence of PT on oxygen ion OPP and energy levels in cubic $BaTiO_3$. Dashed area - the energy level decreasing when $T \to T_c^+$. 1 - OPP far from T_c, 2 - $(T-T_c)=100$ K, 3 - 80 K, 4 - 60 K, 5 - 40 K, 6 - 20 K, 7 - $(T=T_c)$.

$$E_n = \hbar\sqrt{\alpha}/m\,(n+1/2)+3\gamma\,(\hbar^2/m\alpha)\,(n^2+n+1/2)/2 \qquad (12)$$

and probability to find the O ion on corresponding level are

$$P_n = [\exp(-E_n/k_0T)-1]^{-1}/Z_n, \qquad (13)$$

where

$$Z_n = \sum_n [\exp(-E_n/k_0T)-1]^{-1}$$

(chemical potential for phonons is zero). The calculated values E_n and P_n are collected in Table 2. The corrected

Table 2

Energy levels and corresponding probabilities for the O ion OPP in $BaTiO_3$

n	400 K		400 K with PT accounted		1500 K	
	E_n, eV	P_n	E_n, eV	P_n	E_n, eV	P_n
0	0,0124	0,709	0,0122	0,6837	0,0119	0,485
1	0,0368	0,1610	0,0359	0,1598	0,0355	0,179
2	0,0604	0,0646	0,0581	0,0667	0,0581	0,083
3	0,0831	0,0303	0,0788	0,0332	0,0797	0,055
4	0,1050	0,0154	0,0979	0,0182	0,1005	0,040
5	0,1260	0,0081	0,1155	0,0107	0,1204	0,030
6	0,1461	0,0045	0,1325	0,0066	0,1393	0,024
7	0,1654	0,0025	0,1460	0,0043	0,1573	0,020
8	0,1838	0,0015	0,1589	0,0029	0,1744	0,017
9	0,2014	0,0009	0,1703	0,0021	0,1906	0,014
10	0,2184	0,0006	0,1802	0,0016	0,2059	0,012

probability of the oxygen ions with energy higher than the potential barrier (at n>5):

$$P_b = \sum_{n} P_n . \qquad (14)$$

The detecting probability of the O ions with energy higher than level n=15 is small. Value of P_b is growing fast with rising temperature (Table 2). For example - at T=400 K P_b=0,11. That means, that barrier is relatively high. At temperature 1500 K P_b reaches value 0,132 and there is some possibility to find the O ion shifted from symmetrical position. When $T \to T_c^+$ the increase of anharmonic parameters ($\gamma = \Delta$) causes considerable decrease of potential barrier high around the O ion and small lowering of energy level (Fig.4). The probability to detect the O ions shifted from symmetrical positions growth fast when $T \to T_c^+$ and reaches P_b=0,084 at T_c. There is an analogical situation as at the high temperatures and near PT - the

probability to find the O ion shifted from the symmetric positions of cubic lattice grows - the disordering of oxygen sublattice can occur.

The probability to detect the O ions shifted from symmetrical position by some distance can be calculated, using probability density function (PDF). The PDF at T>0 is equal [2]:

$$P(u) = \exp\left[-N(u)/k_0T\right] \Big/ \left\{ \int_{\infty}^{\infty} \exp\left[-V(u)/(k_0T)\right] du \right\} \quad (15)$$

In Fig.5 probability to find the O ion in range 0,001 nm is

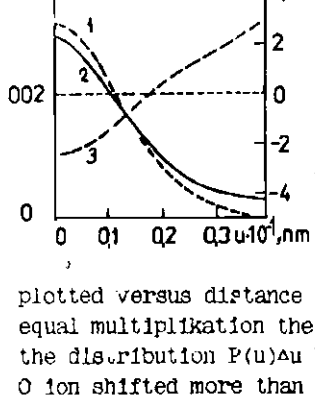

Fig.5. The oxygen ion detecting probability P(u)Δu in region Δu = 0,001 nm in $BaTiO_3$ shifted at distance u. 1 - for anharmonic potential, 2 - change P(u)Δu when anharmonicity near PT is included, 3 - changes in (P(u)Δu), when anharmonicity near T_c is included.

plotted versus distance from lattice site (the probability is equal multiplikation the PDF by range 0,001 nm). Near the PT the distribution P(u)Δu broadened. The probability to find the O ion shifted more than 0,02 nm from lattice point grows (Fig.5,c.3). Similar changes of PDF was observed in $PbCsCl_3$ [10] at $T \to T_c^+$ from neutron data (ΔP changes sign at r=0,035 nm and has maximum at r=0,07 nm).

Discussion

The following approximations have been used in the paper. The OPP model are based on assumption that each atom exists in a seperate potential well, entirely unaffected by the motions of neighbours. In the vicinity of a structural PT it is to be expected that the atomic motions will be characterized by

interparticle correlations. However, we can still work within the framework of the OPP formalism, obtaining atomic OPP's at each individual temperature, recognizing, that the Debye-Waller is an exact one-particle property of the system. The temperature dependence of OPP's may then be related to the cooperative effects in the crystal.

It was assumed the O ion occupy the site with isotropic symmetry. In reality the O ion occupy lattice site with 4/mmm symmetry and corresponding OPP is anisotropic. Therefore calculated anharmonic parameter γ in (1) contains in some combination also the anisotropic parameters γ_i.

The essential feature of determined OPP parameters are following. Far from PT OPP is supposed to be only quasiharmonic dependent on temperature as in papers [3,4,5]. The magnitude of $\langle u^2\rangle(T)$ deviations from stright line $\langle u^2\rangle(T)=k_bT/\alpha$ at high temperatures allows us to determine anharmonic parameter γ. The deviation $\langle u^2\rangle(T)$ up from expexted curve (3) near PT (as a result of appearance $\langle u_s^2\rangle(T) \neq 0$) allows us to determine the growth of anharmonicity in addition to that determined from curves $\langle u^2\rangle(T)$ at high temperatures far from T_c.

Summary

In the frame of mentioned approximations it is shown that the O ion has the softest OPP in $BaTiO_3$. That conclusion is consistent with the theoretical [4] and the previous experimental work [5]. We had shown, that the oxygen ion OPP softened significant when $T \rightarrow T_c^+$. The analogy between ferroelectric phase transition (T_c=400 K) and melting (T=1500 K) have been shown: in both cases the detection probability of the oxygen ion at energies higher than potential barrier reaches value 0,1. Before melting it was caused by growing occupancy higher energy levels by the oxygen ions (the OPP's barrier lowers very little). Near the PT the energy level occupancy changes very little, but the barrier high lowered significant from 0.14 to 0,08 eV from temperature $T=T_c+100$ K to T_c. That phenomenon have been observed only for the oxygen

ion, which thermal vibrations is most anharmonic. Therefore we can conclude, that shift some number of the O ions from high symmetrical positions is the first step in both melting and ferroelectric phase transition.

REFERENCES

1. Mair S.L. // Acta Crystallogr.- 1982.- Vol.A30, N 6. P.790- 796.

2. Willis B.T., Pryor A.W. Thermal vibrations in crystallography. - Cambridge:Univ. press, 1975. - 279 p.

3. Balashov S.M., Venevtsev Yu.N., Fedyanin V.K. // Reports of the Joined Institute of Nuclear Research.- Dubna, 1985.- P.17-85-515-16 (in Russian).

4. Turik A.B., Hasabov A.G. // Fiz.Tverd.Tela.- 1985.- Vol.27, N 8.- P.2510-2513 (in Russian).

5. Tanaka N., Shiozaki Y., Sawaguchi E.// J.Phys.Soc. Jap. - 1979. - Vol.47, N 5. - P. 1588-1594.

6. Zvirgzds J.A. Actual Physical and Chemical Problems of Ferroelectrics.- Riga, 1987.- P.18-44 (in Russian).

7. Kapostins P.P., Zitars I.R., Zvirgzds J.A.// Ferroelectrics. - 1988. - Vol.79. - P. 185-188.

8. Ivanov S.A., Michalchenko V.P., Venevtsev Yu.N. // Dokl.Akad.Nauk SSSR.- 1979.- Vol.248, N 5.- P.865-867.

9. Reiselend J.A. The Physics of Phonons.- M., 1975.- 365 p. (in Russian).

10. Hutton J., Nelmes R.J. // J.Phys. C.: Solid State Phys. - 1981. - Vol.14, N 12. - P.1713-1236.

Received February 6,1991.

UDC 537.226.33

REEXAMINATION OF PHASE TRANSITIONS IN FERROELECTRIC SOLID SOLUTION $Pb_xSr_{1-x}TiO_3$

I.Podlina, A.Cajevskis, G.Liberts
Institute of Solid State Physics, University of Latvia
8, Kengaraga St., 226063 Riga, Latvia

ABSTRACT. To clarify the polar properties and phase diagram of lead-strontium titanate solid solution, dielectric, elastic and non-linear optical properties has been tested and discussed.

INTRODUCTION

There has been continued interest concerning the role of structural disorder in the ferroelectric (FE) phase transition (PT). Behavior of the mixed FE - paraelectric and FE - antiferroelectric systems like $K_{1-x}Li_xTaO_3$, PLZT and others /1-3/ have led to conflicting interpretations which range from a simple increase of the Curie point T_C with concentration x, to their being no phase transitions at all, but merely a " dipole glass " at low temperatures /4/. There has been a special question regarding the polar properties of ferroelectric mixed systems, where some additional disordering takes place due to the well defined structural PT of one of the components e.g. strontium titanate.

Earlier studies of the $SrTiO_3$ based FE solid solutions /5-8/ have revealed some anomalies of physical properties in dilute (small concentration of FE component) solutions. Despite the fairly general character of the Pb induced ferroelectric PT in $Pb_xSr_{1-x}TiO_3$ many questions have arisen about the interval of concentration where both the ferroelectric and structural PT occur.

We have investigated dielectrical, elastic and optical properties of lead - strontium titanate ceramics in a wide region of temperatures

SAMPLE PREPARATION AND EXPERIMENTAL METHODS

Homogeneous ceramic samples of $(Pb,Sr)TiO_3$ were synthesized by conventional two-stage ceramic technology at the Ferroelectric Material Synthesis Division of the Institute of Solid State Physics (University of Latvia). Special procedures to control parameters of PbO ambient during annealing and anatase/rutile (TiO_2) ratio of raw TiO_2 have been applied. Polished ceramic plates with planar Ag electrodes were used for the dielectric constant measurements. Bar shaped samples were used for the sound velocity (longitudinal) measurements by mechanical resonance method. Polished surfaces of the ceramics were utilized for the optical investigations. Dielectrical measurements (dielectric constant) were made over the frequency range 10^2 - 10^7Hz with a SWM-1 and SWM-2 bridges in a wide range of temperature and external bias d.c field. Dielectric hysteresis measurements were performed in quasistatic regime (with bipolar symmetric triangular high-voltage (period 100 s)generator). Conventional longitudinal piezo-resonance method was used to evaluate the sound velocity in the ceramic bars. Initializing bias field up to 100 V/cm was applied along the bar.

Additional noncontact spontaneous polarization vs temperature measurements were made by optical second harmonic generation (SHG) / 9 /in a reflection mode. Our experimental equipment for SHG nondestructive probe has been based on application of a CW pumped mode-locked and Q-switched Nd laser supplied with a gated photon counting system. In our case, when highly-absorbing ceramic samples have been tested, such an approach allows the correct determination of the averaged spontaneous polarization and its dependence on temperature. From the other point of view, SHG technique does not need electrodes to determine polarization and provides a possible method in the case of conductive samples.

RESULTS AND DISCUSSION

Dielectric constant versus temperature curves for $(Pb,Sr)TiO_3$ ceramic samples are compared in Fig.1. Very small amplitudes of measuring ac electric field (0,1 - 2 V/cm) have been used to avoid suppression of the second peak of dielectric constant curve. All the dielectric constant measurements were made at cooling. On the other hand, the ac field frequency was limited to 500 kHz , that means "unclamped" conditions of the sample. Dielectric data presented in Fig.1 indicate, that for dilute solid solutions of $Pb_xSr_{1-x}TiO_3$ ($x<15$ %) two subsequent dielectric constant peaks occurs,indicating the presence of two phase transitions. First observation of such a phenomena in lead-strontium titanate has been reported earlier by Martin et al. / 6 /. Maximum magnitude of dielectric nonlinearity parameter $N = 1/\varepsilon\ \partial\varepsilon / \partial E_{static}$ obtained from the measurements of the dc biased dielectric susceptibility has been observed for x = 6-8 % Pb. It should be stressed that these values of N are very high (N ≈ 1,5 cm/kV) which compares to nonlinearity of pure $SrTiO_3$ /10/ single crystals at liquid He temperatures. Similar properties have been observed for solid solutions of $Ba(Ti_{1-y}Zr_y)O_3$ and $Ba(Ti_{1-y}Sn_y)O_3$ / 11 /,where for y = 0,10-0,15 the same two - ε peaks and extreme nonlinearity takes place. Dielectric constant versus temperature curves fragments for various frequencie and different bias field intensities are shown in Fig.2 and Fig.3 . These fragments clearly demonstrates two pecualiarities- *first* - suppression of the low temperature ε peak by an external field and *second* - frequency dispersion of the dielectric constant maximum peaks. It should be pointed out, that a similar suppression under high pressure for the "high temperature" ε peak has been observed previously / 6 /. Such a different behaviour of two ε peaks is more pronounced for $Pb_{0,07}Sr_{0,93}TiO_3$.

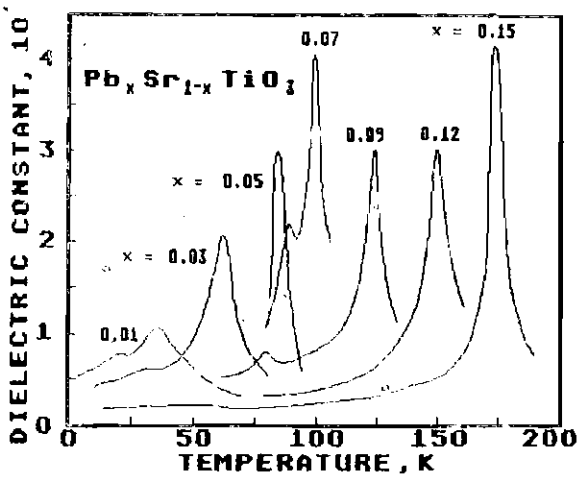

Fig.1. Temperature dependences of the dielectric constant at f=1kHz

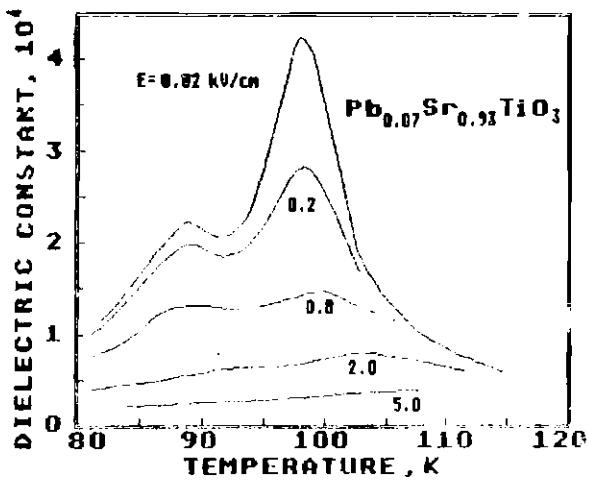

Fig 2. Temperature dependence of the dielectric constant on cooling at various external dc bias field strength for x = 0.07

A remarkable feature of the lead-strontium titanate solid solutions is the strong dependence of sound velocity on temperature, especially for $x \approx 0.07$ (see Fig. 4). For these samples a typical two step decrease of the sound velocity takes place, which indicates the presence of two subsequent structural PT. Such a drastic decrease of the sound velocity values has not been observed for a similar solid solutions of $(Ba,Sr)TiO_3$ /12/, where the two subsequent FE - PT takes place.

SHG measurements, provided for the whole lead strontium titanate system, clearly show the presence of FE PT when increasing the x values. A characteristic PT parameter $dT_C / dx \approx 7$ deg /mol.% has been obtained from the SHG vs temperature curves. An inflection point of the SHG temperature dependence serves for determination of the FE to paraelectric phase transition.

Such an approach seems to be valid for the PT diagram construction, while the use of the SHG data for the "low" temperature PT is under discussion and further investigation. The typical second harmonic temperature dependences are shown in Figs. 5 and 6. These temperature curves, dielectric measurements and acoustic studies give information about the phase diagram of the system, shown in Fig.7.

It is necessary to point out, that for the system under investigation two significant tendencies take place - *first*, the low temperature structural PT temperature (for pure $SrTiO_3 \approx 106$ K respectively) is going down, and *second* the ferroelectric PT T-line ("point") lowered as far as the "crossover" of these two PT lines occurs. The last phenomena seems to be in contradiction with the Gibbs phase equilibrium rule. To solve this disagreement with a thermodynamical principles a region of undetermined symmetry (or mixed phase) has been proposed. It is interesting to point out the early observations of the double hysteresis loops in lead-strontium titanate system /6/, which is similar to the situation taking place in PLZT and related materials. Obviously, the additional structure and dielectric polarization dynamics measurements are needed to clarify the nature of ferroelectricity in the lead strontium titanate system.

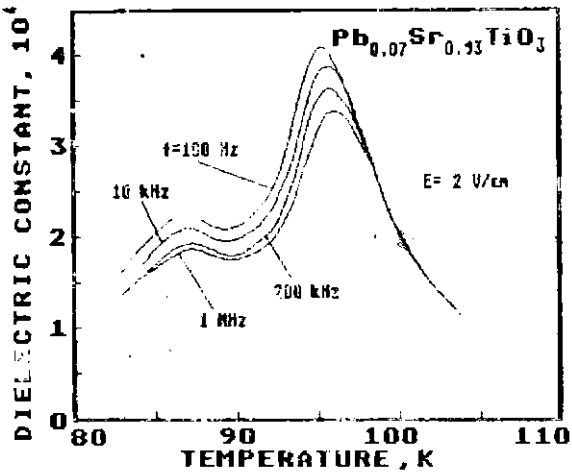

Fig.3. Temperature dependence of the dielectric constant on cooling at various frequecies for the samples with x = 0.07.

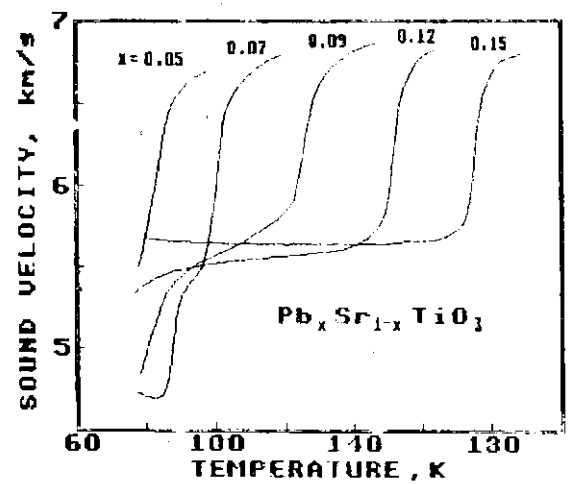

Fig.4. Temperature dependence of the sound velocity for $Pb_xSr_{1-x}TiO_3$

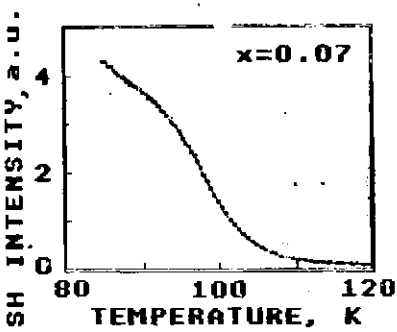

Fig. 5. Temperature dependence of SH intensity of the ceramic $Pb_{0,07}Sr_{0,93}TiO_3$ sample.

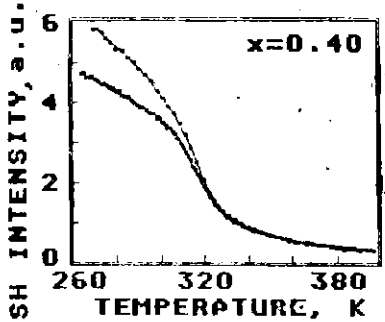

Fig. 6. Temperature dependence of SH intensity of the ceramic $Pb_{0,40}Sr_{0,60}TiO_3$ sample. Upper curve - heating, lower - cooling.

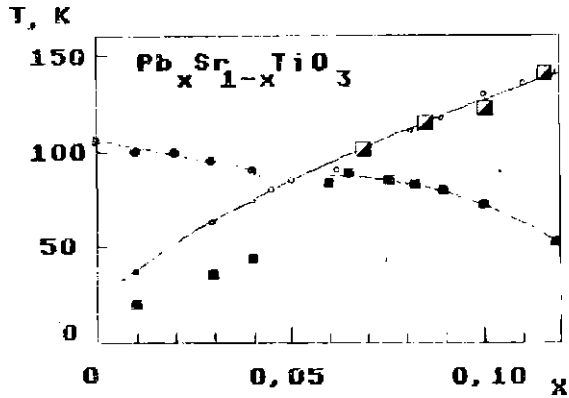

Fig. 7. Phase diagram of the lead strontium titanate dilute solid solution. Collected experimental points corresponds to : open circles - dielectric constant high temperature maxima, fullfilled quadrates - low temperature dielectric constant maxima, fulifilled circles - sound velocity data and half - filled quadrats - SHG data.

CONCLUSIONS

Detailed analysis of polar properties of the $Pb_x Sr_{1-x}TiO_3$ system reveals two subsequent FE phase transitions for small lead titanate concentration . Lead strontium titanate seems to be useful material for various applications due to high dielectric and optical nonlinearity and possibility of the fine "temperature tuning" of such properties.

ACKNOWLEDGMENTS

The authors are indebted to A.Kalvane, M.Kalnberga and A.Rubulis for kindly supplying good quality samples of lead strontium titanate ceramics.

References

1. Van der Klink J.J.,et al.// Phys.Rev.B,- 1983,vol.27,No1.-P.89-101.
2. Ischuk V.M.,et al.// Sov.Solid State Phys.-1986,vol.28,No5,P.1502-1504.
3. Courtens E.//Helvetica Physica Acta,1983,vol.56,P.705-720.
4. Samara G.A.// J.Phys.Chem.-1990.Vol.94,P.1127-1134.
5. Rubulis A.N.,Fritzberg W.// Izv.Akad.Nauk SSSR,Ser.Phys.-1975, vol.39, P.1332-1335 (in Russian).
6. Martin G.,Hegenbarth E.,Fritzberg W.,Romanovskis T. // Sov.Solid State Phys.-1976,vol.18,No1, P.248-250.(in Russian).
7. Klingner E., Hegenbarth E. //Ferroelektrizität'73, Halle (Saale). 1978/39(05), P.99-108.
8. Kersten O.// Ferroelektrizität'85,Halle (Saale) 1986/5 (018),P.62-66.
9. Zauls V.A., Kundzinsh M., // Methods and Instrumentation for the Physical Research,(edited by Ya.Yansons) - University of Latvia,Riga, 1989,P.117-130 (in Russian).
10. Belokopitov G.V.et al.,//Sov.Solid State Phys.- 1981,vol.23,No1,P.141-151.
11. Bethe K. // Philips Research Reports Supplements,1970, No2.
12. Perro I.T.// Physical Properties of ferroelectric Materials.- Riga, University of Latvia,1981, P.90-115 (in Russian).

UDC 538.95.

COEXISTENCE AND EVOLUTION OF THE POLAR PHASE IN $NaNbO_3$ SOLID SOLUTIONS

M.N.Palatnikov, K.J.Borman,* V.Samulyonis,**
Yu.A.Serebryakov, V.T.Kalinnikov
Institute of Chemistry, Kola Scientific Center
Academy of Sciences, Apatity, USSR
*Institute of Solid State Physics, University of Latvia
**Department of Physics, Vilnius University

Dielectric, thermal and acoustic studies of synthesized ferroelectric $Li_xNa_{1-x}Ta_yNb_{1-y}O_3$ solid solution ceramic samples are reported. The obtained results have been used to fix the temperature and character of phase transitions and make presumptions on stable and metastable polar phase coexistence. A slow relaxation of the polar phases has been observed at low temperatures, the ratio of phase concentration at a given temperature being dependent on Ta content.

Introduction

Amongst the perovskite oxides sodium niobate is distinguished by its complex and multiple properties. In pure $NaNbO_3$ at the room temperature T_R there may simultaneously exist apart from the electric field-induced phases two orthorombic phases P and Q [1]. Phase P is an antiferroelectric (AFE) one while the Q phase is metastable its structure being identical to that of the "forced" ferroelectric phase.

To study the evolution of these phases and the change of phase transition (PT) temperature caused by isovalent substitution in A and B sites (of an ABO_3 coumpound) we have used $Li_xNa_{1-x}Ta_yNb_{1-y}O_3$ (LNTN) solid solutions (SS) in the concentration interval of $0 \le x \le 0.16$ and $0 \le y \le 1$. Even a small amount (about 0.02 mole parts) of lithium induces transition of $NaNbO_3$ to ferroelectric (FE) state at T_R [2] and the phase picture of the SS is made complicated by the presence of morphotropic regions [3,4].

Presently hereafter are reported experimental data on

thermal behaviour of dielectric permeability (ε) and thermal expansion (α), conductivity (σ) and resistivity (ρ), acoustic properties and the low-frequency spectra of ε^* in the polar phase of polycrystalline LNTN SS.

The method

The SS samples were prepared by conventional ceramics technology. Density of the material was no less than 95% of that calculated for a structure of close packed ions. The real and imaginary parts of dielectric permeability (ε' and ε'') were determined from the phase shift of current through the sample in circuit series, the measurements being made by automated phase detection in the frequency range from 10 Hz to 1 MHz. AC conductivity was measured at 1 kHz by bridge method while the dc conductivity - by terraohmmeter "E6-13A". The thermal expansion was measured by a mechanic quartz

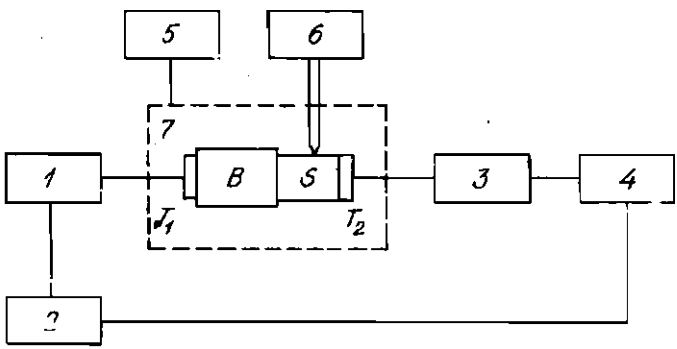

Fig. 1. Shematic diagram of the apparatus of acoustic measurements:

1 - pulse generator, 2 - synchronizer, 3 - wide-band amplifier, 4 - oscilloscope, 5 - thermal stabilizer, 6 - microvoltmeter, 7 - sample chamber, T - electric-acoustic transformer, B - sound delay line, S - sample, T - accustic-electric transformer.

dilatometer, an optical attachment to which provided the accuracy within $\pm 10^{-5}$ cm [5]. Acoustic measurements were made by the pulse method two transmitting wave transformers at 10 MHz frequency being used (Fig.1).

Results and discussion

The linear thermal expansion coefficient (LTEC) α was obtained as function of temperature. In $NaNbO_3$ a sharp minimum of the α (T) curve is observed at -3 °C upon heating (Fig.2). According to the well-known phase sequence it corresponds to transition from the FE N to the AFE P phase. Reverse transition is observed at -60 °C at cooling. The temperature of the P→N transition is dependent on production technology and ceramics history. In our case it has revealed itself as a change of the α (T) minimum from $800 \cdot 10^{-6}$ K^{-1} to $100 \cdot 10^{-6}$ K^{-1}, and a shift of the T_{PT} as low as -190 °C. Gradual substitution of Na by Li decreases the α (T) anomaly, the N→P transition being moved to higher temperature and its diffuseness considerably enhanced.

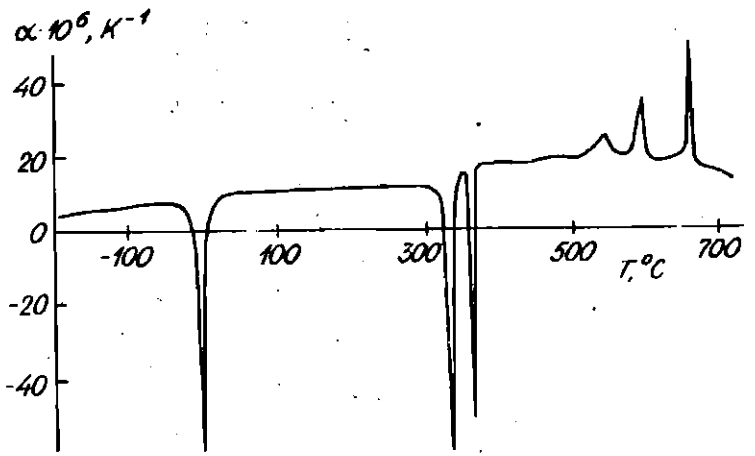

Fig. 2. Thermal behaviour of the LTEC of $NaNbO_3$.

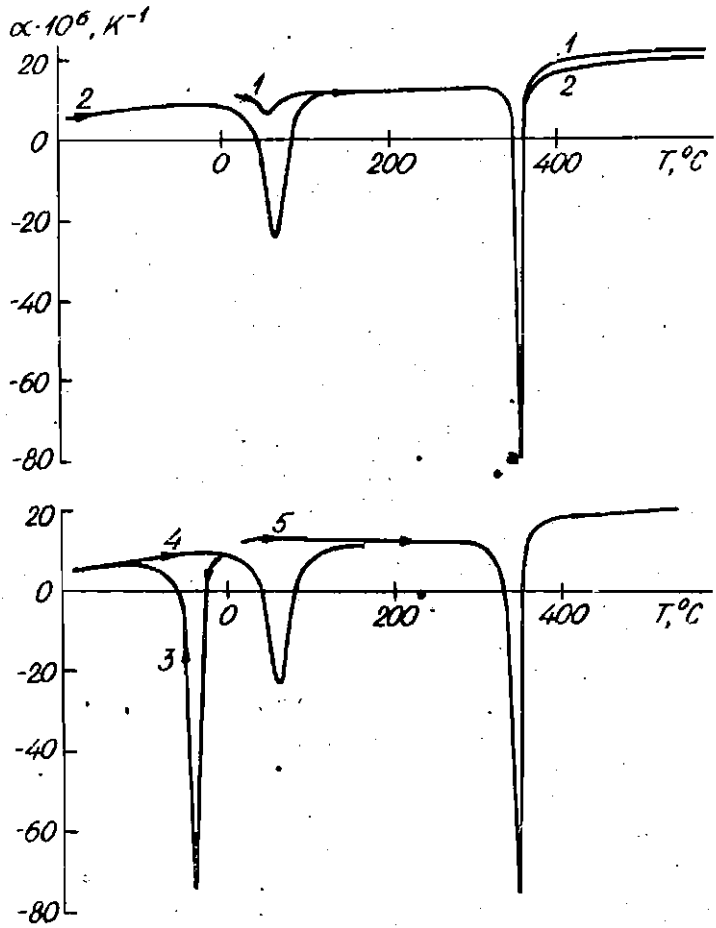

Fig. 3. Thermal behaviour of LTEC 1 SS $Li_{0,08}Na_{0,92}NbO_3$.

1 - the first heating beyond T_R; 2 - heating from 180 °C; 3 - cooling below T_R; 4 - subsequent heating from -190 °C; 5 - repeated heating beyond T_R of a specimen after being cooled down to 20 °C.

Since addition of Li induces transition of $NaNbO_3$ to the FE

state at T_R, it is a transition between FE phases.

A considerable hysteresis of the peaks (ΔT = 102 °C) is observed at the N→P PT in $Na_{0,92}Li_{0,08}NbO_3$. The N→P transition minimum on the α (T) curve at heating from T_R was also observed in a sample never having been cooled below 0 °C. Its value is about 5 times less compared to that observed in the same sample when heated after being cooled down to -180 °C (Fig.3, curves 1,2). At cooling below 0 °C a sharp minimum (curve 3) was observed while at subsequent heating (curve 4) the anomaly of α (T) observed near 64 °C was repeated exactly curve 2. A following fifth heating beyond the T_R did not reveal any anomalies up to nearly 360 °C. The FE N phase may be supposed to exist in LNTN at 20 °C not only as a consequence of N→P transition hysteresis, but also due to relaxation at T_R, the thermodynamic equilibrium between the phases being essentially hindered in LNTN compounds with a high tantalum content. E.g., in SS with y>0,5 complete relaxation of the low-temperature phases takes hundreds of hours at T_R.

Thermal behaviour of acoustic properties (velocity V and absorption a' of sound) indicate that the low-temperature phases lose stability near 30-50 °C and effects characteristic to the first order PT are observed in the first cycle of heating (Fig.4). The measurements made after heating the samples beyound 50 °C reveal quite clearly the low-temperature anomalies (Fig.5). The latter disappear in SS being held for some days at T_R and are restored only upon heating beyond 50 °C. A similar behaviour of ε(T) has been observed in SS with a high content of tantalum.

Anomalies of ε'(T), ε''(T), σ(T), ρ(T) are observed in LNTN SS in the interval -40-0 °C. The anomaly of ρ (as the effect of positive thermal coefficient of resistivity - PTCR) may reach 5-6 orders (Fig.6) and decreases as the frequency grows. The effect of PTCR seems to be caused by the increase of conductivity of the interlayers and the change of potential barriers on grain boundaries [6]. As the field is increased the PTCR appears upon heating at a lower temperature, the anomaly of ρ remaining almost uncharged (Fig.6). At cooling under a high field intensity (~10^3 V·cm^{-1}) the anomalies of ε

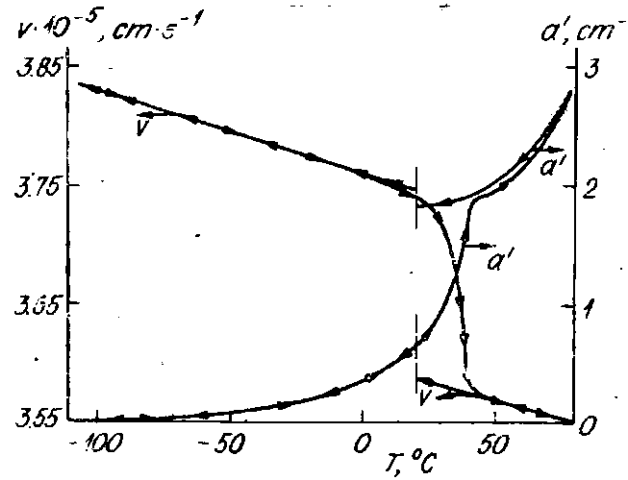

Fig. 4. Thermal behaviour of sound velocity and attenuation in SS $Li_{0,12}Na_{0,88}Ta_{0,7}Nb_{0,3}O_3$ (20→ -120→20→80→20 °C).

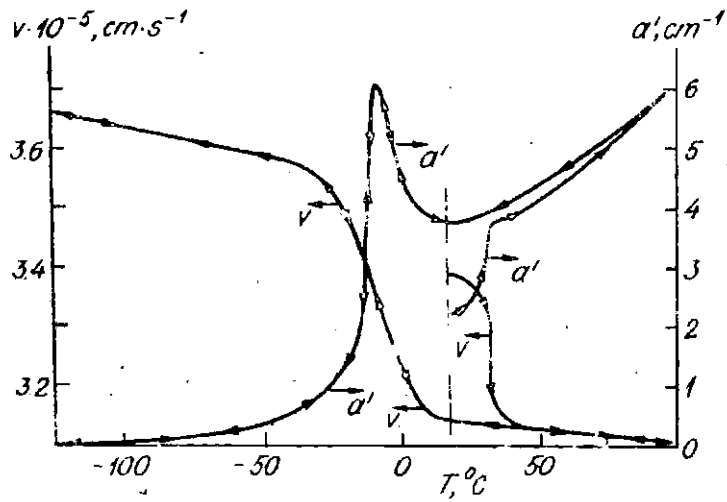

Fig. 5. Thermal behaviour of sound velocity and attenuation in SS $Li_{0,03}Na_{0,97}Ta_{0,5}Nb_{0,5}O_3$ (20→80→20→ -120→20 °C).

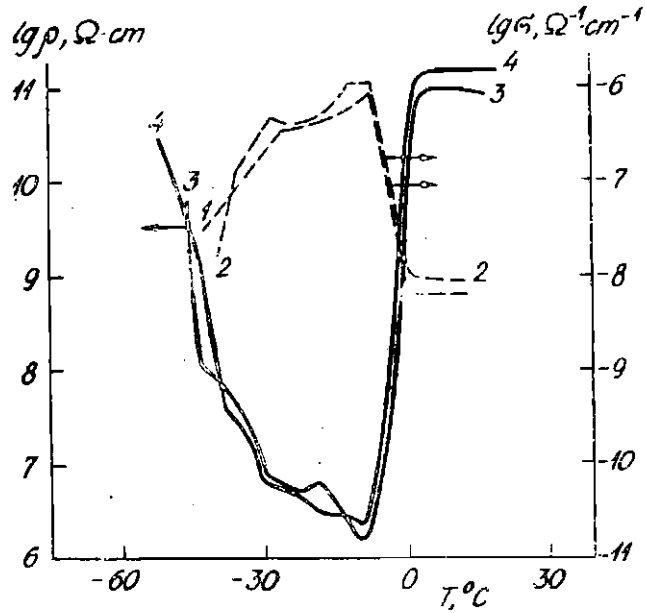

F i g. 6. Thermal behaviour of ac conductivity (1 and 2 at $f = 10^3$ Hz, $E_{\sim 1} = 45$ V·cm^{-1}, $E_{\sim 2} = 450$ V·cm^{-1} and dc resistivity (3 and 4: $E_1 = 10$ V·cm^{-1}, $E_2 = 10^3$ V·cm^{-1}) in S $Li_{0.03}Na_{0.97}Ta_{0.05}Nb_{0.95}O_3$

practically do not show up since the domain reorientation induced by a strong measuring field lowers potential barriers [7].

The anomalous hysteresis of the extremities of $\sigma(T)$ curve, the interval between structure rearrangement (which is related to σ (T) minima) and the electrophysical properties (e.g., PTCR effect, $\varepsilon'(T)$ and $\varepsilon''(T)$ anomalies), seems to be caused by simultaneous existence of several polar phases (N, and Q) in LNTN SS over a wide interval of temperature, the PT occuring in the process of measurement being dependent on the state of crystal lattice subject to external action as well as on the sample history. An essential part of evolution of the metastable phase Q in anomalous behaviour of σ is suggested to

the fact that its anomalous change is decreased by 4-5 orders after a long (about a year) aging of samples and is restored by heating beyond T_c (the Q phase in $NaNbO_3$ is stabilized near T_c [1]).

Dispersion of experimentally observed minimum values of $\sigma(T)$ is mainly caused by coexistence of phases at T_c and microvolumes of phases N, P and Q being present in a sample. Only one of the phases (P or N), i.e., only a part of the sample, is involved in a particular PT. In the processes related to anomalies of ρ and σ (in the region of PTCR effect) most probably clusters of at least two FE phases are involved. Thus, as the field applied to measure conductivity is increased (from 45 to 450 $V \cdot cm^{-1}$ at 10^3 Hz) a second maximum appears on the conductivity vs. temperature curve (Fig. 6, curve 1,2). The same is observed with $\varepsilon'(T)$. This seems to be related to different non-linearity of the coexisting polar phases. Two distinguished dispersion regions appear in dielectric spectra approaching the PTCR effect (Fig.7). The frequencies of dielectric absorption maxima differ by two-three orders. Both of the dispersion regions are closely similar to the Coul-Coul type (Fig. 8) and seem to be due to polarization processes concerned with domain and interphase boundaries. However, to explain the very mechanism of these phenomena requires a further investigation.

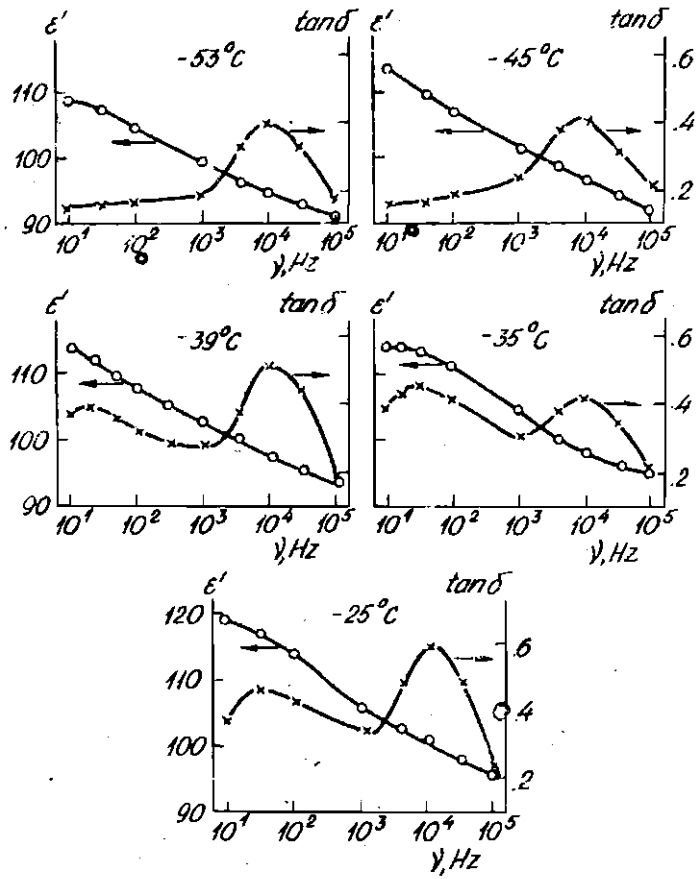

F i g. 7. Dispersion of the dielectric permeability ε' and tan δ in SS $Li_{0.03}Na_{0.97}Ta_{0.03}Nb_{0.95}O_3$.

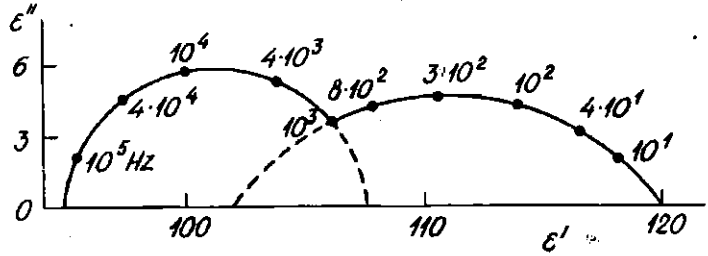

Fig. 8. Coul-Coul diagram in SS $Li_{0.03}Na_{0.97}Ta_{0.03}Nb_{0.95}O_3$ at -25°C.

Conclusion

Studies of low-frequency dielectric spectra, thermal behaviour of conductivity, acoustic properties, the coefficient of linear thermal expansion have suggest coexistence of several polar phases in a wide interval of temperature (-190–80 °C) in LNTN SS, at least one of the phases being metastable. The state of a sample within the interval is essentially determined by its thermal history. A considerable relaxation of the low-temperature phases is found to occur at T_m, the rate of change of the phase ratio increasing with the increase of concentration of tantalum.

REFERENCES

1. Lefkowitz I., Lukoszewich K., Megaw H.D. // Acta Crystallogr.- 1966.- Vol.20, N 5.- P.1670.

2. Sadel A., Von der Mühl R., Ravez J. // Mater. Res. Bull.- 1983.- Vol.18, N 1.- P.45.

3. Reznichenko L.A., Shilkina L.A. // Izv. Akad Nauk SSSR, Ser. Fiz. - 1975.- Vol.38, N 5.- P.1118 (in Russian).

4. Palatnikov M.N., Serebryakov Yu. A. // Abstr.of the III USSR Conf.on Physics and Chemistry of Technology of Perroelectrics and Related Materials.- M., 1988.- P.28 (in Russian).

5. Fritsberg V.J., Borman K.J. // The Phase Transitions in Ferroelectrics with the Perovskite Structure.- Riga, 1974.- P.99-149 (in Russian).

6. Sheftel L.T. Thermoresistors.- M., 1973.- P.251 (in Russian).

7. Rayevsky I.P., Bondarenko E. J. , Pavlov A.M., et al. // Zh.Tekh. Fiz. - 1985.- Vol.55, N 3.- P.596 (in Russian).

Received December 7 , 1990

UDC 537.226.33:537.

MICROMECHANISM OF ELECTRIC FIELD INDUCED PHASE TRANSITION IN PLZT CERAMICS

M.Knite, A.Kapenieks, and A.Sternberg
Institute of Solid State Physics, University of Latvia
8,Kengaraga St., 226063 Riga, Latvia

An experimental study of electric field controlled birefringence and light scattering at wavelength 0.425-5.56 μm in hot-pressed PLZT 8.5/65/35 is reported. The diameter of electric field induced polar microregions vs field intensity is determined.

Dielectric polarization

In coarse grained (4-6 μm) hot-pressed optically transparent PLZT 8.5/65/35 dielectric polarization P vs temperature decreases rapidly at 17 °C. At the temperature of 21 °C a double dielectric hysteresis loop P(E), polarization vs electric field E is observed (Fig.1).

At the field intensity $E > E_{k_1} = 6.8$ kV/cm a ferroelectric phase is induced, a following decrease of E reverts to the non-ferroelectric state at $E < E_{k_2} = 1.6$ kV/cm. It corresponds to the quasiparaelectric-ferroelectric phase transition [1].

Birefringence

In order to eliminate the light scattering and depolarization the measurements of birefringence $\Delta n(E)$ were carried out using a CO cw laser ($\lambda = 5.56$ μm). We observed the quadratic electrooptic effect $\Delta n \sim E^2$ only at temperature higher than 60 °C (Fig.2). At lower temperature the $\Delta n(E)$ dependance changes. At room temperature we observed $\Delta n \sim E^4$) at $4 < E <$ kV/cm. We suppose that it is due to the increase of the amount of field-induced ferroelectric phase according to

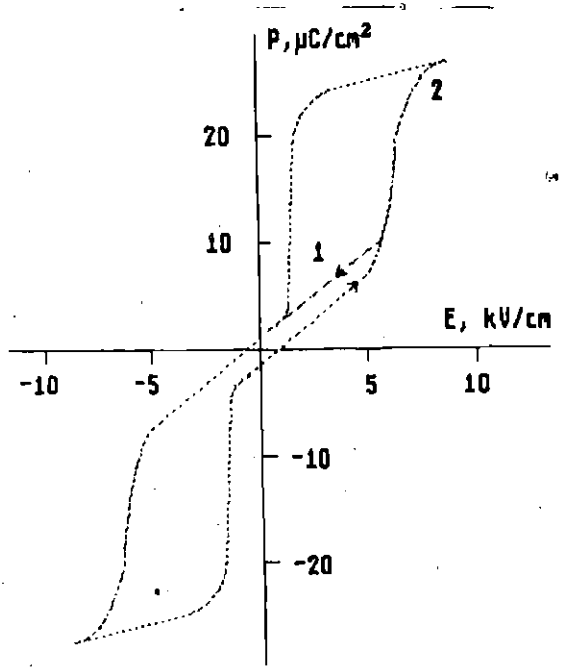

F i g. 1. PLZT 8.5/65/35 polarization P vs electric field hysteresis loop. T = 21 °C. 1 - E_{max}<E_{x1};2-E_{max}>E_{x1}.

$$\Delta n = v \cdot \Delta n_{sp} + 0.5\, n^3 rvE + 0.5\, n^3 R(1-v)E^2, \qquad (1)$$

where v - volume concentration of polar phase, Δn_{sp} - spontaneous birefringence, r and R - electrooptic coefficients, n - refractive index. Δn_{sp} is calculated from the value of spontaneous polarization P_{sp}, determined from P(E) hysteresis loop. The quadratic dependence $\Delta n_{sp} = -0.5\, n^3 M P_{sp}^2$ is typical for all the temperatures investigated. In (1) the first additive characterizes the spontaneous polarized volume vs E. The second additive characterizes linear electrooptic effect inside the small single domain microregions. The third additive

corresponds to the quadratic electrooptic effect, it is typical in paraelectric phase. We calculated the v(E) using Δn(E) curve (Fig.2) and the experimentally determined values for PLZT

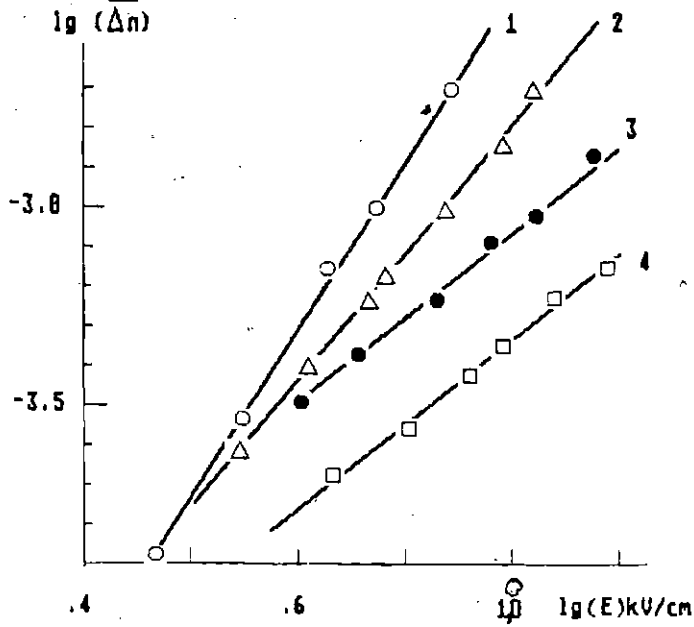

F i g. 2. Birefringence Δn vs electric field E at different temperature. λ = 5,56 μm. 1 - 25 °C, 2 - 40 °C, 3 - 60 °C, 4 - 80 °C.

8.5/65/35: r= $3.75 \cdot 10^{-10}$ m/V at T = 21 °C, E = 10 kV/cm; R = $3 \cdot 10^{-16}$ m^2/V^2 at T=80 °C, E = 8 kV/cm; M = $1.38 \cdot 10^{-2}$ m^4/C^2 at 25 °C; n = 2.28. All the parameters are determined at laser wavelength λ = 5.56 μm. The calculated curve v(E) is shown in Fig. 3, curve 3.

Scattering

The values of the extinction coefficient β determined by scattering were measured vs the light wavelength λ at different constant values of $E < E_{ks}$ (Fig.4). The experimental value of β was calculated from:

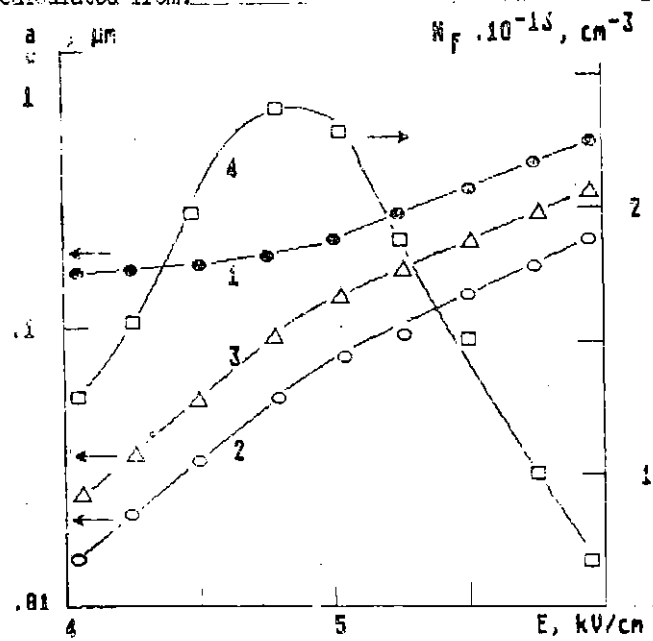

Fig.3. Dependence on the electric field E of: 1 - polarized microregion diameter a; 2,3 - polar phase volume v determined from scattering data (2) and birefringence (3); 4 - concentration of polarized microregions N_r.

$$I = I_o \exp(-\beta d), \qquad (2)$$

where I_o is the intensity of transmitted light at E = 0; I is the intensity of transmitted light at E>0, and d is the sample thickness.

To explain the scattering behavior we use the Usov-Shermergor relationship (3) [2,3] for light scattering on dielectric spheres in homogeneous dielectric. We suppose the scattering on polarized microregions in a paraelectric matrix. The effective difference of refractive index in microregions and matrix is Δn_{eff}. The scattering on another non-electric

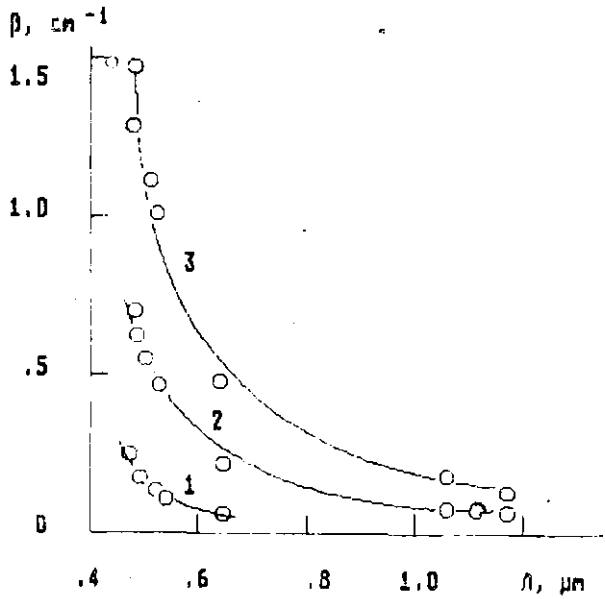

F i g. 4. Spectra of the extinction coefficient β for PLZT 8.5/65/35 at different values of the electric field E.

1 - E = 4 kV/cm; 2 - 5 kV/cm; 3 - 6 kV/cm. Temperature 23 °C. Optical aperture $4 \cdot 10^{-2}$ rad. Circles - experiment, solid curve - calculation according to [3].

field controlled non-homogeneities (pores, grain boundaries) was compensated in the measurement.

$$\rho=\frac{4\pi\nu(1-\nu)\Delta n^2_{ep}}{\lambda n^2}\cdot\left[\frac{\lambda}{4\pi a}-\frac{16\pi^2 a^2}{\lambda^2(1+4\pi^2a^2/\lambda^2)}\cdot\frac{\lambda}{8\pi^2 a}\ln\left(1+\frac{16\pi^2a^2}{\lambda^2}\right)\right]. \quad (3)$$

The linear size of microregions a and the change of volume concentration of ferroelectric phase ν vs E are shown in Fig.3. The amount of microregions per cm^3 N_r is calculated from a and ν. We have obtained both the increase of microregion diameter and the concentration of ferroelectric phase with E. The number of polarized microregions vs E shows the increase up to E = 4.8 kV/cm which is followed by a drop as E>4.8 kV/cm. The concentration of polar phase determined from scattering data (Fig.3, curve 2) and birefringence measurement data (Fig.3, curve 3) are in good agreement. With the increase of the electric field intensity formation of new polar regions is the most important up to E = 4.8 kV/cm. At higher intensities E the increase of the microregion diameter is more important.

REFERENCES

1. Yokosuka M., Marutake M.// Jap.J.Phys.- 1986.- Vol.25.- P.981.

2. Usov A.A., Shermerger G.D. // Zh.Theor.Fiz.- 1978. - Vol.48, N5.- P.1132 (in Russian).

3. Knite M., Kapenieks A., Sternberg A., and Livins M. // Ferroelectrics,- 1989.- Vol.90.- P.71-74.

Received September 11, 1990.

UDC 537.226.33

DIELECTRIC INHOMOGENEITY OF THE SBN SINGLE CRYSTALS

A. KAPENIEKS
Institute of Solid State Physics, University of Latvia
8, Kengaraga St., 226063 Riga, Latvia

R. STUMPE
Institut für Experimentalphysik Johannes Kepler Universität, A-4040 Linz, Austria *)

The contact and bulk dielectric properties are derived from thickness dependent complex impedance of strontium barium niobate (SBN) single crystals with Au-electrodes perpendicular and paralell to the ferroelectric axis. The particular dielectric properties of the surface layer are accounted for by electrical inhomogeneities within the contact region. The types of inhomogeneities possible are evaluted using finite element method computer simulations.

INTRODUCTION

It is known that contact effects (dependence of dielectric constant ε and loss tangent tanδ on sample thickness) are typical in relaxor ferroelectrics / 1 , 2 , 3 /. The contact effects are present in the case of silver paint electrodes. They are also detectable employing high quality vacuum evaporated gold contacts. Here we show that the main aspects of the dielectric behavior of the surface layer of relaxor ferroelectrics can be accounted for by electrical inhomogeneities.

In the recent letter it was reported that the dielectric properties in ferroelectric SBN ($Sr_{3/4}Ba_{1/4}Nb_2O_6$) single crystal the interfacial electrode-crystal layer differs from the bulk / 4 /. Here we present how the surface layer can be accounted for by the electrical inhomogeneities within the contact region.

EXPERIMENTAL PROCEDURE

Samples of about 2·2 mm were cut from the SBN crystals with the polar c - axis normal and parallel to the planes of the rectangle. The thickness of the samples varied between 0.1 and 3 mm. The two faces of the rectangles were electroded with evaporated gold. Then the samples were put in a sample cell.

*) Present adress: *Gablonzerstraße 44, A 4540 Kremsmünster, Austria*

Temperature was varied between - 180 °C and 400 °C with a heating rate of 1 °C per minute. The ambient medium in all of the dielectric measurements was air.

The dielectric measurements have been performed at frequencies ranging from 10 kHz to 10 MHz (Hewlett Packard LCR meter HP 4275A). The parallel circuit mode was used.

EXPERIMENTAL OBSERVATIONS

In order to determine dielectrical properties of the SBN bulk and bulk-electrode interface, we have investigated dependence of the dielectric response on the thickness, for temperatures both below and above the maximum in the dielectric constant of the material, which occurs at $T_m \approx 60$ °C (10 kHz).

Figure 1 shows the dielectric constant ε deduced from capacitance measurements and the geometry of the sample, and the loss tangent. It can be seen from the figure that both quantities are not material constants, but show a marked dependence on the sample thickness. This dependence is more or less pronounced, depending on the electrode material, measuring frequency and temperature. The measured value of ε increases with the sample thickness in the whole temperature range investigated.

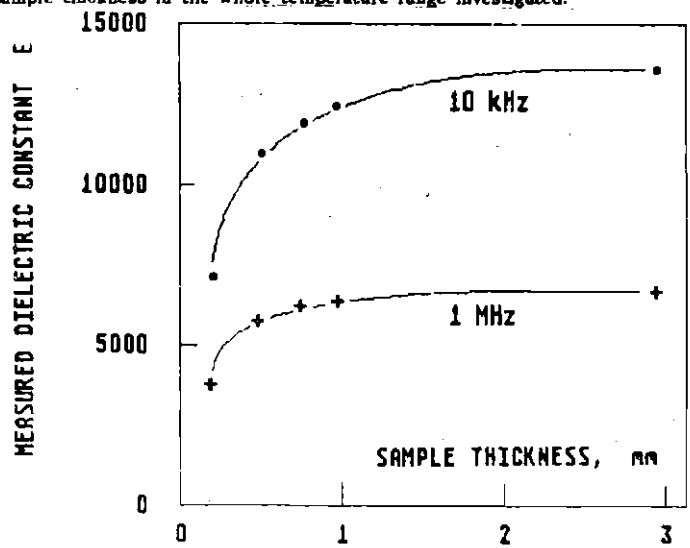

Fig. 1. Measured dielectric constant ε and loss tangent tanδ of SBN as a function of sample thickness at frequencies of 10 kHz (•) and 1 MHz (+). T = 25 °C. E ∥ c axis.

To obtain further information on the contact properties of electrodes we have separated bulk and surface (see Figure 2,a) contributions from the thickness dependence of the (complex) impedance. If neither the bulk nor the contact properties depend on the sample thickness h the measured impedance Z is expected to increase linearly with h. Thus, the bulk dielectric properties can be derived from Z(h) according to

$$\varepsilon_b = \frac{1}{\omega \varepsilon_0 A} \cdot \frac{1}{\{[\partial \mathrm{Re}\, Z(h)/\partial h]^2 + [\partial \mathrm{Im}\, Z/\partial h]^2\}^{1/2}} \cdot \frac{1}{\{\tan^2 \delta_b + 1\}^{1/2}} \qquad (1)$$

$$\tan \delta_b = \frac{\partial \mathrm{Re}\, Z(h)/\partial h}{\partial \mathrm{Im}\, Z(h)/\partial h}, \qquad (2)$$

while the behavior of the contact/surface layer can be evaluated from the extrapolation of Z(h) to zero thickness, i.e. $h \to 0$, according to

$$C_s/A = \frac{1}{\omega A} \cdot \frac{1}{\{[\mathrm{Re}\, Z(0)]^2 + [\mathrm{Im}\, Z(0)]^2\}^{1/2}} \cdot \frac{1}{\{\tan^2 \delta_s + 1\}^{1/2}} \qquad (3)$$

$$\tan \delta_s = \frac{\mathrm{Re}\, Z(0)}{\mathrm{Im}\, Z(0)}, \qquad (4)$$

where C_s is the surface layer capacitance, A is the electrode area, ε_0 is the vacuum permittivity and ω is the angular frequency. Re and Im denote the real and imaginary part of Z. The method also works for deducing the bulk properties when employing "bad" electrodes (silver paint).

Figures 3,4,5,6,7,8 show the bulk and contact properties derived from eqs. (1) - (4) for various frequencies as a function of the sample temperature. The experimental data were taken during the heating cycle.

It becomes evident from the Figures that dependences of bulk and surface properties are different. Both parallel and perpendicular to the ferroelectric c-axis the measured dielectric constant increases with increasing sample thickness suggesting, in a superficial point of view, that a low permittivity surface (contact) layer masks the bulk dielectric properties. On the other hand the temperature dependence of the surface capacitance qualitatively resembles the bulk behavior, which is in contradiction to the flat response expected. A reasonable explanation for the empirical dielectric response is that the transport properties within the metal - SBN - junction are determined by electrical inhomogeneities macroscopically resulting in a deficiency of *surface volume* contributing to the response.

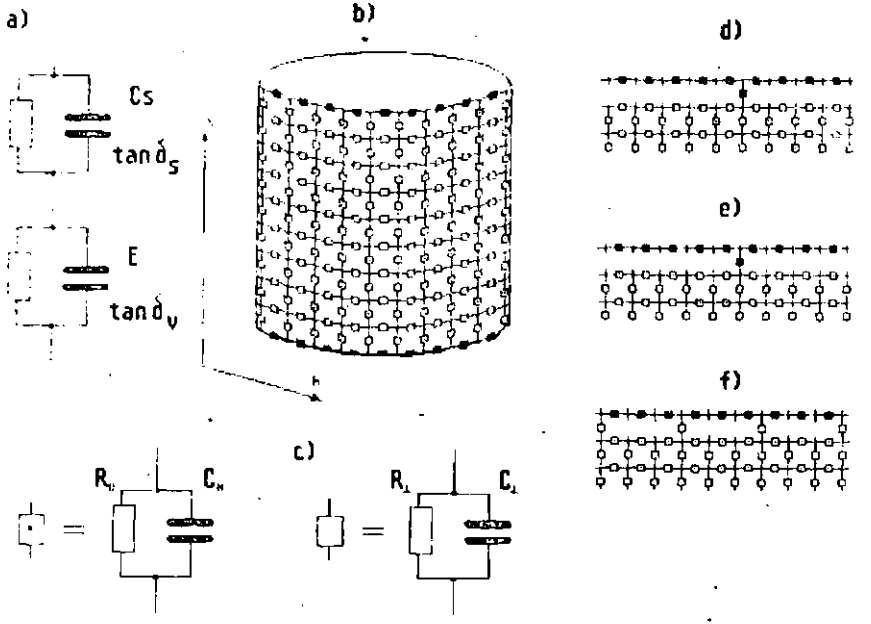

Fig. 2. Equivalent circuits for SBN samples with electrodes.
a) equivalent circuit, calculated from experimental results; b) circuit for computer simulation c) explanation for elements (b), black elements are ideal conductors.
R_v, C_v values are determined from Fig. 4 and Fig. 6 ; $R_\perp$, $C_\perp$ values are determined from Fig. 3 and Fig. 5; d) computer-simulated surface-bulk interface inhomogeneities $E_\parallel$ c-axis, e) computer-simulated surface-bulk interface inhomogeneities, $E_\perp$ c-axis; f) another version of inhomogeneities.

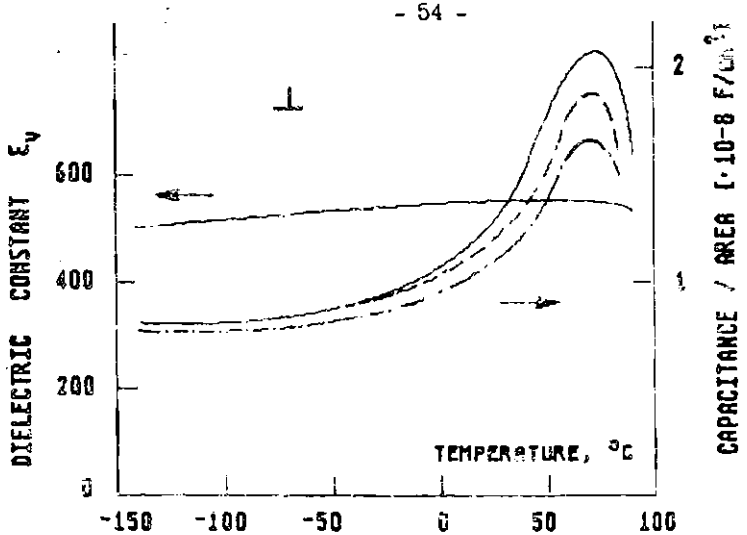

Fig. 3. Bulk dielectric constant ε_v and surface capacitance/area C_s of SBN single crystals with Au-evaporated electrodes at frequencies 10 kHz (————), 100 kHz (- - - - -) , 1 MHz (—·—·—), calculated from the thickness dependance of the impedance according to eqs. (1) - (4), as a function of temperature; electric field E ⊥ c-axis.

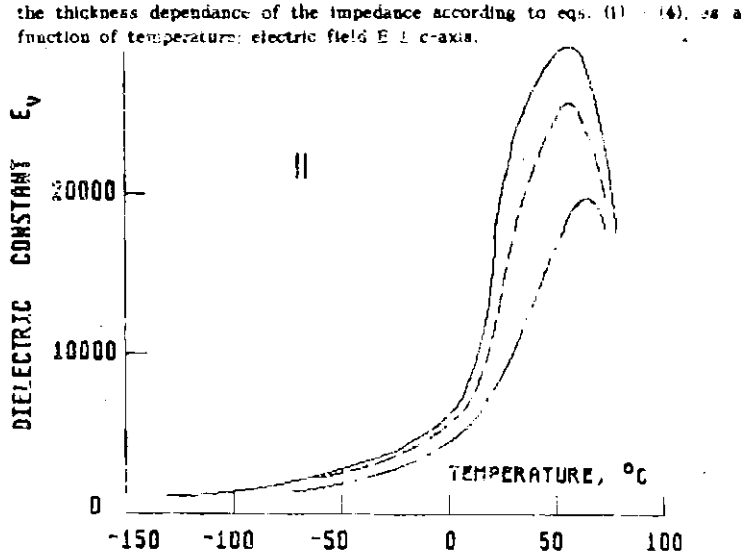

Fig. 4 . Bulk dielectric constant ε_v of SBN single crystals with Au-evaporated electrodes at frequencies 10 kHz (————), 100 kHz (- - - - -) , 1 MHz (—·—·—), calculated from the thickness dependence of the impedance according to eqs (1) - (4), as a function of temperature, electric field E ∥ c-axis.

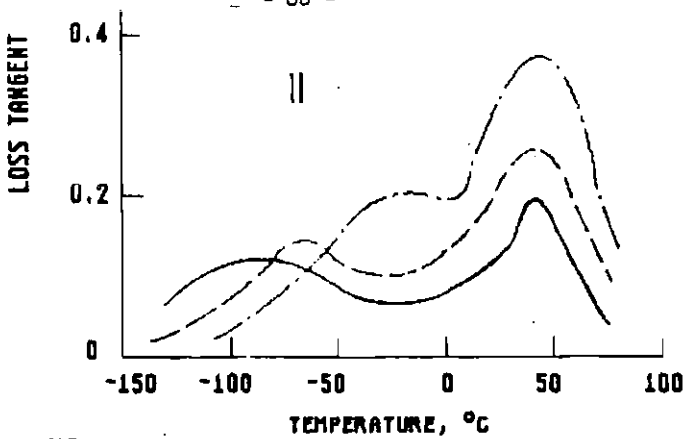

Fig. 5 . Bulk loss tangent $\tan\delta_v$ and surface loss tangent $\tan\delta_s$ of SBN single crystals with Au-evaporated electrodes at frequencies 10 kHz (————), 100 kHz (- - - - -) , 1 MHz (—·—·—), calculated from the thickness dependence of the impedance according to eqs. (1) - (4), as a function of temperature; electric field E ⊥ c-axis.

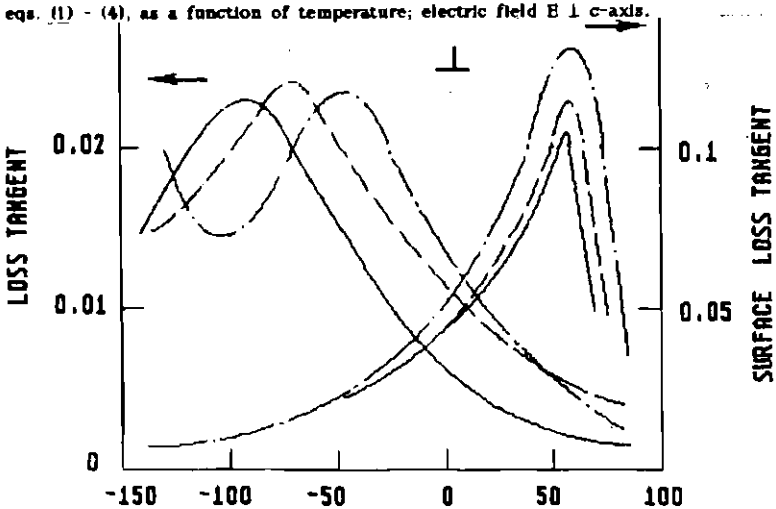

Fig. 6 . Bulk loss tangent $\tan\delta_v$ of SBN single crystals with Au-evaporated electrodes at frequencies 10 kHz (————), 100 kHz (- - - - -) , 1 MHz (—·—·—), calculated from the thickness dependence of the impedance according to eqs. (1) - (4), as a function of temperature; E ⊥ c-axis.

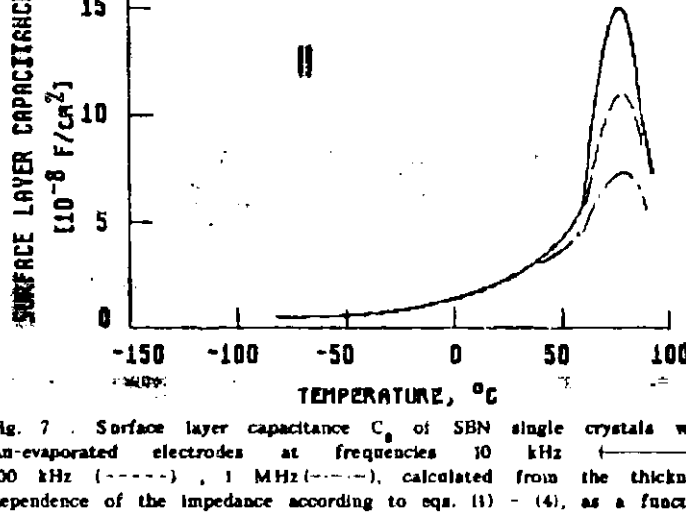

Fig. 7 . Surface layer capacitance C_s of SBN single crystals with Au-evaporated electrodes at frequencies 10 kHz (————), 100 kHz (- - - - -) , 1 MHz (—·—·—), calculated from the thickness dependence of the impedance according to eqs. (1) - (4), as a function of temperature; electric field E ⊥ c-axis.

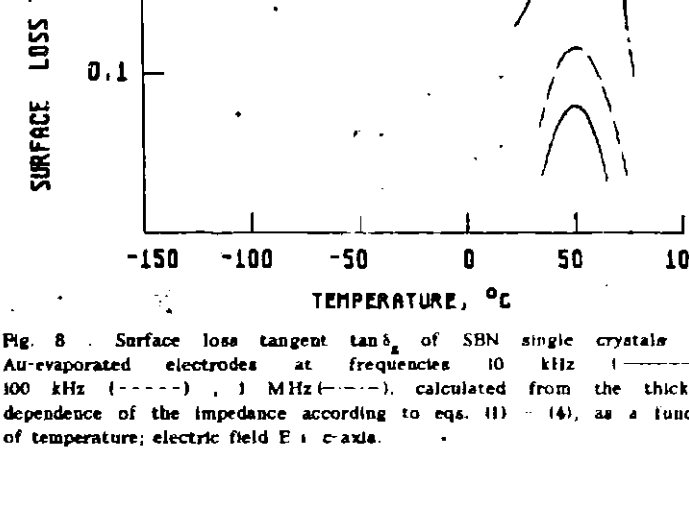

Fig. 8 . Surface loss tangent $\tan\delta_s$ of SBN single crystals with Au-evaporated electrodes at frequencies 10 kHz (————), 100 kHz (- - - - -) , 1 MHz (—·—·—), calculated from the thickness dependence of the impedance according to eqs. (1) - (4), as a function of temperature; electric field E ⊥ c-axis.

CALCULATIONS

In order to validate the kinds of inhomogeneities possible the following model calculations have been performed employing some idealized assumptions on the electrical structure of the junction. We explain the experimental results Figs. 3,4,5,6,7,8 with the local distortion in the bulk-electrode interface. In order to do the calculations we simulate the sample with a cylindric net of complex impedances (Fig. 2, b). The values of R, e.g., tanδ and C were taken equal to the experimentally determined ε and tanδ for bulk perpendicular and parallel to c-axis, correspondingly (Figs. 3,4,5,6). Different surface layers were proved to vary the values of R and C in the surface layer

The values of macroscopic C and tanδ of the simulated sample were calculated from the current in the sample and voltage on the electrodes.

Potential at every point of the intersection U_p was calculated from the potential in four neighbouring points of the intersection U_j and the values of C_j and R_j to neighbour points:

$$U_p = \frac{\sum_{j=1}^{4} U_j \left(\frac{1}{R_j} + i\omega C_j \right)}{\sum_{j=1}^{4} \left(\frac{1}{R_j} + i\omega C_j \right)} \qquad (3)$$

With the 300 - 6000 cyclic calculations of U_p for all the points of the intersection we obtain the values of U_p for all the simulated sample. From the values of U_p we determine the current in the sample and calculate the C and R e.g. ε and tanδ of the sample. Using the equivalent circuit (Fig. 2, a) we calculated the *effective* parameters of surface C_s and $\tan\delta_s$.

We tried to do the explanation without the occurrence of elements with turned direction of c-axis. The increase of the imaginary as well as the real part of the impedance due to electrodes we introduce in our calculation with the presence of holes between the electrode and bulk (Fig. 2,f). With such an approximation it was possible to explain the experimental results of dielectric parameters measured with electrodes perpendicular but not parallel to the ferroelectric axis .

The next step was the occurrence of conducting (metallic) elements in our calculation. In order to increase the value of computer-simulated sample up to the experimental value we introduce the hole under the electrodes. The calculation of this configuration yielded qualitatively agreeable results for situation with electrodes perpendicular to c-axis. In the next step, we locally changed the elements (turned c-axis by 90^0) at the conducting element (Figs. 2,d ; 2,e). Results of calculation of this configuration are presented in Figs. 9,10.

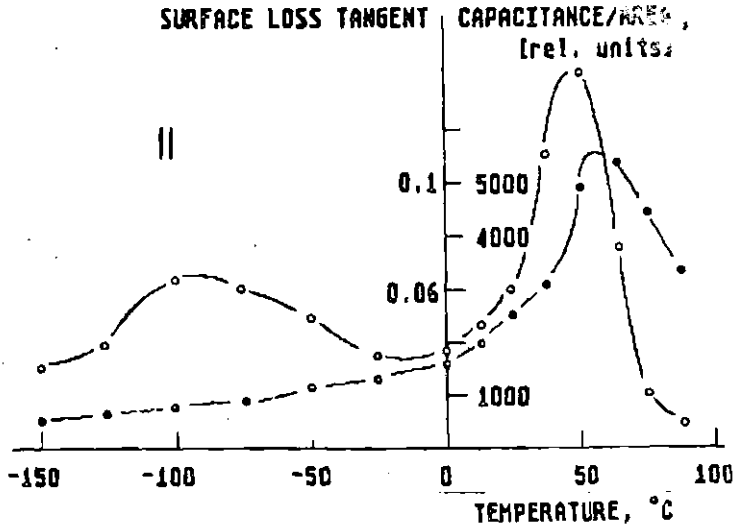

Fig. 9 . Computer-simulated dielectric properties capacitance/area ϵ_s (—o—●—) and surface loss tangent $\tan\delta_s$ (—o—o—) for Figure 2,d bulk-electrode interface. Equivalent circuit was a cylinder 20 elements high and 6 elements in perimeter; electric field E ⊥ c-axis.

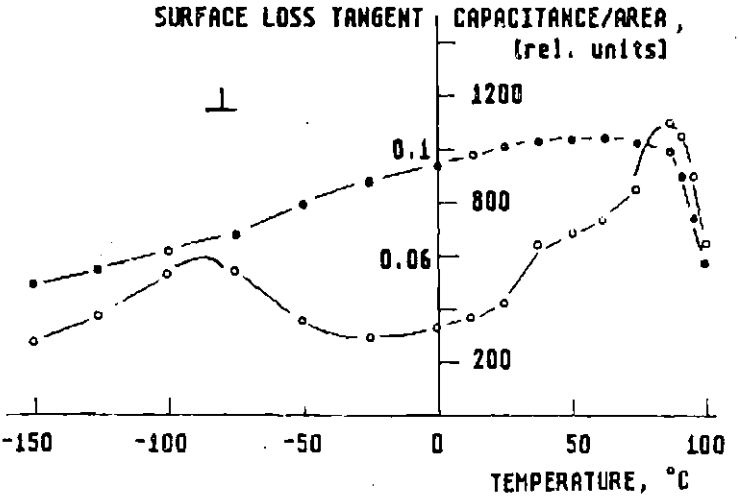

Fig. 10 . Computer-simulated dielectric properties capacitance/area ϵ_s (—o—o—) and surface loss tangent $\tan\delta_s$ (—o—o—) for Figure 2,e bulk-electrode interface. Equivalent circuit was a cylinder 20 elements high and 6 elements in perimeter; electric field E ⊥ c-axis.

The results of calculation from Fig. 3,d,e are presented in Fig. 4,a,b. The character of $C_s(T)$ and $\tan\delta_s(T)$ are similar to experimental and computer-simulated results. The differences are caused by the simple two-dimensional model applied . The simple " geometrical" variation can change the maximum temperature of $\tan\delta_s$. As following from the model calculations the homogeneity of the electrical field is disturbed in regions exeeding the extension of the inhomogeneity by far (20 elements). Therefore an inhomogeneity within a thin surface layer (interface, junction) leads to an " effective" surface layer of appreciable thickness. The results of computer-simulation show that simple changes in the bulk-electrode interface can cause the effects in the dielectric response of SBN single crystals, similar to the experimentally determined.

At the present state of investigation, in order to evalute the dominating mechanism, the model calculations have been restricted to the assumption of some extreme kinds of inhomogeneity. For further improvement a broad distribution of properties, as typical for relaxor ferroelectrics, has to be taken into account. The best agreement with the experimental data is obtained by presuming both insulating and highly conducting ("metallic") regions. The results are compatible with an increase of the electrical inhomogeneity, inherent in the material, within a thin surface layer.

REFERENCES

1. Glass A.M. // J. Appl. Phys. – 1968.– Vol.40.– P.4699.

2. Kapenieks A., Stumpe R., Eyett M., and Bäuerle D.// Proc. of the Sixth IEEE Int. Symp. on Applications of Ferroelectrics.– Lehigh University, Bethlehem, PA USA, 8-11 June ,-1986. - P. 696-699.

3. Stumpe R., Wagner D., Bäuerle D., Hagemann H.J. // Ferroelectric Lett. - 1985.– Vol.4 – P.143.

4. Kapenieks A., Stumpe R.// Abstr. of the III Soviet Seminar "Production, Research and Application of Transparent Ferroelectric Ceramics.– Latvian State University,-Riga, 1988.– P 66 - 68.

UDC 537.226.4:620.1..

DOMAIN STRUCTURE OF DOPED PLZT CERAMICS

A. Plaude
Institute of Solid State Physics, University of Latvia
8, Kengaraga St., 226063 Riga, Latvia

Results of microstructure studies of Cr, Mn, Fe, Co, Ni and Cu doped PLZT 8/65/35 ceramics are reported. Most of them are explained by dopant-induced domain structure formation in PLZT ceramics.

Introduction

A number of studies of PLZT 8/65/35, where the notation refers to atomic % La/Zr/Ti, have been reported [1-6]. It has been indicated that structure and domain structure of the material depend on the thermal and electrical history of the material. In thermally depolarized state it belongs to the so called undefined symmetry state [4]. Some results of X-ray diffraction and microstructure measurements of PLZT 8/65/35 ceramics doped by Fe, Co and Eu have been reported [7,8], however full mictrostructure examinations have not be made before.

Experimental

We have studied microstructure of hot-pressed PLZT 8/65/35 ceramics doped by Cr, Mn, Fe, Co, Ni and Cu with different concentrations up to 3% of weight. The grain boundaries and domain structure were revealed by TEM chemical etching and replica technique or by SEM with Au coated specimens.

Results

The domain structure in thermally depolarized PLZT 8/65/35 is absent. It is induced by applying electric field or uniaxiall stress. We noticed forming of domain structure in doped PLZT 8/65/35 without external fields. In the case of small dopant concentration the effect is small and there is no unabiguous interpretation of it, while as the dopant concentration increases, the microformations are anhanced and the domain structure becomes evident.

For PLZT 8/65/35 + Fe, Co and Ni the microstructure in etched patterns suggest the presence of domains in all of the dopant concentration range (Fig.1).When the concentration of Fe, Co and Ni increases, the domains grow but never cross the grain boundaries. Regular lamellar structures were observed in each grain in electrically polarized material (Fig.2,a).

For PLZT 8/65/35 + Cr changes in microstructure which we may relate to domain structure, appear when dopant concentration reahes 0,5 % of weight (Fig.2,b).

For PLZT 8/65/35+Cu in the case of small dopant concentration domains were noticed in some grains, not throughout of the whole sample at concentration increase up to 1% of weight, domain concentration becomes regular (Fig.2,c).

For PLZT 8/65/35+Mn in the case of small dopant concentration there is no unambiguous interpretation of microstructure, but when dopant concentration rises up to 3% of weight, microstructure consists of large grains and wide grain boundaries without domain structure (Fig.2,d).

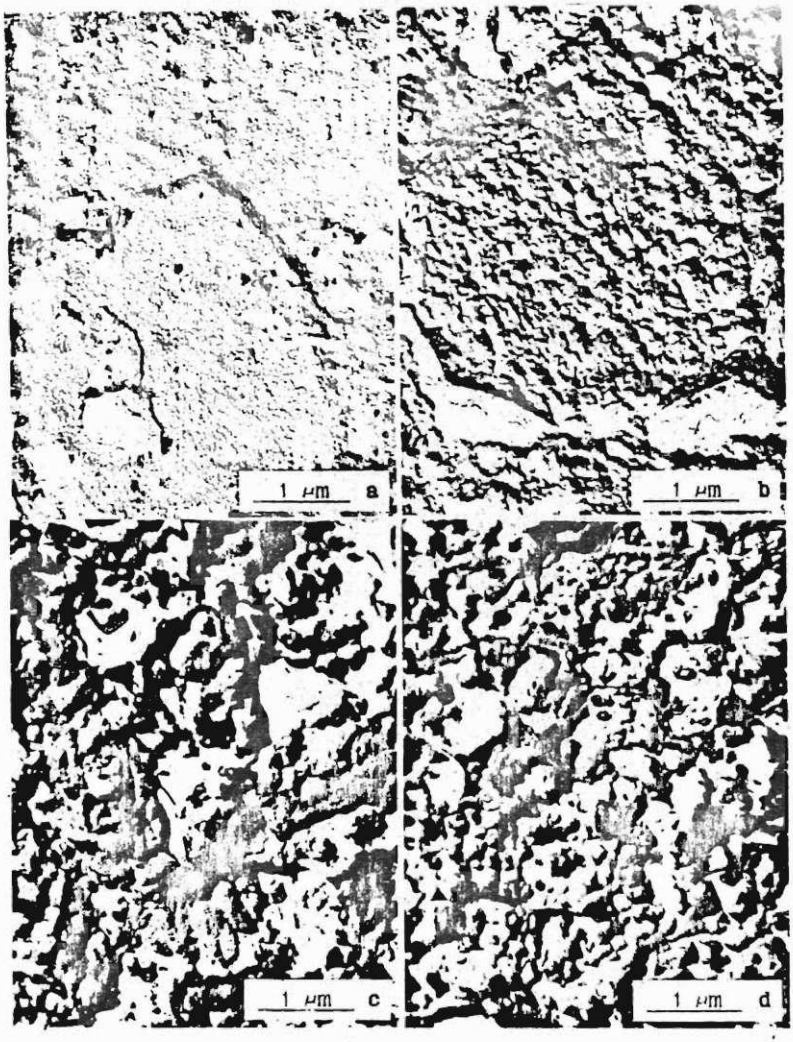

Fig. 1. Microstructure of chemically etched PLZT 8/65/35 ceramics. a - 0,05 wt.%Fe; b - 0,5 wt.% Fe; c - 1 wt.% Fe; d - 3 wt.% Fe.

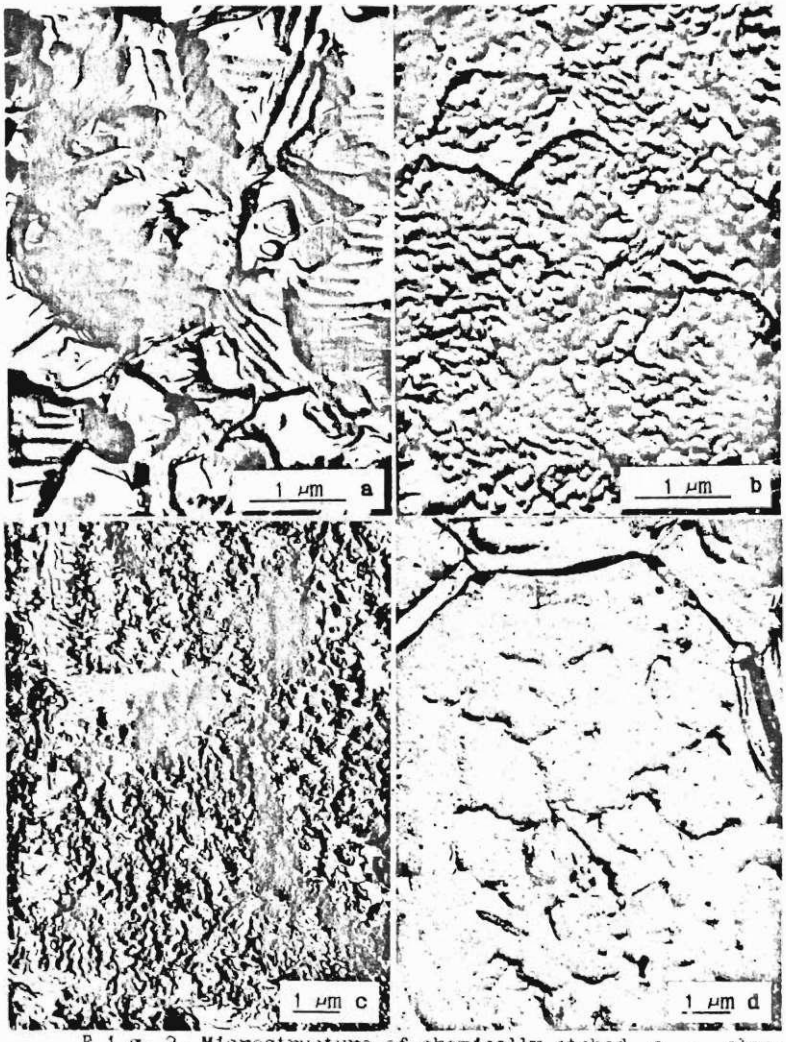

Fig. 2. Microstructure of chemically etched. a - electrically poled PLZT 8/65/35+0,1 wt.% Co; b - PLZT 8/65/35+0,5 wt.% Cr; c - PLZT 8/65/35+1 wt.% Cu; d - PLZT 8/65/35+3 wt.% Mn.

Conclusion

Doping of PLZT 8/65/35 ceramics by Cr, Mn, Fe, Co, Ni and Cu essentially changes microstructure, but not in the same manner in all cases. Comparatively less concentration of Fe, Co and Ni caused domain formation in PLZT 8/65/35. With the growth of dopant concentration domain structure appears in PLZT 8/65/35 doped by Cr and Cu but disappears in PLZT 8/65/35 doped by 3 wt.% Mn. Domain structure in doped ceramics grains is regular, but domains do not cross grain boundaries in the case of thermally depoled material.

REFERENCES

1. O'Bryan H.M., Meitzler A.H.// Bull.Amer.Ceram.Soc.- 1972.- Vol.51, N5.-P.479-485.

2. Michel C., Sicignano A.// Appl.Phys.Lett.-1974.- N11.- P.559-562.

3. Keve E.T., Bye K.L.// J.Appl.Phys.- 1975.- Vol.46, N2.- P.810-818.

4. Sternberg A., Pritsberg V., Shebanov L., et al.// Electrooptic Ceramics.- Riga, 1977.- P.138-167 (in Russian).

5. Schmit G., Arndt H., Borchardt G., et al.// Phys. status solidi, a.- 1981.- Vol.63.- P.501-509.

6. Plaude A.V. // Actual Physical and Chemical Problems of Ferroelectrics.- Riga, 1987.- P.130-139 (in Russian).

7.Dimza V.I., Sprogis A.A., Kapenieks A.E., et al.// Ferroelectrics.- 1989.- Vol.90.- P.45-55.

8. Plaude A., Dimza V., Sternberg A.// Abstr. International Symposium on Domain Structure of Ferroelectrics and Related Materials.- Volgograd, 1989.- P.62.

Received December 21, 1990.

UDC.548.0:537.226.33

POLARIZATION SWITCHING IN TRANSPARENT PLZT CERAMICS

L.I.Dontsova
Civil Engineering Institute,
1, Akademicheskaya St., 400074 Volgograd, USSR

The process of polarization switching was observed in transmitted light under polarizing microscope, the time of complete switching of the samples being measured as the time required for transition of the sample from one single domain state to the other of antiparallel direction of $\vec{P}_s$.

Introduction

Polarization switching in PLZT ceramics has been studied by Barkhausen method [1,2] providing information of the discontinuous change only, by polarization loops [3], pyroelectric response [4], by the change of light scattering coefficient and other indirect methods.

In the studies being reported the switching process in PLZT ceramics has been examined by the nematic liquid crystal (NLC) method [5,6] in unannealed samples of PLZT 7/65/35, PLZT 8/65/35 and PLZT 8/65/35:Ne. The process of polarization switching was observed in transmitted light under polarizing microscope, the time of complete switching of the samples being measured as the time required for transition of the sample (its part seen in the microscope) from one single domain state to the other of antiparallel direction of $\vec{P}_s$. It has to be noticed that with the NLC method the polarization switching of a ferroelectric occurs under conditions of dielectric gap when the process is essentially slowed and the absolute values of τ_s are increased as compared to the process in the presence of well conducting (e.g., metal) electrodes. However, as shown in [7], the features of the process are maintained, and such

characteristics of the material as activation field of switching do not depend on the type of electrodes.

Results

1. In the initial (non-polarized) state the PLZT samples with a thin layer of NLC between its polished surface and a transparent electrode (SnO_2 fired on glass plate) appears to be oriented, and the NLC-PLZT cell - transparent. A picture of inhomogeneous electric potential distribution is seen on the PLZT surface reflecting the features of sintering technology and other "defects" caused, e.g., by mechanical treatment of the surface.

2. As in single crystals (TGS, GASH, $BaTiO_3$ a.o.)[6,8] the switching of PLZT ceramics from one polarized (single domain) state to the opposite occurs by forming domain nuclei (with $\vec{P}_s$ directed along $\vec{E}$) at places predetermined by local distinctions of the sample, their growth and widening throughout the sample. Upon coalescing of several closer domains, switching "fronts" (boundaries between the part switched and that unswitched) of arbitrary shapes - closed, extended, often starting from the sample sides - are formed. Since the boundaries are not flat they coalesce at separate places as the regions of unswitched phase disappear. This last stage of the switching process we shortly call "erasing" [8]. With the increase of applied field the number of domain nuclea, number of boundaries and propagation velocity of the latter grow, the complete switching time τ_s being shorter (Fig.1.).

3. At the beginning of the switching process a large number of domain nuclea arise, and a strong scattering of light is observed - the cell darkens, then the switched regions become transparent, their growth and coalescing makes transparent the whole cell as the switching process ends (the cell returns to the initial state of light transmittance). In a number of earlier studies [3,9] an interrelation between the light scattering and appearance of polarized regions or their switching by applied field in PLZT ceramics has been noticed.

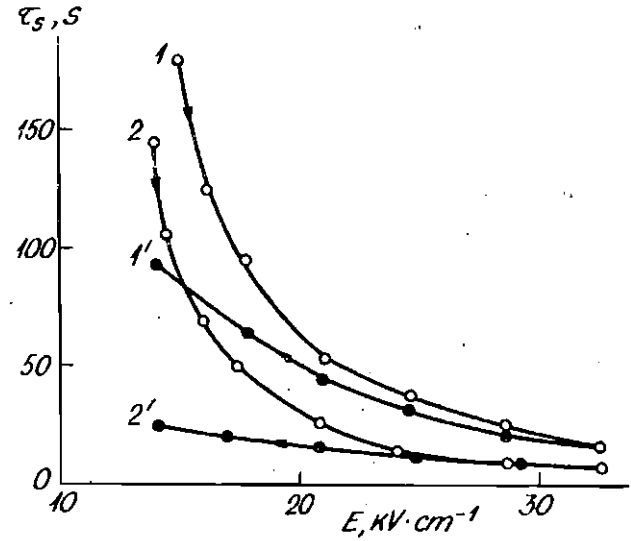

F i g. 1. Unipolarity and hysteresis of the total switching time.

τ_s in PLZT ceramics represented as function of the applied dc field E at increase (1,2) and decrease (1', 2') of the intensity of the opposite field (1 and 1', 2 and 2').

4. Disinclination lines in the NLC layer and remnants of the switching boundary coalescence observed upon the end of the switching process suggest the presence of defects in PLZT. A highly possible appearance of the latter in PLZT has been noticed in [10]. Some of the defects behave like twin boundaries where domains arise under electric field widening and propagating in both directions (similar to the loop domains in GASH crystals [11]). Different parts of these domain boundaries move with a different velocity resulting (at E = const) in branching, partitioning and coalescing of those moving towards each other.

5. As a rule, the distribution of the field-induced domain nuclea over the sample is random which suggest a random

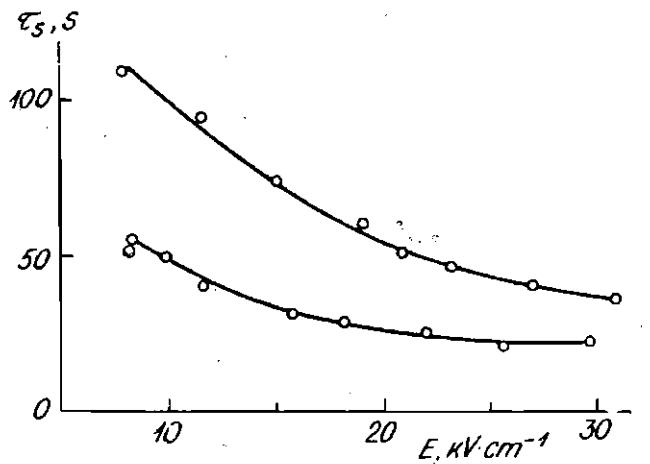

F i g. 2. The total switching time τ_s as function of dc field intensity E for two parts of an PLZT 8/65/35 sample.

distribution of point defects or their clusters being the nucleation centers. The number, localization and activity (evaluated from the threshold field at switching) of the domain nucleation centers being different for different directions of the field ±E the switching characteristics become unipolar: $\tau_s^+ \neq \tau_s^-$ (Fig.1). The unipolarity determined by $/ \tau_s^+ - \tau_s^- // \tau_s^+$ is high (0,6-0,7) for PLZT 7/65/35 and essentially less (0,1-0,4) for PLZT 8/65/35. It has also to be noticed that the switching time may differ twice or more for different parts of a sample (Fig.2) suggesting the distribution of defects being not homogeneous. The switching boundaries arising in PLZT 8/65/35 under applied field are made smaller at doping (Mn, Fe, Eu, Co). In PLZT: Fe ceramics, besides a random distribution of domain nuclea, in some areas they are observed to be arranged in rows.

6. Any state induced during the polarization switching in a sample upon taking off the applied field is more stable in

the case of PLZT 7/65/35 as compared to PLZT 8/65/35 where a rather quick spontaneous decay of the field induced state and return to the initial one (the state before the field was applied) is observed to take place. The "decay" time is different for opposite directions of the applied field suggesting the initial state of the ceramics being a unipolar one.

7. A considerable difference of switching time curve $\tau_s(E)$ between direct (increasing) and reverse (decreasing) change of the applied field is observed in PLZT ceramics (Fig.1.): the reverse values of τ_s are less, i.e., the value and duration of the previous field are important.

8. Dependence of the switching time τ_s on the applied dc field intensity is described, as for a lot of single crystals, by exponential law (Fig.3): $1/\tau_s = (1/\tau_{s\infty})\exp(-\alpha/E)$ which correlates with the time of transition from optically depolarized to OP-state: $t = t_\infty \exp(\alpha/E)$ [12]. However, as seen from the $\ln(1/\tau_s)$ vs $(1/E)$ diagrams there are two values of the activation field α observed within the field interval examined (4-40 kV/cm). Mn and Fe dopands cause a shift of the $\ln(1/\tau_s)$ vs $(1/E)$ diagram to smaller τ_s values and change the value of α (determined from the slope of the linear interval). The values of α_I and α_{II} for the intervals I and II, respectively, determined for the samples examined, are given in the Table. The change of the $\ln(1/\tau_s)$ vs $(1/E)$ diagram and the α value upon doping show that Mn is a more efficient dopand as compared to Fe. This agrees with the change of fundamental absorption edge: the higher is the number of the dopand element the less is the shift [13].

9. The total switching time τ_s is a general characteristic of the switching process. Particular stages contribute to it: generation and toward-growth of the domain nuclea - τ_I, side movement of the domain walls and their coalescing at separate areas - τ_{II}, and "erasing" time - τ_{III}. For PLZT ceramics as in the case of TGS single crystals [8] $\tau_I \ll \tau_s$ within the whole interval of field values. "Erasing" time remains less than the time of side movement of the domain walls τ_{II}, but the relative contribution of the first is growing with the intensity of the applied field (Fig.4).

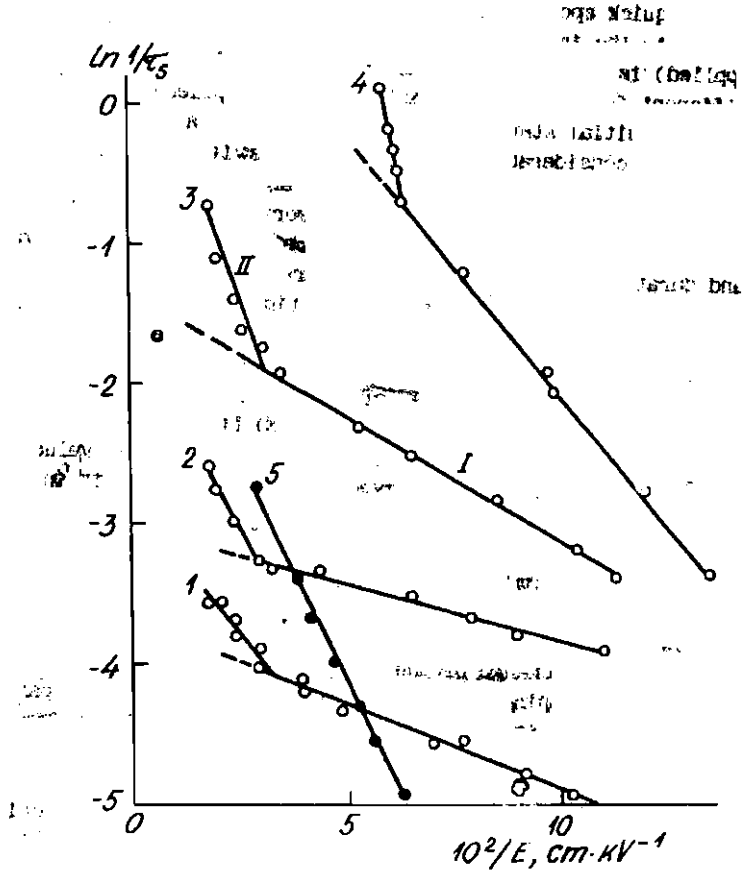

F i g. 3. The total switching time representation by ln $(1/\tau_s)$ (τ_s in seconds)) vs 1/E diagram for ceramics samples: 1 - PLZT 8/65/35 (undoped); 2 - PLZT 8/65/35: 0.01 Fe; 3 - PLZT 8/65/35: 0.01 Mn; 4 - PLZT 8/65/35: 0.1 Mn; 5 - PLZT 7/65/35 (undoped).

Table

The values of the activation field for the undoped and doped samples

Compound	Activation field, kV·cm^{-1}		Transition field between I and II E_t, kV·cm^{-1}
	α_1	α_2	
PLZT 8/65/35, undoped	5.5-9.5	20-33	20
PLZT 8/65/35: 0.01 Fe	9	72	33
PLZT 8/65/35: 0,01 Mn	19	110	31
PLZT 8/65/35: 0,1 Mn	40	200	15
PLZT-7/65/35, undoped	-	70-82	-

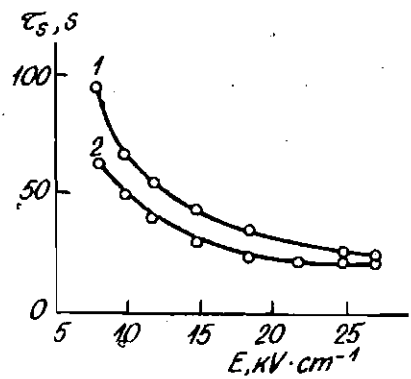

Fig. 4. Total time ($\tau_I + \tau_{II}$) of nucleation, growth and side propagation of domains or "switching frontiers" (curve 1) and erasing time τ_{III} (curve 2) as functions of the dc field E in PLZT 8/65/35 (undoped) ceramics.

Discussion

The switching of the PLZT ceramics has many features common with the 180°- switching of single crystals (TGS, $BaTiO_3$ a.o.). It includes the same stages and follows the same law. The polycrystalline structure of PLZT does not exhibit itself, at least at the stage of extending the switched areas providing the most considerable contribution to the total switching time. The size of crystallites is possibly important at forming regions polarized parallel to the applied field.

Different from single crystals in PLZT ceramics there is no anisotropy of the velocity of side movement of the domain walls which is naturally expected in polycrystals. Unusual for ceramics is the switching unipolarity in PLZT despite the different orientation of crystallites with respect to the sample surface to which the field is applied. The 180°-switching is likely to be the only to speak about in PLZT.

Really, if the initial state of PLZT ceramics is a ferroelectric macroscopically polarized one, the crystallites consisting of domains with different orientation of $\vec{P}_s$ with respect to the sample surface (which is possible in PLZT at room temperature), then as the field is applied, i.e., during the polarization, the domain structure is destroyed, and the sample changes its state from optically and electrically isotropic to another one of field-induced anisotropy, the ceramic material being turned similar to a single domain uniaxial crystal, the optical and polar axis of which is parallel to the applied field. The following cycles of reversing the field (±E) will result in 180° polarization switching from one single domain state to another. The switching is not related to the initial static domain structure (if it has been) and in any field interval the change of polarization inevitably proceeds the stage of forming nuclei with $\vec{P}_s$ parallel to the applied field.

Assuming the electronic state of the sample being responsible for domain nucleation [14,15], and the new polarization under applied field being induced by exciting electrons from the surface states the concentration of domain

nuclea at a given value of E is determined by the depth of the levels and number of electrons on them. Distribution of electrons in the surface states is strongly dependent on defects. PLZT is known [16,17] to have a high defect concentration, the lead vacancies being about 10^{21} cm^{-3}, the donor (La^{3+} ions) concentration - about 10^{22} cm^{-3}. Doping introduces additional localized states. The unipolarity of PLZT switching characteristics thus may be due to the surface states being different with respect to opposite directions of the applied field and to the bipolar conductivity being also different for $\pm E$. The latter is due to a higher mobility of holes in PLZT [17]. A somewhat less unipolarity of PLZT 8/65/35 samples as compared to PLZT 7/65/35 may be explained by the difference of T_c. Besides, appearance of polarized regions under applied field is possibly easier in the case of macroscopically nonpolarized matrix (PLZT 8/65/35) as compared to reorientation of $\vec{P}_s$ (PLZT 7/65/35).

The total switching time, i.e., the speed of polarization switching, is determined by the speed of compensation of the polarization charge (external - from the electrodes, internal - from the bulk and surface states of the ferroelectric sample).

The growing contribution of "erasing" time with the applied field (Fig.4) (similar to what is observed in TGS single crystals [15]) suggests that the charge stored by surface states is smaller than required for fast compensation of considerable bounded charge appearing in a strong field because of "momentaneous" nucleation of a large number of domains and fast growth of their size. Therefore the propagating domain wall (the "switching fronts") will have a tail of uncompensated charge the compensation of which will be continued by carriers from the electrodes and the bulk even after the polarization switching is finished (the single domain state being achieved). Because of a small conductivity of PLZT ($\sim 10^{-15}$ $1/\Omega \cdot cm$ [16]) the relaxation time of charge carriers is rather large ($\sim 10^4$ s at room temperature). If the applied field is removed before full compensation a decay of the polarized state will take place because of depolarizing field and, the speed and degree of the decay obviously depending on the intensity and endurance of preceding field.

The hysteresis of τ_s (E) at increase or decrease of the applied field (Fig.1) may be explained in a similar way. The effects, however less pronounced, should be observed, in the case of well conducting electrodes since, according to calculations [18], the density of the injected charge of free carriers is small as compared to density of the bounded charge ($\sim 10^{14}$ cm^{-2} at $P_s \sim 20$ μ C/c^2).

Conclusion

1. The polarization switching of PLZT ceramics proceeds the same stages and follows the same laws as the 180° polarization switching of single crystals. The 180° switching of PLZT compared to single crystals is distinguished by a rather high threshold field (some kV/cm) and absence of anisotropy of the domain wall side velocity.

2. Unipolarity of the total switching time $\pm\tau_s$ for opposite directions of applied dc field $\pm E$ has been observed. The unipolarity of switching is assumed to be related to difference of surface states of the sample with regard to the sign of E and to the bipolar conductance of PLZT ceramics.

3. The total switching time τ_s is shown to depend on the value and duration of the preceding field. A direct observation has confirmed the decay of polarized state in PLZT ceramics after applied field is removed. The effects are tentatively explained by depolarizing field being left uncompensated during the switching: the charge of carriers injected from the electrodes and the charge accumulated in surface states is insufficient to achieve a fast and complete compensation of the polarization charge while the relaxation of majority carriers from the bulk in PLZT, because of small conductivity (dispite a high concentration), is slow and may take much longer time than the applied field takes.

4. At doping by Mn, Fe, Eu, the density of domain nucleas (with $P_s \| E$) appearing under applied field in PLZT 8/65/35 is increased causing an increase of the number of switching "frontiers", for which reason the switching proceeds faster (τ_s decreases) and the activation field is changed.

5. The study of polarization switching in PLZT by means of NLC may be used as express - examination of sample quality - to reveal inhomogeneity of switching in different parts of the sample and the distribution of point as well as extended defects in the sample.

REFERENCES

1. Bolshakova N.N., Rudyak V.M., Sokolova I.D. // Abstr. of Third Soviet Seminar on Production, Research and Application of Transparent Ferroelectric Ceramics.- Riga, 1988.- P 72 - 74 (in Russian).

2. Bolshakova N.N., Zharov S.Yu.. Rudyak V.M., et al.- Ibid.- P.127-129 (in Russian).

3. Krumin A.E., Seglinsh Y.A., Knite M.E., and Rupp V.A. -Ibid.- P.101-103 (in Russian).

4 Bogomolov A.A., Dabizha T.A. - Ibid.- P.130-132 (in Russian).

5. Tikhomirova N.A., Dontsova L.I., Pikin S.A., and Shuvalov L.A. // Pis'ma Zh. Eksp.Teor.Fiz.- 1979.- Vol.29.- P.37-40 (in Russian).

6. Dontsova L.I., Bulatova L.G., Popov E.S., et al. //Kristallografiya.-1982.- Vol.27, N 2.- P.305-312 (in Russian).

7. Dontsova L.I., Tikhomirova N.A., Bulatova L.G., et al.//Fiz.Tverd. Tela .- 1987.- Vol.29, N 4.- P.1041- 1047 (in Russian).

8. Tikhomirova N.A., Dontsova L.I., Ginsberg A.V., et al. // Fiz.Tverd. Tela.- 1986.- Vol.28, N 11.- P.3319-3328 (in Russian).

9. Shilnikov A.V., Burkhanov A.I., Dontsova L.I., et.al.// Ferroelectrics.- 1986.- Vol.69, N1-2.- P.111-115.

10. Prisedsky V.V., Golubitsky V.M., But V.E., et al.// Izv. Acad. Nauk SSSR.Neorg. Mater.-1981.-Vol.17.- P.1875 (in Russian).

11. Dontsova L.I., Tikhomirova N.A., Pikin S.A., and Shuvalov L.A.// Zh. Eksp. Teor. Fiz.-1982.- Vol. 36 N 6.- P.181-184 (in Russian).

12. Wolfram S. // Ferroelectrics.- 1976.- Vol.10, N 1-4.- P.39-42.

13. Dimza V.I., Arndt H., Sprogis A.A., et al.// Actual Physical and Chemical Problems of Ferroelectrics.- Riga, 1987.- P.45-65 (in Russian).

14. Guro G.M., Ivanchik I.I., and Kovtonyuk M.P.// Fiz. Tverd. Tela.- 1968.- Vol.10, N.1.-P.135-140 (in Russian).

15. Dontsova L.I. and Tikhomirova N.A. // Pis'ma Zh. Eksp. Teor. Fiz.- 1985.- Vol.41, N.5.- P.183-185 (in Russian).

16. Krumin A.E.// Phase Transitions and Related Phenomena in Ferroelectrics.- Riga, 1984.- P.3-67 (in Russian).

17. Rouchon J.M., Vergnolle M., and Micheron F.// Ferroelectrics.- 1976.- Vol.11.- P.389-392.

18. Ormancey G. and Godefroy G.// J. Phys.- 1974.- Vol.35.- P.135-139.

Received December 7, 1990.

UDC 537.226.4:539.4

MECHANICAL STRENGTH OF METAL-DOPED PLZT CERAMICS

M.Katrich*, V.Dimza**, I.Bespaltseva*,
K.Borman**, A.Plaude**
*Civil Engineering Institute,
1, Akademicheskaya St., 400074, Volgograd, USSR
**Institute of Solid State Physics, University of Latvia
8, Kengaraga St., 226063 Riga, Latvia

Analysis of indentation diagrams has shown that properties of ferroelectric ceramics are characterized by microhardness H, fracture toughness K_{1c}, intrinsic tension σ and critical size of cracks c^*. No change of microhardness has been observed in PLZT 8/65/35 upon doping by Mn, Fe, Co, Cu, Eu. Mn, Fe, Co, Eu dopants cause an increase of parameter K_{1c}, C^* and σ values. A minimum is observed on concentration curves $K_{1c}(x)$ and $c^*(x)$ at x = 0.1 wt.% of Cu-doped PLZT 8/65/35 ceramics.

Introduction

Deformation and fracture of ceramics is a rather complicated phenomenon and physical processes of indentation of the material have not been cleared completely. Speaking of such a complicated compound as PLZT [1] in terms of plasticity and resistance to deformation of solids, the contribution of different components to its resistance to deformation and fracture is determined by ceramic characteristics (grain size, composition and structure of the interlayer etc.) as well as by a good number of characteristics of the crystallites themselves concerning ionic and valent bonding, defectness (vacancies, dislocations etc.) and heterogeneity (compositional fluctuations, enclousures of different phase etc.). Since these problems presently are far from having been solved even in pure PLZT, the more it is true for metal-doped PLZT+Me ceramics and

any discussions of the deformation mechanisms concerning the latter are to be regarded as preliminary assumptions only.

To vary the light absoption, dielectric and another properties of PLZT ceramics different dopands are used to extend application of the material in optoelectronics [2,3]. Technological processing of PLZT+Me ceramics has been developed and the structure, dielectric and optical properties of the obtained samples studied [2,3]. To continue the studies mechanical properties of Mn-, Fe-, Co- and Eu-doped PLZT ceramics are presently reported. Apart from utilitarian purposes the present studies allow to understand the tension being formed at doping and to make quantitative estimates of it.

The method of structural test

Mechanical properties of undoped and 0.01, 0.1 and 1 mol.% Me-doped (by Mn, Fe, Co, Eu) PLZT 8/65/35 ceramics were examined by the indentation method on polished surfaces of non-polarized, unannealed samples.

Testing was performed by a Vicker's indentor on a "PMT-3" microhardness meter in the load interval P = 0.1-2.0 N. At a given load value the average values (from a number of at least 20 tests) of the pit diagonal d and the length of the radial crack c were measured. The information is presented as the lgP (lg d) and lg P (lg c) diagrams (Fig.1), where from the elastic-plastic deformation and fracture of the material may be examined to select criteria for mechanical strength and stress estimates of the material.

The study of indentation diagrams. Criteria of mechanical strength

1. For all the samples examined within the load interval $P \sim d^2$. In this case the microhardness $H = 1.854\ P \cdot d^{-2}$ does not depend on the load.

2. The curve lg P (lg c) is known[4] to have three linear intervals determined by 3 stages of crack development. The I and III regions are characterized by $P \sim c^2$, the II - by $P \approx c^{1.5}$. For all the examined samples within the load interval mainly the II stage - a distinct growth of cracks has been observed which makes it possible to calculate the intrinsic fracture toughness (resistance to cracking) of the material K_{1c}, independent on the load [5,6]

$$K_{1c} = 0.0726\ P \cdot c^{-1.5}.$$

The H and K_{1c} values were calculated at the load P = 0.2 N at which the II stage of the crack development is observed in all the examined samples.

3. In some of the samples within the load interval the III stage of crack development was also observed. To reveal transition to the III stage in all the samples the load need to be increased. Unfortunately, the small thickness of electrooptic samples has not allowed for that. Determination of the inflection point between the II and III regions of the indentation diagram is important for the following reasons. Relation between the effective K'_{1c} and intrinsic K_{1c} fracture toughness has been obtained [7] to be

$$K'_{1c} = K_{1c} + 2\sqrt{c/\pi}\ \sigma$$

and the averaged internal stress σ is determined (for $Pb_{1-1.5x}La_xTiO_3$ ceramics) from the slope of experimental K'_{1c} ($\sqrt{c}$) line. With regard to the linar dependence of $K'_{1c}(\sqrt{c})$ at the III stage of crack development (where $P \sim c^2$), a simple method to determine σ from fixed coordinate values P_o and c_o of the point between the II and III regions of the indentation diagram is suggested:

$$\sigma = 0.0726\ P_o c_o^{-2} \quad \text{or} \quad \sigma = K_{1c} c_o^{-0.5}.$$

4. An important characteristic of mechanical tension is the critical size of the crack c^*, obtained as the crosspoint of the indentation diagrams lg P (lg d/2) and lg P(lg c). As shown earlier, e.g. [8], the value of c^* is characteristic to the scale of the region wherein the tensions are localized.

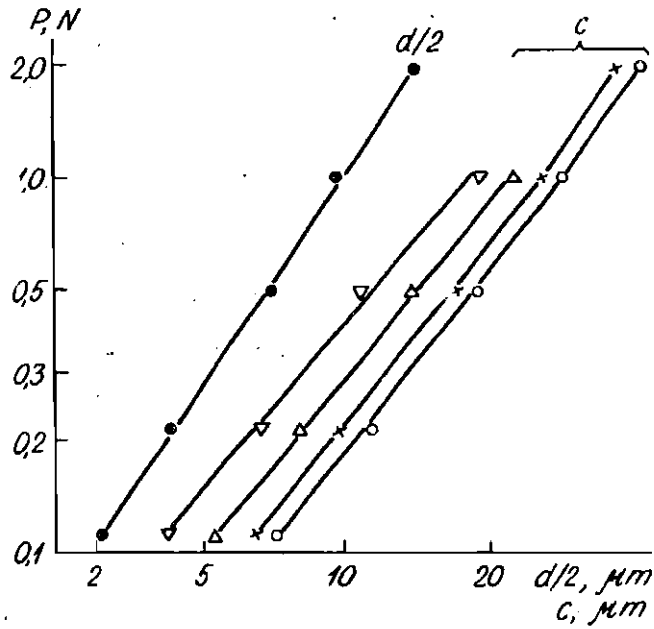

F i g . 1. Indentation diagram (half diagonal of the imprint d/2 and length of the crack c nearby it as functions of the indentor load P) for PLZT 8/65/35 (o) and PLZT 8/65/35+Mn (x-0.01%, Δ-0.1%, ▽-1 wt. %).

Thus, results of structural tests of PLZT 8/65/35+Me ceramics are represented by the values of microhardness H and fracture toughness K_{1c} determining resistance of the material to elastic-plastic deformation and brittle destruction, respectively, as well as by the values of σ and c^* which characterize the value of internal stress and the size of the region of their localization, respectively.

Experimental results

Microhardness H

Indentation measurements of the pit diagonal d are presented in the form lg P (lg d/2). In the case of PLZT 8/65/35 + Mn it is shown (Fig.1) that lg P (lg d/2) is a linear function and all the points regardless to the concentration of Mn as well as other dopants lay on the same line. Herefrom the microhardness value of all the examined PLZT 8/65/35 + Mn materials occurs to be the same and equal to H=6.1±0,1 GPa.

Fracture toughness K_{1c}

Results of experimental study of the damaged samples (area around the indentation mark - the length of the most extended radial crack) are presented as lg P (lg c). The linear intervals of this function in doped PLZT 8/65/35+Me samples shift to the left as the Me concentration grows (except Cu at small concentrations) and little depend on the element used as dopant (Fig.1). The fracture toughness K_{1c} is determined for each compound and the function K_{1c} (x) found (Fig.2).

Internal stress σ

Internal stress σ are determined from the coordinates of the inflection point between the II and the III intervals of the indentation diagram lg P (lg c). Experimental conditions have allowed to determine the σ values for some particular compounds: for pure PLZT σ = 80 MPa; parameter σ increases at doping by Fe - from 130 (0.01 wt.% Fe) to 146 (0.1 wt.% Fe) MPa; by Co - from 137 (0.01 wt.% Co) to 160 (0.1 wt.% Co) MPa; by Eu - from 128 (0.01 wt.% Eu) to 140 (0.1 wt.% Eu) MPa; but at doping by Cu σ at first increases to 134 MPa (0.01 wt.% Cu) then decreases to 106 MPa (0.1 wt.% Cu).

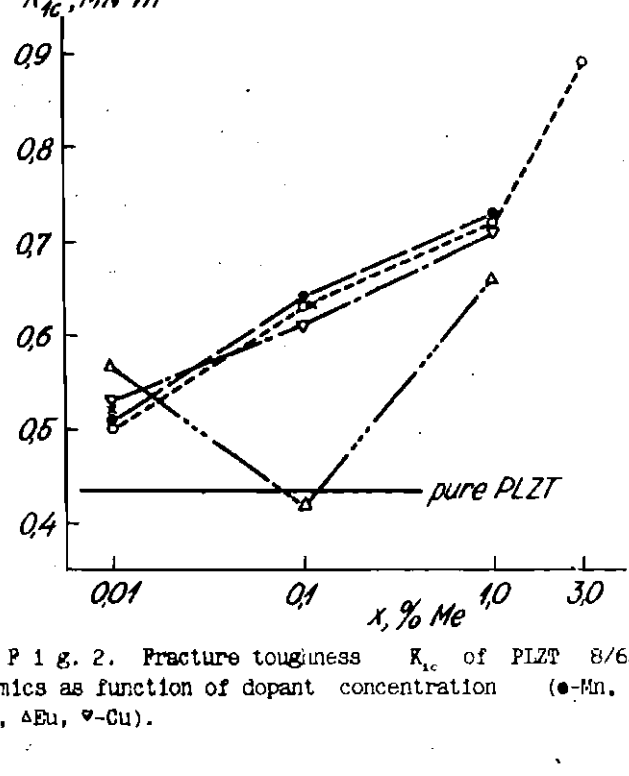

P i g. 2. Fracture toughness K_{1c} of PLZT 8/65/35+Me ceramics as function of dopant concentration (●-Mn, o-Fe, x-Co, ▵Eu, ▽-Cu).

The critical size of cracks c^*

The critical size of cracks c^* is determined as the coordinate of intersection of linear extrapolations of lg P (lg d/2) and lg P (lg c) (Pig.1). The concentration curves $c^*(x)$ (Pig.3) are characterized by monotonous growth in concentration interval $0.01 < x < 3.0\%$ for all the dopants except Cu in the case of which c^* has a minimum at x=0.1 wt.% Cu.
The obtained results show some general features:

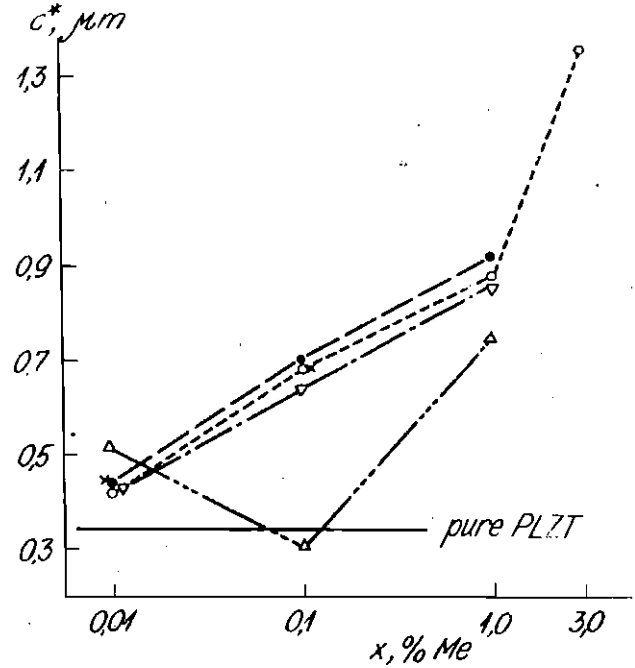

P 1 g. 3. The critical size of cracks c* in PLZT 8/65/35+Me ceramics as function of dopant concentration (●-Mn, o-Fe, x-Co, ▽-Eu, △-Cu).

1. No change of elasto-plastic properties characterised by microhardness H has been observed in PLZT 8/65/35 upon doping by the elements Mn, Fe, Co, Eu, Cu.

2. Introduction of Mn, Fe, Co and Eu in PLZT cause an increase of K_{1c}, c* (Fig.2,3) and ε values, the concentration curves $K_{1c}(x)$ and c*(x) are monotonously ascending with x.

3. The concentration curves of $K_{1c}(x)$ and c*(x) in PLZT 8/65/35+Cu have a minimum at x 0,1 wt.% Cu.

Discussion

1. Internal stress in ceramics may be due to structural defects of different scale. As shown earlier [8], the values of c^* and grain size do not correlate in PLZT (in contrast to other types of ferroelectric ceramics). This agrees with the conclusions in a number of papers concerning the small effect of grain boundaries on other physical properties in PLZT [9,10]. Present investigations show, that there has not been revealed any correlation between the strength and the size of crystallites. Really, our studies by means of scanning electron microscope (SEM) (detailed results are reported in a separate paper), the fractograms of PLZT and PLZT+Me have shown, that Fe and Mn dopants reduce the grain size from 3-8 μm for pure PLZT to 1-3 μm in the case of 1% Fe and 1% Mn, however, a farther increase of Mn concentration up to 3% weight cause an increase of the grain size to 10-20 μm. At the same time from Figs. 2,3 it is seen that the concentration curves $K_{1c}(x)$ and $c^*(x)$ for Mn- and Fe-doped as well as for the Eu- and Co-doped samples (where the change of grain size has not been observed) are monotonously growing in a similar way.

2. As shown earlier [8], the increase of K_{1c} caused by the growth of La concentration in PLZT X/65/35 ceramics may be a consequence of the decrease of unit cell volume V. The change of structure parameters in PLZT+Me caused by acceptor admixture is opposite to that of the donors. At doping by Mn, Fe, Co, being 3d-elements and Eu-lanthanoid, i.e., the difference of the electron shells of the elements, as well as Mn, Fe, Co occupying B site while Eu, obviously - the A site is less important than the unit cell volume V of PLZT being reduced by Mn, Fe and Co dopants while increased by Eu, the change of the ratio of X-ray diffraction maxima integrated intensities I_{210}/I_{211} caused by Eu also being opposite to that of other dopants /3/.

However, the present discussion reveals that microhardness H is not changed by doping, the growth of $K_{1c}(x)$ and $c^*(x)$ being similar in PLZT at doping by Mn, Fe, Co and Eu. This

means that in this case behaviour of mechanical resistance characteristics is not determined by the change of structure-sensitive characteristics ν and I_{210}/I_{211}.

3. At the same time, the strength properties to some extent are determined by two other structure-sensitive characteristics: the width of the X-ray diffraction maxima D and the Poisson's coefficient σ. As compared with PLZT+Mn,Fe,Co and Eu (at the same dopant concentrations) smaller values of K_{1c} and c^* have been observed in PLZT+Cu ($x \geq 0.1$ wt.%) which most likely is due to the same reasons as the discrepant behaviour of σ and D at doping by Cu, on one hand, and Mn, Fe, Co and Eu - on the other. Really, if linewidth D is decreased and σ increased by adding copper, then in the case of Mn-, Fe-, Co- and Eu-doped samples the change of the two parameters is either weak or of opposite character [3] (σ = 0,28; 0,32; 0,27; 0,25; 0,24; 0,26 correspondingly for pure PLZT 8/65/35 and PLZT 8/65/35+Cu, Mn, Fe, Co, Eu at x = 1 wt.% Me). The details of the mechanism of this phenomenon are not clear so far, however, the character of the change of D and σ suggests that by introduction of copper the structure is made more homogeneous. It has to be noticed that the value of the coefficient necessary to calculate K_{1c} depends, to some extent on the value of Poisson's coefficient, the latter having no effect on the corresponding factor in the formula used to calculate H [11].

Behaviour of $K_{1c}(x)$ and $c^*(x)$ in PLZT+Cu seems to suggest a one-dimensional superposition of two opposite contributions: 1) a decrease of K_{1c}, c^* and σ due to homogenization of the material at concentration of Cu 0.1 wt.% and 2) an increase of K_{1c} and c^* at large concentrations of Cu, i.e., strengthening of the samples due to similar mechanism as at doping by Mn, Fe, Co and Eu dopants.

4. From what has been told above one may presume that introduction of dopants in PLZT ceramics (a strongly defectful material [1]) the defect concentration is increased, clusters and, possibly, extended defects being formed [12]. All of this extends the regions of localization of tensions and explains appearance of additional internal stress (as compared to pure PLZT) the presence of which as well as inhomogeneity of grains

is shown by examining etched surfaces of doped and undoped PLZT samples [3]. The values of σ estimated in the present study allow to make some evaluation of the tension appearing upon doping PLZT: if in the case of undoped ceramics they are about 80 MPa, then at doping (up to 1% of admixture) they are increased by 60-100%. Besides, it seems possible to estimate the size of the regions of defect clusters in doped and undoped PLZT. The studies of radiation damage in TGS crystals [13] have shown that the size of radiation defects and the regions of localization of tensions (characterized by the critical size of cracks c^*) in TGS are close to each other. Assuming this to be true in the present case, one obtains (see Fig.3) that in undoped ceramics the clusters of defects are of the size of 0.3 μm while at doping (up to 1% admixture) they increase to 0.7-1.5 μm.

Thus, some conclusions and suggestions concerning the nature of micromechanisms responsible for mechanical resistance of PLZT and PLZT+Me we have been able to obtain by comparing the characteristics of strength properties with other structure-sensitive characteristics obtained by other methods, particularly by SEM, ultrasonic, X-ray diffraction.

In the present paper we do not make more speculations concerning the details responsible for the observed phenomena as the studies of structure and possible microscopic models of the relevant changes of PLZT+Me are being continued. Besides, more detailed farther studies of the rules revealed at indentation are needed.

REFERENCES

1. Haertling G.H. // Perroelectrics.- 1987.- Vol.75.- P.25.

2. Dimza V.I. , Arndt H. , Sprogis A.A., et al. // Actual Physical and Chemical Problems of Perroelectrics.- Latv. State Univ., Riga, 1987.- P.45-65 (in Russian).

3. Dimza V.I., Sprogis A.A., Kapenieks A. E., et al.// Perroelectrics.- 1989.- Vol.90.- P.45-55.

4. Berdikov V.F.// Physics of brittle fracture.- Kiev, 1976.- Vol.1. - P.208-210 (in Russian).
5. Evans A.G., Charles E.A.// J.Amer.Cer.Soc.- 1976.- Vol.59, N 7,8.- P. 371-373.

6. Grabko D.Z., Bojarskaja Yu.S., Zhitaru R.P. // Superconductivity: phys., chem., techn.- 1989.- Vol.2, N 6.- P.67-71 (in Russian).

7. Yamamoto T., Igarashi H. and Okazaki K.// J.Amer. Cer. Soc. 1976.- Vol.66.- P.363-366.

8. Katrich M.D., Dontsova L.I., Shilnikov A.V. // Ferroelectrics.- 1986.- Vol.69, № 1/2.- P.117-123.

9. Little J.A. and Yao P.C.// J.Amer. Cer. Soc.- 1984.- Vol.67.- P.29.

10. Krumin A.E. // Phase Transitions and Related Phenomena in Ferroelectrics.- Riga, 1984.- P. 3-62 (in Russian).

11. Lawn B.R., Jensen T., Arora A.et al. // J. Mater.Sci.- 1976.- Letters.- Vol.11 (3).- P.573-575.

12. Prisedskij V.V., Golubitskij V.M., But V.E., et al.// Izv.Akad. Nauk SSSR. Neorg.Mater . - 1981.-Vol.17.- P.1875. (in Russian).

13. Dontsova L.I., Katrich M.D., Tikhomirova N.A., et al. // Abstr. Int.Symp. on Domain Structure of Ferroelectrics and Related Materials.-Volgograd., 1989.- P.98.

Received December 7 , 1990.

UDC 537.226.4:539.16.043

RADIATION EFFECTS ON OPTICAL AND DIELECTRIC PROPERTIES OF PLZT X/65/35 CERAMICS

A. Sternberg, A. Krumina, A. Sprogis, A. Rubulis, and G. Grinvalds
Institute of Solid State Physics, University of Latvia,
8, Kengaraga St., 226063 Riga, Latvia

H.W. Weber, H. Klima, and H. Schwabl
Atominstitut der Österreichischen Universitäten,
Schüttelstraße 115, A-1020 Wien, Austria

S. Dindun and U. Ulmanis
Institute of Physics, Latvian Academy of Science,
32, Miera St., 229021 Salaspils, Latvia

Comprehensive studies of radiation effects on the optical and dielectric properties of PLZT X/65/35 ceramics have been made. The samples have been exposed to gamma-, electron and reactor neutron irradiation.

With regard to the optical properties, a maximum in the absorption difference with respect to the pre-irradiated state, appears in samples of PLZT 8-1/65/35 at wavelength of 380 nm, irrespective of the type of radiation.

With regard to the dielectric properties, the radiation-induced effects have been found to be strongly dependent on the sample composition, especially their La-content. Those samples, which are characterized by a slim hysteresis loop, show linear correlations between the 380 nm-maximum of the optical density difference, which is presumably proportional to the defect concentration, and the change of polarization in the neutron-irradiated state.

Introduction

Transparent ferroelectric ceramics (TFC) are promising materials for a number of optoelectronic devices [1,2] including electrooptical modulators for various functional purposes. Some of these applications may also involve radiation environments. In addition to this applied point of view, studies of radiation damage processes in TFC seem to represent an interesting aspect of materials science. Furthermore, TFC, in particular the well-known system of La-doped zirconate-titanate (PLZT X/Y/Z, X = La, Y = Zr, Z = Ti) has become a model material for studies of diffused phase transitions.

Many basic properties of ferroelectric materials and, in particular, their optical quality and electrooptical properties, are controlled by defects such as oxygen vacancies, redistributions of vacancies between the A and the B sites or additions of transition metal ions [3]. Hence, studies of radiation effects represent an interesting possibility to change the defect structure in a controlled way and to introduce new defects into the material. Preliminary results of our studies on radiation effects in TFC have been reported previously [4-6] and reviewed recently [7]. In the present paper we will report on radiation-induced property changes in a series of PLZT X/65/35 ceramics. Special emphasis will be placed on first results of optical property changes upon reactor neutron irradiation.

Experimental

The experiments were made on ceramic specimens of PLZT X/65/35 (X = 4.5 - 10.5 at.% La). Starting from chemically coprecipitated raw material, the TFC were prepared by a two-stage hot pressing technique. The lattice parameters and the phase composition of the samples were determined by X-ray diffraction, the detection of the stoichiometry was made by neutron activation analysis.

The optical measurements were made on thin polished samples of rectangular shape (10x10x0.2 mm^3), in order to achieve an uniform distribution of defects also in the case of electron irradiation. For the dielectric measurements, larger samples (5x5x1 mm^3) with fired silver paste electrodes were used.

The irradiation was done at three different facilities. The samples were exposed to gamma-irradiation in the gamma-loop of the Salaspils research reactor (average gamma-energy: 1.15 MeV; dose rate: 1050 r/s; doses up to $6 \cdot 10^6$ rad; sample temperature during irradiation: 45-60 °C); secondly, to electron-irradiation at the linear accelerator in Salaspils (electron energy: 4.5 MeV; flux density: 10^{12} electr./cm^2.s; fluences up to $4 \cdot 10^{17}$ electr./cm^2); and, thirdly to neutron and gamma-irradiation in the TRIGA MARK II reactor [8] in Vienna

(flux density at a reactor power of 250 kW: $2.1 \cdot 10^{13}$ n/cm^2.s (total), $7.6 \cdot 10^{12}$ n/cm^2.s (E > 0.1 MeV); fluences up to $1 \cdot 10^{18}$ n/cm^2; gamma-dose rate: $\leq 2.7 \cdot 10^4$ r/s; sample temperature: ≤ 60 °C).

The spectra of the optical absorption difference ΔD between the irradiated and a reference sample were obtained by an automatic double-beam spectrometer (Perkin-Elmer Lambda 9) over a wide range of wavelengths (340-3200 nm). The hysteresis loops were measured by quasi-static Sawyer-Tower techniques using an ultralow-frequency special-shape high-voltage generator "Cilpotājs 2000 EP" developed at the Institute of Solid State Physics, Riga. Duration of the whole measuring cycle was set to 60 s. Capacity and dielectric losses of the samples at 1 kHz were measured using a GR 1657 Digibridge. All the optical and dielectric measurements were made at room temperature. The annealing experiments were made in a thermostat using fixed preset rates of temperature change and employing especially fast cooling rates to room temperature after each annealing cycle, in order to preserve the particular defect structures.

Results and discussion

Optical properties

Visual inspection of all the irradiated PLZT samples showed a change of color to yellow, suggesting radiation-induced absorption in the UV part of the spectrum. This was indeed confirmed by the spectroscopy data. A typical example (PLZT 9/65/35), which is characteristic for all the results obtained on samples with a La-content between 7 and 11 at %, is shown in Fig. 1. The main features may be summarized as follows.

A pronounced maximum in the absorption difference ΔD as a function of wavelength occurs at a wavelength of ~380 nm in all of the irradiated samples, i.e., irrespective of the kind of radiation used (neutron, electron, and gamma-irradiation). This seems to indicate, that only one type of defects, which

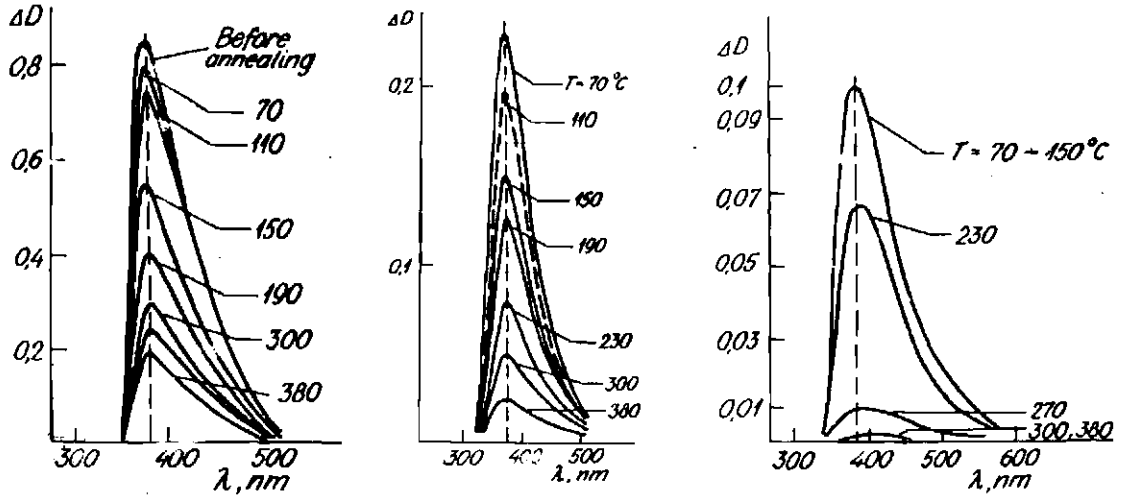

F i g. 1. Optical density difference ΔD versus wavelength of PLZT 9/65/35 ceramics:

a) neutron irradiated (fluence $5 \cdot 10^{17}$ n/cm^2); b) electron irradiation (fluence $4.2 \cdot 10^{17}$ electr./cm^2); c) gamma-irradiation (dose: $6.36 \cdot 10^6$ rad).

The numbers refer to the annealing temperatures (an annealing time of 8 min was employed through the experiments). The upper curves show the state of the irradiated sample before annealing.

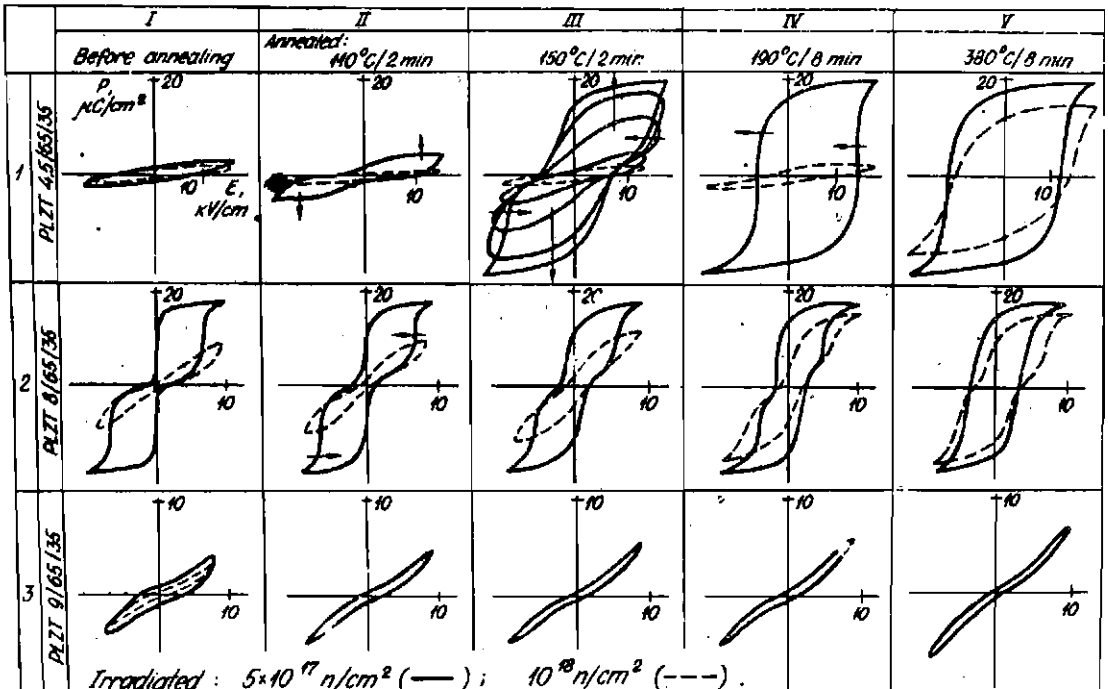

F i g. 2. Dielectric hysteresis in PLZT X/65/35 ceramics subjected to reactor neutron irradiation and annealing treatments. All measurements were done at room temperature.

can be produced by all kinds of radiation, is involved in the optical property changes of the PLZT ceramics investigated.

These defects have a rather low activation energy, since they can be annealed out already at temperatures between 400 and 500 °C.

The most significant changes of the optical properties are observed after reactor neutron irradiation to a fluence of $5 \cdot 10^{17}$ n/cm^2, E > 0.1 MeV, ($\Delta D \approx 0.8$), followed by electron irradiation ($4.2 \cdot 10^{17}$ electr./cm^2, E = 4.5 MeV), $\Delta D \approx 0.2$, and finally by gamma-irradiation to a dose of $6.36 \cdot 10^6$ rad ($\Delta D \approx 0.1$). However, since no damage calculations are available yet for this compound, a comparison between these different types of radiation is difficult.

The effect of annealing temperature seems to be different for the different types of radiation (Fig. 1). Whereas the annealing processes presumably begin already at room temperature in the neutron-irradiated samples (note the small differences between the upper curves in Fig.1a), significant annealing effects in the electron- and gamma-irradiated samples occur only at temperatures of ≈ 110 and ≈ 140 °C, respectively.

The initial optical properties are restored at temperatures between 400 and 500 °C in the cases of neutron and electron irradiation, whereas the differences between the gamma-irradiated and the reference samples fall below the experimental resolution already at a temperature of ≈ 300 °C.

Very similar results, in particular, the maxima around 380 nm, have been obtained also for PLZT 4.5-7/65/35 samples. However, depending on the actual composition as well as on the state of polarization, some qualitative and quantitative differences have been observed, which require additional experimental examination.

Dielectric properties

A summary of neutron irradiation effects on the dielectric properties (quasi-static hysteresis) is shown in Fig.2 for two fast neutron fluences ($5 \cdot 10^{17}$ and $1 \cdot 10^{18}$ n/cm^2). An electric field strength of 15 kV/cm was used for the samples PLZT 4.5/65/35 and 10 kV/cm for the other materials.

The pre-irradiation properties of all the materials are represented very closely by the solid lines in column V of Fig. 2 (annealed at 380 °C following irradiation to $5 \cdot 10^{17}$ n/cm^2). The effect of neutron irradiation (column I, Fig. 2) is very significant in all the samples investigated. The most pronounced change occurs in the shape of the hysteresis loops in samples PLZT 4.5/65/35. This may be explained by the classical mechanism [9] leading to the appearance of intrinsic radiation-induced bias fields in ferroelectric substances. Accordingly, the radiation-induced defects are responsible for stabilizing the direction of spontaneous polarization, which leads to an increase in the coercive field and prevents switching processes. For samples PLZT 4.5/65/35, e.g., no switching can be achieved by a 15 kV/cm field, unless annealing temperatures of ≈ 150 °C ($5 \cdot 10^{17}$ n/cm^2) or even ≈270 °C ($1 \cdot 10^{18}$ n/cm^2) have been employed (cf. row 1 in Fig.2). In addition, the defects reduce the magnitude of the spontaneous polarization by screening the long-range interaction and, hence, the phase transition in the material becomes more diffused. This is illustrated nicely by the last graph in row 1 (column V), where the completely annealed data (solid line, fluence: $5 \cdot 10^{17}$ n/cm^2) are compared to incompletely annealed results (dashed line) obtained after exposure to a fluence of $1 \cdot 10^{18}$ n/cm^2.

Due to the radiation-induced bias field, the hysteresis loops become asymmetric in "hard" ferroelectrics such as PLZT 4.5/65/35 (row 1, column IV in Fig. 2), while double loops appear in "soft" ferroelectrics (row 2, Fig. 2) or "propeller shaped" curves in slim-loop samples (row 3, Fig.). The bias field strength increases with decreasing La-concentration and increasing neutron fluence.

After each annealing stage a more or less pronounced build-up of the loop size has been observed under repeated field cycling conditions (cf. the arrows in Fig. 2 indicating the direction of loop formation). Such a building-up process can be related to a rearrangement and relaxation of radiation-induced defects. The most efficient build-up has been observed, when the sample is brought into a state, where the applied field compensated the defect-induced intrinsic field

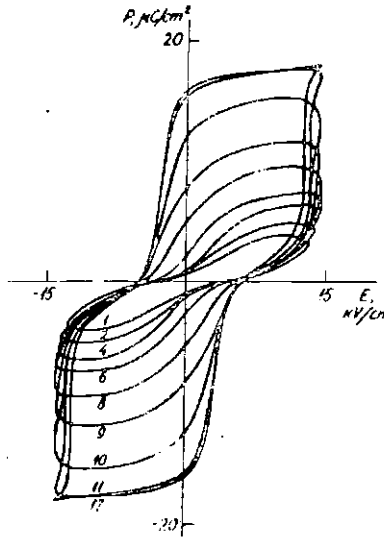

F i g. 3. Formation of hysteresis loops in PLZT 4,5/65/35 ceramics irradiated by reactor neutrons (fluence $5 \cdot 10^{17}$ n/cm^2) and annealed (150 °C for 2 min) at repeated switching (the number of cycles is given at each curve) under applied field.

and the spontaneous polarization started to reverse its direction under the applied field. The value of the switched polarization grows and is then stabilized after a certain number of cycles (Fig.3). This unique formation of the hysteresis loop has been observed in PLZT 4.5/65/35 after neutron irradiation to $5 \cdot 10^{17}$ n/cm^2 and an annealing treatment at 150 °C for 2 minutes (Fig.2, row 1, column III, and Fig.3).

Regarding this loop formation, an additional interesting feature has been observed. As depicted in Fig. 3, the hysteresis loop becomes practically symmetric after a certain number of cycles. However, upon increasing the temperature to the next annealing stage, the loop starts out asymmetrically again (cf. row 1, columns III and IV in Fig. 2), a feature

hich can be explained by a redistribution (diffusion, drift) of the radiation-induced defects.

Because of a small rhombohedral distortion of their crystal lattice in the polarized state, PLZT X/65/35 ceramics with $7.5 \leq X < 9$ are extremely sensitive to all external effects, such as electric field and mechanical pressure [10], and show the largest electrooptic coefficients. Irradiation leads to a more diffused phase transition: the maximum of the $\varepsilon(T)$-curve broadens and both the polarization and the coercive field are decreased. A change of the ion charge and redistributions of vacancies in the A and B sublattices may be considered as being the responsible irradiation mechanisms [7]. This sensitivity is also observed with regard to the radiation-induced bias field as shown by the hysteresis loops in row 2, columns I and II in Fig. 2: these nearly rectangular loops with an obvious narrowing in the center, which were observed in PLZT 8/65/35 following neutron irradiation to $5 \cdot 10^{17}$ n/cm^2, are very similar to loops observed in irradiated multidomain single crystals. Due to the small values of E_c, the remanent polarization goes practically to zero when the field is removed. This process occurs within a few seconds after the field removal and follows a nearly exponential law.

In PLZT X/65/35 compounds with $9 \leq X \leq 11$, irradiation leads to a decrease of the total polarization and to the appearance of small remanent polarized volumes. The annealing behavior (Fig. 2, row 3) differs from the results obtained on the materials with lower La-content and the loop shapes are nearly identical for the two neutron fluences investigated, at least at annealing temperatures above 110 °C.

A common feature observed in all irradiated samples is the decrease of the dielectric permeability ε at room temperature. Dielectric permeability has been measured after each annealing step as well as immediately after hysteresis loop experiments. In the latter case, the ε-values were always found to be higher initially and to decrease with time following roughly an exponential law. This behavior is typical for structure stabilization and defect relaxation processes.

Summary

We have observed significant changes in the optical and dielectric properties of PLZT X/65/35 ceramics following irradiation with neutrons, electrons and gamma-rays.

With regard to the optical properties, we have found a characteristic maximum in the absorption difference ΔD (prior to and following irradiation) at a wavelength of ~380 nm, irrespective of the type of radiation employed. However, some differences in the annealing behavior have been observed depending on the type of irradiation. The radiation-induced defects have a rather low activation energy, since they can be annealed out at temperatures between 400 and 500 °C (and even at lower temperatures, ≈ 300 °C, in the case of gamma-irradiation).

With regard to the dielectric properties, neutron irradiation leads to significant effects on the shape and size of the hysteresis loop, especially in materials with low La-content. In some cases, an interesting loop build-up has been observed under field cycling conditions. In all cases, the dielectric permeability ε at room temperature decreased upon irradiation.

In conclusion, we wish to point out an interesting correlation between the change of optical and the dielectric properties which seems to prevail at least in materials with X > 9 at.-% La, and lattice structure approaching cubic symmetry. Since the spectral distribution of the optical absorption difference ΔD is constant and the absolute values of ΔD depend on fluence and annealing temperature, ΔD may be assumed to be proportional to the defect concentration. Fig. 4 shows that the relevant change of sample total polarization, $|\Delta P| = P_{irr} - P_{unirr}$, is in fact linearly correlated to ΔD. The magnitude of the slope, however, becomes smaller with increasing La-content. This suggests that the influence of radiation-induced defects on polarization becomes smaller with the increase of La-content. It should be noted that the absolute values of polarization and of the electrooptical coefficients also become smaller in this series of materials as the structure approaches cubic symmetry. In the case of

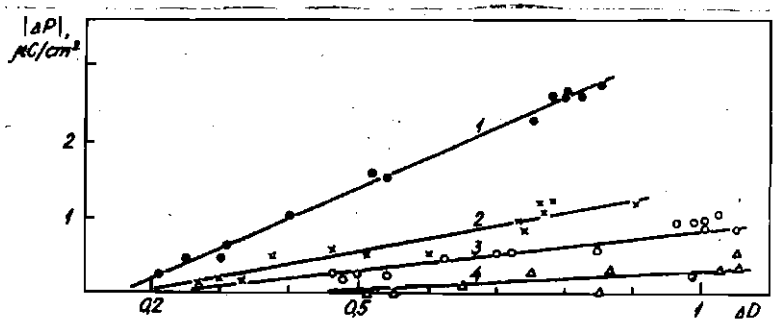

F i g.4. Neutron-induced (fluence $5 \cdot 10^{17}$ n/cm^2) polarization change |ΔP| versus radiation-induced optical density difference ΔD at 380 nm in PLZT samples subjected to sequential annealing. 1 - PLZT 9/65/35; 2 - PLZT 9.75/65/35; 3 - PLZT 10.5/65/35; 4 - PLZT 8/65/35.

ceramics with X < 9 at.% La (non-cubic materials), this correlation becomes less obvious (curve 4 in Fig.4). This is not unexpected, since the interaction between the defects and the structure of macroscopic polarization is more complicated, the optical properties of the ceramics depending on the state of polarization itself.

In order to obtain more information about the nature of th radiation-induced defects as well as their activation energies, further optical, electrooptical and structural investigations will be needed.

Acknowledgements

The authors are thankful to colleagues in the Laboratory of Chemical Synthesis of the Ferroelectric Physics Department at the Institute of Solid State Physics for providing the samples, to Dr. L. Shebanov for the X-ray diffraction measurements and to Dr. I. Popova for the neutron activation analysis. This work is supported in part by Bundesministerium für Wissenschaft und Forschung, Wien.

REFERENCES

1. Haertling G.H.// Ferroelectrics. - 1987. - Vol.75. - P.25-58.

2. Sternberg A. // Ferroelectrics. - 1989. - Vol.91. - P.53-67.

3. Dimza V.I., Sprogis A.A., Kapenieks A.E.,et al. // Ferroelectrics. - 1989. - Vol.90. - P.45-55.

4. Sternberg A., Shebanov L., Rubulis A., et al.// Ferroelectrics. - 1986. - Vol. 69. - P.95-104.

5. Sternberg A., Dimza V., Sprogis A., et al. // Ferroelectrics. - 1988. - Vol.80. - P.949-954.

6. Grinvalds G.Z., Dimza V.I., Dindun S.S., et al. // Autometria. - 1988. - Vol.4. - P.50-58 (in Russian).

7. Sternberg A., Rubulis A., Shebanov L., et al. // Ferroelectrics. - 1989. - Vol.90. - P.89-101

8. Weber H.W., Beck H., Unfried E., and Greenwood L.R. // J.Nucl.Mater.- 1986.- Vol.137. - P.236.

9. Lines M.E., Glass A.M. Principles and Applications of Ferroelectric and Related Materials.- Oxford, Clarendon Press, 1977. - 736 p.

10. Sternberg A.R., Fritsberg V.J., Borman K.J., et al. // Electrooptic Ceramics.- Riga, 1977.- P.138-167 (in Russian).

Received December 7 , 1990.

UDC 546.815-546.825

FABRICATION OF PLZT CERAMICS FROM CHEMICALLY PURIFIED SOURCE MATERIAL

M.Dambekalne, M.Antonova, L.Ravina, I.Popova, and V.Belov*
Institute of Solid State Physics, University of Latvia
8,Kengaraga St.,226063 Riga ,Latvia
* Institute of Extra Pure Substances, Moscow

Lead nitrate and zirconyl chloride salts, the basic source materials used in PLZT powder synthesis by chemical coprecipitation, have been purified by recrystallization and sedimentation. Concentration of impurities was measured in the source material before and after purification as well as in the synthesized PLZT powder. Amount of many impurities (Zn, Ni, Cr, Co, Cu) was decreased by an order while content of Fe, Si, Al, Mg - by several times; this has increased the light transmittance of the end product by 5% and reduced scattered light by 10%.

Introduction

Successful application of the lanthanum-doped lead titanate-zirconate (PLZT) transparent electrooptic ceramics in optical electronics requires improved quality (optical transmittance and homogeneity) and a good reproducibility of properties. This can be achieved by exact stoichiometry, of chemical homogeneity and high purity of the synthesized stock. The study was mainly aimed at improvement of the quality of PLZT ceramics by use of chemically purified lead nitrate ($Pb(NO_3)_2$) and zirconylchloride ($ZrOCl_2 \cdot 8H_2O$) - source material for stock synthesis by chemical coprecipitation.

The salts were purified by recrystallization and sedimentation on rather commonly practiced in laboratories due to simplicity and effectiveness. The method of recrystallization is based on the increase of solubility at heating used to obtain saturated solutions. At cooling solubility of salts decreases and crystals of purified substance separate out of the cooled solution which is saturated with respect to the basic substance while smaller

amounts of admixtures remain solved. This method is used as well to obtain extra pure chemicals as in production common substances. The effect of purification is enhanced by repeated procedure.

Another commonly used method of purification is sedimentation of admixture (or basic substance) by use of suitable chemical agent to form insoluble compounds of the substance to be filtered from the solution.

Analysis of impurities

We used an EMAL-2 mass-spectrometer and automated data processing (improved in the ISSP) for fast impurities detection. Samples of the size from 2x3 to 40x40 mm^2 and 0.5 to 3 mm thick were pressed from the powders subject to examination.

For more complete detection of impurities kind and concentration the instrumental neutron activation analysis (INAA) reported in [1,2] was used. The method allows to detect about 22 admixture elements in lead and titanium compounds, and 18 - in zirconium and lanthanum compounds.

Experimental procedure.
Purification of lead nitrate $Pb(NO_3)_2$

Several methods described in [3,4] were tried to find the optimal one.

1. To obtain extra pure lead nitrate, nitric acid is used to sediment it from concentrated solutions. With the purpose 37.5 g of lead nitrate are solved in 95 ml water, by stirring intensively during an hour 100 ml of nitric acid of 41.4% concentration (density 1.24) is added to the solution. Sedimented crystals are filtered through Büchner's funnel, repeatedly rinsed by distilled water and dried at 60-70 ^{o}C. The processing reduces copper, iron and zinc admixture content by two orders (100 times). The process is often made less efficient because of isomorphic admixture being encloused in the solid phase. This is avoided if (1) the radii of equivalent

Table 1

Impurity concentration in lead nitrate $(Pb(NO_3)_2$ by INAA

Impurity	Concentration, wt.%		
	unpurified	purified	
		HNO_3 sedimentation	recrystallization
Na	$(2,0\pm0,1)\cdot10^{-4}$	$(6,0\pm0,1)\cdot10^{-4}$	$(4.0\pm0,1)\cdot10^{-4}$
Ba	$\leq0,7\cdot10^{-4}$	$\leq0.8\cdot10^{-4}$	$\leq0,8\cdot10^{-4}$
Fe	$(1,5\pm0,1)\cdot10^{-4}$	$(1,0\pm0,1)\cdot10^{-5}$	$(1,5\pm0,1)\cdot10^{-5}$
Mn	$(0,37\pm0,03)\cdot10^{-4}$	$(0,25\pm0,03)\cdot10^{-4}$	$(0,30\pm0,03)\cdot10^{-4}$
V	$\leq0,01\cdot10^{-4}$	$\leq0,01\cdot10^{-4}$	$\leq0,01\cdot10^{-4}$
Al	$(0,40\pm0,05)\cdot10^{-4}$	$(0,10\pm0,05)\cdot10^{-4}$	$(0,15\pm0,05)\cdot10^{-4}$
Se	$(0,5\pm0,05)\cdot10^{-5}$	$(0,5\pm0,05)\cdot10^{-5}$	$(0,6\pm0,05)\cdot10^{-5}$
Cr	$(1,6\pm0,1)\cdot10^{-5}$	$(0.60\pm0,1)\cdot10^{-6}$	$(1,0\pm0,1)\cdot10^{-6}$
Au	$(1,4\pm0,1)\cdot10^{-7}$	$(1,6\pm0,1)\cdot10^{-7}$	$(1,4\pm0,1)\cdot10^{-7}$
Ni	$\leq0,9\cdot10^{-5}$	$\leq0,7\cdot10^{-6}$	$\leq0,8\cdot10^{-6}$
Zn	$(2,8\pm0,1)\cdot10^{-5}$	$(2,6\pm0,1)\cdot10^{-6}$	$(5,6\pm0,1)\cdot10^{-6}$
Ag	$(0,70\pm0,05)\cdot10^{-5}$	$(0,50\pm0,05)\cdot10^{-5}$	$(0,60\pm0,05)\cdot10^{-5}$
Br	$\leq0,2\cdot10^{-6}$	$\leq0,2\cdot10^{-6}$	$\leq0,2\cdot10^{-6}$
Co	$\leq0,2\cdot10^{-6}$	$\leq0,5\cdot10^{-7}$	$\leq0,15\cdot10^{-6}$
Sb	$(4,5\pm0,1)\cdot10^{-6}$	$(4,0\pm0,1)\cdot10^{-6}$	$(4,3\pm0,1)\cdot10^{-6}$
La	$\leq0,6\cdot10^{-6}$	$\leq0,4\cdot10^{-6}$	$\leq0,6\cdot10^{-6}$
Sc	$(0,8\pm0,1)\cdot10^{-6}$	$(0,78\pm0,1)\cdot10^{-6}$	$(0,75\pm0,1)\cdot10^{-6}$
Ta	$(3,0\pm0,2)\cdot10^{-7}$	$(3,0\pm0,2)\cdot10^{-7}$	$(3,0\pm0,2)\cdot10^{-7}$
Cu*	$2.0\cdot10^{-5}$	$1,0\cdot10^{-5}$	$5,0\cdot10^{-4}$

* Emission spectral analysis.

ions differ more then 10–15%, as it is in the case of Pb^{2+} and Cu^{2+} (the ion radii being 1.26 Å and 0,8 Å respectively), (2) the formula or structure of the salts are different, e.g., $Pb(NO_3)_2$ and $Cu(NO_3)_2\cdot6H_2O$, (3) admixture components are more solvable compared to basic substance.

It is possible to reduce iron and copper impurity amount about ten times again by repeated sedimentation.

2. Efficient and simple enough is recrystallization of lead nitrate from saturated solution. Dissolve 150 g lead nitrate in 150 ml of distilled water by intense stirring and

heating, then filter the hot solution and let it crystallize while cooling. The crystallized substance is separated in Büchner's funnel and dried at 60-70°C. As seen from Table 1 this method is an easier one, however purification from admixtures is less efficient as compared to sedimentation by nitric acid.

Purification of zirconylchloride ($ZrOCl_2 \cdot 8H_2O$)

Chemical grade zirconylchloride also contains undesired impurity admixture, mainly Fe^{3+}, Cu^{2+}, Mg^{2+}, Cr^{3+} a.o. We tried the methods described in [3,4] and based on zirconylchloride recrystallization from hydrochloric acid solutions to eliminate impurity contents. The following zirconylchloride purifying techniques were developed from the methods.

1. 1000 g of zirconylchloride is solved in 1200 ml of distilled water.

Table 2

Impurity concentration of zirconylchloride ($ZrOCl_2 \cdot 8H_2O$) by INAA

Impurity	Concentration, wt.% unpurified	purified
La	$\leq 4 \cdot 10^{-3}$	$\leq 2 \cdot 10^{-3}$
Al	$\leq 3 \cdot 10^{-3}$	$\leq 5 \cdot 10^{-3}$
Mg	$(60 \pm 3) \cdot 10^{-3}$	$(80 \pm 3) \cdot 10^{-3}$
Ba	$(7800 \pm 200) \cdot 10^{-4}$	$(7600 \pm 200) \cdot 10^{-4}$
Rb	$\leq 10 \cdot 10^{-4}$	$\leq 10^{-4}$
V	$\leq 20 \cdot 10^{-5}$	$\leq 2,5 \cdot 10^{-6}$
Hf	$(230 \pm 15) \cdot 10^{-3}$	$(200 \pm 15) \cdot 10^{-3}$
Fe	$\leq 2 \cdot 10^{-2}$	$\leq 6 \cdot 10^{-4}$
Sb	$\leq 2 \cdot 10^{-5}$	$\leq 2 \cdot 10^{-5}$
Sc	$(1,7 \pm 0,1) \cdot 10^{-5}$	$(1,5 \pm 0,1) \cdot 10^{-5}$
Ta	$(10 \pm 0,5) \cdot 10^{-5}$	$(8 \pm 0,5) \cdot 10^{-5}$
Co	$\leq 7 \cdot 10^{-5}$	$\leq 8 \cdot 10^{-5}$
Eu	$0,2 \cdot 10^{-4}$	$0,2 \cdot 10^{-4}$
Cu*	$2 \cdot 10^{-3}$	$2 \cdot 10^{-4}$

* Emission spectral analysis.

2. To separate mechanical admixtures solution is filtered in Buchner's fannel through double filter paper.

3. Solution is once more filtered through Buchner's fannel and a mixture of activated charcoal and ZrO_2 powder. The filtrate must be clear as water without any opalescence.

4. The cleared solution is poured into thermoresistant glass and an equal volume of 25% chemical grade hydrochloric acid added. Then it is heated up to 80 ^{o}C and stirred until the sediment is completely dissolved, after which solution is left overnight to cool.

5. Sediment of zirconylchloride is filtered through Buchner's fannel and rinsed by distilled water.

6. To the salt, placed into a thermoresistant glass, is added 25% hydrochloric acid, stirred and left overnight.

7. The chrystals are filtered through Buchner's fannel. If they are yellowish, they are rinsed with 500-600 ml of extra pure hydrochloric acid.

8. The obtained salt then is dissolved in up to 1500 ml of water, and the zirconylchloride concentration of the solution is about 20%.

The method is labor-consuming and complicated however it is good to clean away microadmixtures (see Table 2).

Results and discussion

Copper, iron, zinc and other admixtures from lead nitrate are most efficiently removed by sedimentation in HNO_3 (see Table 1). The concentration of these admixtures is reduced about 100 times with respect to chemical grade lead nitrate. However, the method is not convenient because of concentrated acid and hot solutions. Recrystallization can be regarded to be rather efficient amount of iron, zinc and copper being reduced by 10 times. Efficient reducing of admixture concentration in practice often fails not because of chemical purifying process but accidental contamination during the technological course by water, chemical agents and instruments. This is, particularly, the case of powders and ceramics the synthesizing of which is a long technology.

Table 3

Mass-spectrometric impurity analysis of PLZT-10/65/35 ceramics

Impurity, wt.%	Sample	
	from unpurified surce	from purified surce
Fe	$3 \cdot 10^{-3}$	10^{-3}
Si	$3 \cdot 10^{-2}$	10^{-2}
Al	$3 \cdot 10^{-2}$	10^{-2}
Mg	$3 \cdot 10^{-2}$	10^{-2}
Cr	10^{-3}	10^{-4}
Co	10^{-3}	10^{-4}
Ni	10^{-3}	10^{-4}
Zn	10^{-2}	10^{-3}
Na	10^{-1}	$5 \cdot 10^{-1}$
Cu	$5 \cdot 10^{-2}$	$4 \cdot 10^{-3}$
Ca	10^{-2}	$3 \cdot 10^{-2}$

Admixture contents of purified and unpurified stock of PLZT are given in Table 3. It is seen that concentration of Fe, Si, Al, Mg and other admixtures is reduced by several times, Zn, Ni, Cr and Co - by 10 times while concentration of Na and Ca has increased a little. These are admixtures of high abundance: Si, Al, Na, Ca, K, Mg, Fe, Ti, Mn, Cl, P, N, S a.o. Microadmixtures of this kind is difficult to remove since they are easily brought from environment during the technological process - by water, chemical glass, ware, instruments etc. It has to be noticed that concentration of Si, Al, Mg, Ca, Na microadmixtures in synthesized stock and ceramics is relatively high. PLZT ceramics produced from purified stock is of better quality because of reduced contents of so called color elements Fe, Cr, Co, Ni, Zn. Transmittance of the purified ceramics is increased by 5%, the scattering of light being decreased by 10%.

REFERENCES

1. Popova I.//Izv.Akad.Nauk Latv.SSR. Ser.Fiz.Tekh.- 1980.- N 5.- P.9-14.

2. Popova I.//Izv.Akad.Nauk Latv.SSR. Ser.Fiz.Tekh.- 1984.- N 3.- P.3-8.

3. Karjagin J.V. and Angelow. Pure Chemicals.- M., 1984.- P.176 (in Russian).

4. Stepin B.D., Gorstein I.G., Blum G.Z., and Ogloblina I.P. Producing of Extra Pure Chemical Compounds.- L., 1979.- P.480 (in Russian).

Received February 14, 1991.

UDK 543.53:537.226.33

SIMULTANEOUS DETERMINATION OF LEAD, LANTHANUM, ZIRCONIUM AND TITANIUM BY 14 MeV NEUTRON ACTIVATION ANALYSIS

I.Popova
Institute of Solid State Physics, University of Latvia
8, Kengaraga St., 226063 Riga, Latvia

Instrumental neutron activation analysis (INAA) has been used to determine simultaneously four macrocomponents in PLZT ferroelectric materials. Pb, Zr, Ti have been detected by nuclides ^{203}Pb, ^{95}Zr, ^{46}Sc created by fast neutron (14 MeV) activation. The application of paraffin to slow down and reflect neutrons allowed to determine simultaneously lanthanum by nuclide ^{140}La. The accuracy of determination of zirconium, titanium and lanthanum was ±0,1 wt.%, lead ± 0,7 wt.%.

Introduction

The content of four macroelements (Pb, La, Zr, Ti) in ferroelectric transparent materials can be determined by using nuclear IRT-type reactor with flux density $1,6 \cdot 10^{17}$ $n \cdot m^{-2} \cdot s^{-1}$ [1]. The accuracy of determination was ±0,07 wt.% for lanthanum; ± 2,0 wt.% for lead; ± 1,8 wt.% for zirconium and ± 0,1 wt.% for titanium. But there was influence of lanthanum on titanium determination and the accuracy of determination of three elements (Pb, Zr, Ti) was insufficient for our technological purposes. This method was used as a sensitive one for La determination (the deviation 0,07 wt.% corresponds to 0,0 at.% lanthanum).

The aim of this work was investigation of using 14 MeV neutron generator for simultaneous determination of Pb, La, Zr and Ti.

Experimental

As source of fast neutrons with energy 14 MeV and thermal neutrons neutron generator NG-200 was used [2]. Density of neutron flux in the place of radiation was approximately

neutron flux in the place of radiation was approximately $1 \cdot 10^{12}$ $n \cdot m^{-2} \cdot s^{-1}$. The part of thermal neutrons in fast neutron flux was small, their relation being $1{,}4 \cdot 10^{-4}$. Production of radioactive nuclides in Table 1 [3] was estimated by 14 MeV neutron irradiation of PLZT material. The detection limits were calculated from $3\sqrt{N_r}$ [4], where N_r - experimental counts of background. The calculation of gamma ray spectra was done by COVELL's method. Samples were prepared as powder (tablets) about 100 mg or small ceramic plates with diameter 6 mm and thickness ≤ 0,5 mm. Standards - pure metals Pb, Zr, Ti and La in identical shape as samples with mass 50, 20, 15 and 10 mg, respectively. These samples and standards were each encased in polyethylene and arranged in the following order: Pb, sample, La, Zr, Ti, sample, Pb. Then all three packets were irradiated with 14 MeV neutrons.

As the size and mass of samples were small, the corrections for geometry of radiance [5] and measurements [6], and also selfshielding [6] and self-absorption of gamma-radiation [6,7] had not been taken into consideration.

It was assumed that the part of thermal neutrons in total neutron flux had been increased by using paraffin block around the target of generator and the packets (in order to slow down and reflect neutrons). Then thermal to fast neutrons ratio increased appr. 6 times i.e. to $0{,}8 \cdot 10^{-3}$ [8]. and the reaction $^{139}La(n,\gamma)$ ^{140}La may go together with fast neutroninduced reactions in elements Pb, Zr, Ti.

After investigation of a wide-spread variety of materials the following parameters of INAA method were chosen: time of irradiation on neutron generator with paraffin - 6 h and cooling time - 20 h. Then, the gamma ray spectra of each sample and standard were measured during 20 min. The spectrometric system consisted of a Ge detector with an active volume of 20 cm^3 and 800-channel analyzer LP 4840. The resolution of the spectrometric system was 3 keV for 1,332 MeV gamma-line of ^{60}Co. The gamma ray spectrum of PLZT specimen irradiated by 14 MeV neutrons is shown in Fig.

Table 1 gives the radionuclides produced by thermal and fast neutron reactions with major elements of PLZT, except oxygen. Neighbouring, disturbing reactions with respect to

^{204}Pb (n,2n) ^{203}Pb are not known under these experimental conditions [9].

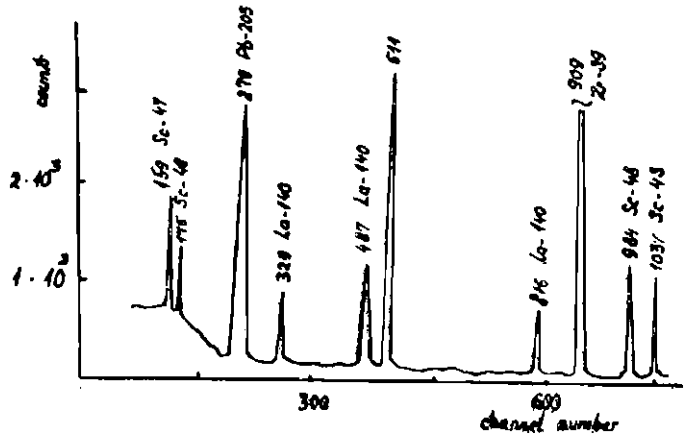

Fig. The gamma ray spectrum of one PLZT sample irradiated by 14 MeV neutrons.

Table 1

Nuclear data for elements detected in PLZT material by INAA

Element	Nuclear reaction	Neutron energy, MeV	Product nuclide	$T_{1/2}$ days	Photopeak used, keV	Nat. isotopic abundance, %	Concentration found, wt.%
Pb	n,2n	14	^{203}Pb	2,17	279,1	80	$4\cdot10^{-2}$
Zr	n,2n	14	^{89}Zr	3,27	909,2	99	$2\cdot10^{-3}$
Ti	n,2n	14	^{46}Sc	1,83	983,5	100	$7\cdot10^{-3}$
La	n,γ	therm. neutr.	^{140}La	1,66	487,0	48	$2\cdot10^{-2}$

Table 2

Accuracy in measuring the concentration of elements in PLZT 9,25/65/35 material

Element	Pb	La	Zr	Ti
Concentration, wt.%	58,184	3,972	17,920	5,067
Photopeak counts for 1 g specimen	25000	4000	56000	4000
Standard deviation	±300	±140	±260	±90
Coefficient of variation,%	1,2	3,5	0,5	2,2
Quantity of standard deviation, wt.%	±0,70	±0,13	±0,06	±0,11

Results

Table 2 shows the results for PLZT 9,25/65/35 material. They are given as counts obtained in 20 min counting per gram of each element. Coefficient of variation for 3 parallel determinations is 1,2 % for Pb; 3,5 % for La; 0,5 % for Zr; 2,2 % for Ti, in wt.% appr. ± 0,1 % for Zr, Ti, La and ± 0,7 % for Pb.

The accuracy of determining Zr is improved by an order of magnitude, but for lead - 2 times compared with the experiment [1]. After 30 days of cooling irradiated specimens can be used for further measurements as nonradioactive.

The accuracy of chemical analysis [10] of PLZT materials is as follows: PbO ± 0,23 wt.%; La_2O_3 ± 0,07 wt.%; ZrO_2 ± 0,13 wt.%; TiO_2 ± 0,12 wt.%. Required quantity for analysis is 1 g, analysis time is 6-7 h per sample, the specimens being destroyed during the experiment.

Conclusion

The method is most suited for simultaneous analysis of 4 major components in ferroelectric PLZT materials.

The method can be recommended for rapid and sufficiently

accurate determination of stoichiometric changes and can be used to develop high quality transparent PLZT ferroelectric materials.

REFERENCES

1. Popova I.L., Pelekis Z.E., Pelekis L.L. // Proc.10th USSR Conf.Perroel.- Minsk, 1982.- P.82 (in Russian).

2. Mednis I.V., Seimanis J.J., Jurka J.A. // Activation Analysis.- Riga, 1976.- P.32-36 (in Russian).

3. Mednis I.V. Tables of data for NAA.- Riga, 1974.- 409 p.

4. Gunne H.E., Pelekis L.L. // Activation Analysis.- Riga, 1966.- P.5-14 (in Russian).

5. Van Grieken R., Speecke A., Hoste J. // J.Rad.Chem.- 1972.-Vol.10, N.1 - P.95-104.

6. Pelekis L.L., Jurka J.A.// Izv. Acad. Nauk Latv. SSR, Ser. Fiz. Tekh.- 1976.- N.4 - P.6-11 (in Russian).

7. Jurka J.A. // Izv.Acad.Nauk Latv.SSR. Ser.Fiz. Tekh.- 1977.- N.3 -P.8-12 (in Russian).

8. Pelekis L.L., Jurka J.A. // Izv. Acad. Nauk Latv.SSR. Ser.Fiz.Tekh.- 1976.- N.5 - P.3-7 (in Russian).

9. Maslov J.A., Luknickii P.A. Tables of NAA. L.,1971.- 312 p.

10.Belov V.V., Vigdorovich V.N., Derbeneva T.A., et al. // Abstr.of 1st Interdepartm. Seminar.- Riga, 1982.- P.7, 8 (in Russian).

Received July 12 , 1990.

CONTENTS

* *

ACTUAL PHYSICAL AND CHEMICAL PROBLEMS OF FERROELECTRICS
Zinātniskie raksti, 559. sējums.

Recenzenti **E.Šiliņš**, LU Eksperimentālās fizikas kat.doc., fiz.un mat.zin.kandidāts;
U.Ulmanis, LZA Fizikas institūta laboratorijas vad., tehn.zin.kandidāts.

Redaktori A.Šternbergs, V.Polmane
Tehniskā redaktore M.Dreimane
Korektore I.Meldere

Parakstīts iesp.21.05.91. Licence Nr.000224. Papīra formāts 60x84/16. Papīra Nr.1. 7,5 fiz.iespiedl. 7,0 uzsk.iespiedl. 5,5 uzsk.izdevn.l. Metiens 350 eks. Pasūt.Nr. 332

Latvijas Universitāte. 226098 Rīga, Raiņa bulv. 19. Iespiests LU **rotaprintā**. 226050 Rīga, Veidenbauma ielā 5.